

COMPOSITIONAL MODELING OF SABRIYAH NATURALLY FRACTURED GAS
CONDENSATE RESERVOIR, KUWAIT

by
Mesferah Al Qahtani

A thesis submitted to the Faculty and the Board of Trustees of the Colorado School of Mines in partial fulfillment of the requirements for the degree of Master of Science (Petroleum Engineering).

Golden, Colorado

Date _____

Signed: _____

Mesferah Al Qahtani

Signed: _____

Dr. Hossein Kazemi
Thesis Advisor

Golden, Colorado

Date _____

Signed: _____

Dr. Erdal Ozkan
Professor and Head
Department of Petroleum Engineering

ABSTRACT

The thesis pertains to numerical modeling of Sabriyah gas-condensate reservoir in Kuwait. Sabriyah is an abnormally high-pressure, 11,000 psi, naturally fractured carbonate reservoir. The bottom hole temperature is 262 degrees Fahrenheit and the dew-point pressure for a reservoir fluid sample is about 5241 psi.

The purpose of modeling was to evaluate the potential of improving conventional production from Sabriyah SA-01 Well without any re-drilling to extend the well length except for placing three transverse hydraulic fractures in the well. The underlying problem is that reservoir gas is condensate and the well productivity is compromised because of liquid condensation both in the matrix and in the fracture pore space in the vicinity of the wellbore. Specifically, condensation begins from the wellbore into the well drainage volume as the bottom hole pressure drops below the dew point pressure of the reservoir hydrocarbon fluid. Liquid condensation causes two problems. The first problem is that the gas condenses below the dew-point pressure and the resulting gas-condensate becomes immobile. The second problem is that the permeability of the matrix pores and the fracture become essentially an order of magnitude smaller. The thesis specifically addresses these issues and examines a practical approach for alleviating this problem.

The research scope included: (1) Understanding the geologic characteristics of Sabriyah reservoir, (2) Building a dual-porosity model, (3) Analyzing well performance and pressure buildup behavior of horizontal well SA-01, (4) Conducting a history match of the well production, and (5) Evaluating the improved performance of the same well using three transverse hydraulic fractures in the well.

To achieve the thesis objectives, I utilized the well's production data, a pressure buildup test, core characterization, permeability, relative permeability, capillary pressure, porosity, and PVT data from the well. The reservoir model surrounding the well is a sector of Sabriyah reservoir. The dynamic behavior of the well was modeled using CMG's compositional reservoir simulator and the geological and petrophysical data for the model was obtained from Schlumberger's Petrel. After history matching, six potential production scenarios involving the three-stage hydraulic fracture stimulation were evaluated. It was concluded that a horizontal well, without any extensions, performs nearly as effective as having a three-stage hydraulic fracture embedded in

the well. The reason is that the natural fractures provide the improved flow path to the well. If the well could be elongated, we anticipate to obtain additional improvements; however, because of the large reservoir depth the cost is a major issue. Thus, the latter was not included in this thesis, but we recommend it as a future study.

TABLE OF CONTENTS

ABSTRACT.....	iii
TABLE OF CONTENTS.....	v
LIST OF FIGURES	viii
LIST OF TABLES.....	xii
LIST OF SYMBOLS AND ABBREVIATIONS	xiii
ACKNOWLEDGEMENTS.....	xvii
DEDICATION.....	xviii
CHAPTER 1 INTRODUCTION	1
1.1 Research Motivation and Objectives.....	1
1.2 Background	2
1.3 Thesis Organization.....	2
1.4 Research Location.....	3
1.5 Research Methodology.....	3
1.6 Available data.....	4
CHAPTER 2 LITERATURE REVIEW	5
2.1 Gas Condensate	5
2.2 Naturally Fractured Carbonate Reservoirs	7
2.2.1 Dual-Porosity Flow Modeling.....	8
2.2.2 Fracture Porosity	9
2.2.3 Fracture Permeability	10
2.2.4 Effective Fracture Permeability	10
2.2.5 Shape Factor.....	10

2.3	Hydraulic fracturing	11
2.4	Reservoir Simulation.....	12
2.4.1	WinProp	12
2.4.2	Builder.....	12
2.4.3	GEM.....	12
2.4.4	Results Modules	13
CHAPTER 3 GEOLOGY OF THE SABRIYAH JURASSIC RESERVOIR.....		14
CHAPTER 4 RESERVOIR ROCK AND FLUID PROPERTIES.....		17
4.1	Sabriyah Jurassic Rock Properties	17
4.2	Fluid Description.....	17
4.3	EOS Modeling and Tuning	23
CHAPTER 5 RESERVOIR CHARACTERIZATION BY WELL TEST		32
5.1	Pressure Transient Analysis	32
5.1.1	Pressure Transient Analysis Theory.....	32
5.2	Rate Transient Analysis (RTA).....	36
CHAPTER 6 NUMERICAL MODELING		42
6.1	Model Construction.....	42
6.1.1	Base Case Scenario	46
6.1.2	Grid Size Sensitivity.....	47
6.1.3	Relative Permeability and Capillary Pressure Data	50
6.1.4	Well Trajectory and Completion.....	53
6.1.5	Well Production.....	55
6.2	History Matching.....	57

6.3	Hydraulic Fracturing	60
6.3.1	Case 1: Constant Rate: 2.7MMscf/day, Water Saturation Variant.	61
6.3.2	Case 2: Constant Rate: 2.7 MMscf/day, Irreducible.	65
6.3.3	Case 3: Constant Rate: 4 MMscf/day, Water Saturation Variant.	68
6.3.4	Case 4: Constant Rate: 4 MMscf/day, Water Saturation Variant.	72
6.3.5	Case 5: Constant Rate: 2.7MMscf/day, switched to Constant Pressure.....	74
6.3.6	Case 6: Constant Rate: 2.7MMscf/day, switched to Constant Pressure.....	79
CHAPTER 7 CONCLUSIONS AND RECOMMENDATIONS		82
7.1	Conclusions	82
7.2	Recommendations	83
REFERENCES		84
APPENDIX CMG RUN EXAMPLE		888

LIST OF FIGURES

Figure 1.1	Map of Kuwait with field location circled (Rao 2010).....	3
Figure 2.1	Phase diagram of reservoir fluids (Terry and Rogers 2014).....	6
Figure 2.2	Dual porosity Model, taken from Warren and Root (1963).....	9
Figure 3.1	SA-01 horizontal well in Sabriyah (Narhari et al. 2012).....	15
Figure 3.2	Stratigraphic section of Kuwait (Carman 1996).....	16
Figure 4.1	SA-01 percentage of V^{liq}/V^{sat}	19
Figure 4.2	Relative Volume for SA-01.....	19
Figure 4.3	SA-01 Fluid density.....	20
Figure 4.4	Z factor Constant Composition Expansion output for SA-01.....	20
Figure 4.5	SA-01 Total gas recovery.....	21
Figure 4.6	SA-01 Z factor from CVD.....	21
Figure 4.7	SA-01 Gas Viscosity from CVD.....	22
Figure 4.8	Gas Formation Volume Factor from CVD for SA-01.....	22
Figure 4.9	SA-01 fluid composition in mole %.....	25
Figure 4.10	SA-01 lumped component composition in mole fraction.....	27
Figure 4.11	SA-01 CCE ROV experimental vs. final simulated data after tuning.....	28
Figure 4.12	SA-01 gas viscosity experimental vs. tuned simulated data.....	28
Figure 4.13	SA-01 Gas z factor experimental vs. tuned simulated data.....	29
Figure 4.14	SA-01 Gas density experimental vs. tuned simulated data.....	29
Figure 4.15	SA-01 Liquid and produced gas experimental vs. tuned simulated data.....	30
Figure 4.16	SA-01 Gas z factor experimental vs. tuned simulated data.....	30
Figure 4.17	SA-01 Two phase envelope.....	31

Figure 5.1	Diagnostic plot for SA-01 PTA.	34
Figure 5.2	Radial flow analysis for SA-01.....	35
Figure 5.3	Linear flow analysis for SA-01.....	36
Figure 5.4	Diagnostic plot for SA-01 RTA.....	38
Figure 5.5	Linear flow analysis for SA-01 using RTA.	39
Figure 5.6	Diagnostic plot for SA-01 RTA.....	40
Figure 5.7	Linear flow analysis for SA-01 using RTA.	40
Figure 6.1	Sector Model 2D I-J view.	42
Figure 6.2	Sector Model 2D I-K view.....	43
Figure 6.3	Sector Model 2D J-K view.	43
Figure 6.4	Sector Model 3D view.	44
Figure 6.5	SA-01 well diagram.	44
Figure 6.6	Zoomed diagram of perforated section.	45
Figure 6.7	Original Petrel sector model with large block dimensions in ft.	48
Figure 6.8	Refined version of sector model with block dimensions in ft.	49
Figure 6.9	Additional Local refinement for the sector model with dimensions in ft.	49
Figure 6.10	W-O Relative permeability curve for matrix rock SA-01.....	50
Figure 6.11	G-O Relative permeability curve for matrix rock of SA-01.	51
Figure 6.12	Matrix Capillary Pressure Data (Oil-Water) for SA-01.....	51
Figure 6.13	Matrix Capillary pressure curve for Oil-Gas of matrix rock of SA-01.....	52
Figure 6.14	Fracture Relative Permeability Data (Oil-Water).	52
Figure 6.15	Fracture Relative Permeability Data (Oil-Gas).....	53
Figure 6.16	SA-01 Well Schematic.....	54

Figure 6.17	Well path along Jurassic formations.	55
Figure 6.18	BHP and WHP data for SA-01.....	56
Figure 6.19	SA-01 Production history for oil, water, and gas.	57
Figure 6.20	SA-01 well bottom hole pressure simulated VS actual.....	59
Figure 6.21	SA-01 Gas rate simulated VS actual.	60
Figure 6.22	Case 1, comparative plot of BHP with and without HF.....	61
Figure 6.23	Case 1, comparative plot for gas rate with and without HF.....	62
Figure 6.24	Case 1, comparative plot for oil rate with and without HF.	62
Figure 6.25	Case 1, comparative plot for water rate with and without HF.	63
Figure 6.26	Case 1, comparative plot for cumulative gas with and without HF.	63
Figure 6.27	Case 1, comparative plot for cumulative water with and without HF.....	64
Figure 6.28	Case 1, comparative plot for cumulative oil with and without HF.	64
Figure 6.29	Case 1, comparative plot for GOR and WOR with and without HF.....	65
Figure 6.30	Case 2, comparative Plot for well BHP with and without HF.	65
Figure 6.31	Case 2, comparative plot for gas rate with and without HF.....	66
Figure 6.32	Case 2, comparative plot for oil rate with and without HF.	66
Figure 6.33	Case 2, comparative plot for cumulative gas with and without HF.	67
Figure 6.34	Case 2, comparative for cumulative oil with and without HF.	67
Figure 6.35	Case 3, comparative plot of well BHP with and without HF.....	68
Figure 6.36	Case 3, comparative plot of gas rate with and without HF.	68
Figure 6.37	Case 3, comparative plot for oil rate with and without HF.	69
Figure 6.38	Case 3, comparative plot for water rate with and without HF.	69
Figure 6.39	Case 3, comparative plot for cumulative gas with and without HF.	70

Figure 6.40	Case 3, comparative plot of cumulative oil with and without HF.....	70
Figure 6.41	Case 3, comparative plot of cumulative water with and without HF.....	71
Figure 6.42	Case 3, comparative plot of WOR and GOR with and without HF.....	71
Figure 6.43	Case 4, comparative plot for well BHP with and without HF.....	72
Figure 6.44	Case 4, comparative plot for gas rate with and without HF.....	72
Figure 6.45	Case 4, comparative plot for oil rate with and without HF.....	73
Figure 6.46	Case 4, comparative plot for cumulative gas fluid with and without HF.....	73
Figure 6.47	Case 4, comparative plot for cumulative oil fluid with and without HF.....	74
Figure 6.48	Case 5, comparative plot for well BHP with and without HF.....	75
Figure 6.49	Case 5, comparative plot for gas rate with and without HF.....	75
Figure 6.50	Case 5, comparative plot for oil rate with and without HF.....	76
Figure 6.51	Case 5, comparative plot for water rate with and without HF.....	76
Figure 6.52	Case 5, comparative plot for cumulative gas with and without HF.....	77
Figure 6.53	Case 5, comparative plot for cumulative oil with and without HF.....	77
Figure 6.54	Case 5, comparative plot for cumulative water with and without HF.....	78
Figure 6.55	Case 5, comparative plot for WOR and GOR with and without HF.....	78
Figure 6.56	Case 6, comparative plot for well BHP with and without HF.....	79
Figure 6.57	Case 6, comparative plot for gas rate with and without HF.....	80
Figure 6.58	Case 6, comparative plot for oil rate with and without HF.....	80
Figure 6.59	Case 6, comparative plot for cumulative gas with and without HF.....	81
Figure 6.60	Case 6, comparative plot for cumulative oil with and without HF.....	81

LIST OF TABLES

Table 2.1	Gas Condensate Reservoir Characteristics (Terry and Rogers 2014).....	5
Table 2.2	Classification of naturally fractured reservoirs (NFR) (Nelson 2001)	8
Table 4.1	Grid Properties	17
Table 4.2	Flash Data for bottom hole sample of SA-01	18
Table 4.3	Compositional Summary for the bottom hole sample of SA-01.....	18
Table 4.4	General reservoir conditions and fluid properties.....	18
Table 4.5	Crude Oil Assay for SA-01	23
Table 4.6	SA-01 Compositional Analysis.....	25
Table 4.7	Lumped Components Composition for SA-01	27
Table 6.1	Model cases description for SA-01	46
Table 6.2	Grid Properties	47
Table 6.3	SA-01 Well Data.....	53
Table 6.4	Input parameters for prehistory matching sensitivity analysis	58
Table 6.5	Modified parameters in history matching process	58
Table 6.6	Model cases description for SA-01.....	61

LIST OF SYMBOLS AND ABBREVIATIONS

B_g	Formation volume factor of gas, L^3/L^3 (RCF/SCF)
B_o	Formation volume factor of oil, L^3/L^3 (RB/STB)
B_w	Formation volume factor of water, L^3/L^3 (RB/STB)
c_g	Compressibility of gas, L^2/F^{-1} (1/psi)
\hat{c}_o	Compressibility of oil, L^2/F^{-1} (1/psi)
c_{oa}	Compressibility of apparent, L^2/F^{-1} (1/psi)
$C_{r,m}$	Compressibility of total reservoir matrix, L^2/F^{-1} (1/psi)
$C_{r,f}$	Compressibility of total reservoir fracture, L^2/F^{-1} (1/psi)
c_t	Compressibility of total reservoir, L^2/F^{-1} (1/psi)
c_w	Compressibility of water, L^2/F^{-1} (1/psi)
c_ϕ	Compressibility of rock, L^2/F^{-1} (1/psi)
c_w	Compressibility of water, L^2/F^{-1} (1/psi)
c_t	Compressibility of total reservoir, L^2/F^{-1} (1/psi)
D	Decline rate, T^{-1} (day) ⁻¹
D_0	Initial decline rate, T^{-1} (day) ⁻¹
$G_p(t)$	Cumulative gas production at time t, L^3 (SCF)
h	Formation thickness, L (ft)
i, j, k	direction in space
k	Formation permeability, L^2 (md)
$k_{f,eff}$	Effective fracture permeability, L^2 (md)
k_{hf}	Hydraulic fracture permeability, L^2 (md)
$k_{m,i}, k_{m,j}$	Matrix permeability L^2 (md)
$k_{r,\phi}$	Relative permeability of fluid phase ϕ , L^2 (md)
L	fracture spacing length L, (ft)
m_{bl}	Special slope for bilinear flow regime, $1/4$
m_l	Special slope for linear flow regime, $1/2$

m_{unit}	Special slope for boundary-dominated flow regime, 1
$N_p(t)$	Cumulative oil production at time t, L ³ (STB)
n_{hf}	Number of hydraulic fractures
p_i	Initial formation pressure, FL ⁻² (psi)
p_{wf}	Flowing bottom-hole pressure, FL ⁻² (psi)
q	Production rate, L ⁻³ T ⁻¹ (BBL/D, Mscf/d)
q_g^f	Free gas production rate, L ⁻³ T ⁻¹ (BBL/D, Mscf/d)
q_g^t	Total gas production rate at surface, L ⁻³ T ⁻¹ (BBL/D, Mscf/d)
q_{gc}	Gas-condensate production rate, L ⁻³ T ⁻¹ (BBL/D, Mscf/d)
$q_{gc.eq}$	Equivalent gas-condensate production rate, L ⁻³ T ⁻¹ (BBL/D, Mscf/d)
q_g	Gas production rate per unit rock volume, T ⁻¹ (1/D)
q_0	Initial production rate, L ⁻³ T ⁻¹ (BBL/D, Mscf/d)
q_o	Oil production rate, L ⁻³ T ⁻¹ (BBL/D, Mscf/d)
q_o	Oil production rate per unit rock volume, T ⁻¹ (1/D)
$q_{o,calc}$	Calculated oil production rate, L ⁻³ T ⁻¹ (BBL/D, Mscf/d)
q_{total}	Total production rate, L ⁻³ T ⁻¹ (RB/D)
q_w	Water production rate, L ⁻³ T ⁻¹ (BBL/D, Mscf/d)
q_w	Water production rate per unit rock volume, T ⁻¹ (1/D)
Q	Cumulative production, L ⁻³ (Mscf, RB)
Q_{total}	Total cumulative production, L ⁻³ (RB)
R_{so}	Solution gas-oil ratio, L ⁻³ / L ⁻³ (SCF/BBL)
R_{sw}	Solution gas-water ratio, L ⁻³ / L ⁻³ (SCF/BBL)
S_{hf}^{face}	Skin factor at the hydraulic fracture face
S_{hf}^{well}	Skin factor (choking effect) in hydraulic fracture
S_g	Saturation of gas, (fraction)

S_o Saturation of oil, (fraction)
S_{or} Saturation of residual oil, (fraction)
$S_{o,rem}$ Saturation of remaining oil, (fraction)
SRV Stimulated reservoir volume, L ³ (ft ³)
S_w Saturation of water, (fraction)
S_{wr} Saturation of residual water, (fraction)
t Time, T (Day)
t_i Initial production time, T (Day)
t_D Dimensionless time
t_{MB} Material balance time, T (Day)
T_φ Transmissivity of fluid phase φ , L ⁴ T/m (cp)
T_t Total transmissivity, L ⁴ T/m (cp)
w_{hf} Hydraulic fracture width, L (ft)
x_e Distance between hydraulic fractures, L (ft)
y_{hf} Hydraulic fracture half- length, L (ft)

Greek

∇ Divergence
λ Mobility, LT/m (1/cp)
λ_g Mobility of gas, LT/m (1/cp)
$\lambda_{gc,eq}$ Mobility of equivalent gas-condensate, LT/m (1/cp)
λ_o Mobility of oil, LT/m (1/cp)
λ_t Total mobility, LT/m (1/cp)
λ_w Mobility of water, LT/m (1/cp)
Δp_{wf} Well flowing bottom-hole pressure change, FL ⁻² (psi)
ϕ Porosity, (fraction)

φ	Fluid phase (gas, oil and water)
\varnothing_m	Matrix Porosity, (fraction)
\varnothing_f	Fracture Porosity, (fraction)

Abbreviations

BHP	Bottomhole Pressure (psi)
CCE	Constant Composition Expansion
CGR	Condensate-gas ratio at the separator conditions, L ³ /L ³ (STB/MMscf)
CVD	Constant Volume Depletion
DFN	Discrete Fracture Network
DP	Dual Porosity
FWL	Free Water Level
GLR	Gas-liquid ratio at the separator conditions, L ³ /L ³ (STB/MMscf)
GOR	Gas-oil-ratio at the separator conditions, L ³ /L ³ (STB/MMSCF)
HF	Hydraulic Fracture
KOC	Kuwait Oil Company
MCERS	Marathon Center of Excellence for Reservoir Studies
MFS	Maximum Flooding Surface
PBT	Pressure buildup Test
PTA	Pressure Transient Analysis
PVT	Pressure, Volume, Temperature study of fluid
ROV	Relative Oil Volume
RTA	Rate Transient Analysis
WHP	Well Head Pressure (psi)

ACKNOWLEDGEMENTS

Thank you God!

I'm finally at the stage of writing this acknowledgement, to which so many people (and things) have participated together to help me reach where I am today.

I extend my deepest thanks and appreciation to my advisor Professor Kazemi, not only did he act as a mentor, a drive source, an inspiration, but continuously made me believe in myself more than anyone else. Every letter in this document, and all the hard work behind it could not have materialized without him.

To KOC and Staff for sponsoring me, and supporting me in the information needed to realize this work, and helping out every step of the way, thank you.

Along the lines of colleagues, I thank Ilkay the most, she has been a constant support, and not once has she let me on my own unless she was 100% sure I was capable.

To my friends in MCERS, and Mines as a whole, we have had great conversations, and survived the road together. I also wish to thank the Community in Islamic Center of Golden. God knows how much I needed my social fix, spiritual support, international family atmosphere... couldn't have asked for a better environment.

I want to thank my husband Othman, he really pulled it off these two years, and endured a situation not too easy for a man, I Love you and I hope to always be happy with you.

To my two gems, Hajar the ever so hyper and kind, and Ebraheem the bundle of joy. I'm so thankful I have you too as my kids, and can't wait to see how beautifully amazing you will become in the future!

Now to things... I must thank the Play Station, Netflix, Golden Library and Swimming Pool. It made many days easy for the family to wake up again and do it all over until the finish line. Thank you!

Mesferah Al Qahtani

August 29th, 2017, Golden, Colorado.

DEDICATION

To my Wonder woman, my all-time inspiration, my mother.

To my father may he rest in the highest of heavens.

This is another chapter in my life
to show you how much I appreciate everything you have done to me, and my continuous
effort to make you proud.

CHAPTER 1

INTRODUCTION

This thesis presents a numerical modeling of a sector of Sabriyah gas condensate reservoir. Sabriyah is an abnormally high-pressure (11,000 psi) naturally fractured carbonate reservoir. The purpose is to determine an enhanced production method to increase the ultimate gas and gas-condensate recovery from the entire Sabriyah. The research was conducted at the Marathon Center of Excellence for Reservoir Studies.

The project scope was

- (1) Understanding the geologic characteristics of Sabriyah naturally fractured carbonate reservoir, which contains a gas-condensate fluid system.
- (2) Building a dual-porosity model via CMG simulation software.
- (3) Examining and analyzing well performance.
- (4) Conducting history match production of an existing horizontal well, and forecast its future performance.
- (5) Evaluate the performance of the same well using proposed hydraulic fracture stimulation.

To achieve these objectives, I utilized well production data, including pressure buildup tests, core characterization, such as permeability, relative permeability, capillary pressure, and porosity, and measured PVT data.

1.1 Research Motivation and Objectives

The objective of this research is to find ways to enhance long-term production from Sabriyah gas condensate reservoir in Kuwait. To do this, I needed to understand the reservoir geology, the porous media complexity, and the actual performance of a typical well. With this information in hand, the plan was to build a dual-porosity compositional model to simulate well performance and to evaluate the extent of the liquid condensation from the gas phase in the reservoir. Finally, the ultimate objective was to use the research findings to devise a procedure to achieve optimal enhanced condensate production from the field.

The reservoir is currently producing by natural depletion drive, and has an immense potential based on the estimated in place hydrocarbons. Furthermore, the reservoir has not undergone well stimulation nor has any enhanced recovery method been applied—hence, the motivation for this thesis.

1.2 Background

Naturally fractured carbonate reservoirs have come to play a significant role in Kuwait crude production, even more interestingly, they are the sole source for gas production in Kuwait. The field of interest in this study, Sabriyah field, comes from a successful exploration in North Kuwait, that has led to the discovery of six major tight gas fields, resulting in Kuwait's first free-gas fields. Put on production in 2008, the reservoirs provided a highly competitive range of hydrocarbon fields, ranging from black oil to gas condensate, typically producing up to 5000 BOPD/BCPD. And 10 MMscf/d (Rao et al. 2010).

Coming with that, an extensive list of complexities; the reservoir is tight with an average porosity of 2-6 PU, and has low matrix permeability (~ 0.1 md). Given that this is a gas reservoir, the depth is penetrating through Jurassic formation and producing from a source rock (Najma Sarjello; MFS Zone) that is 13500 ft. deep. Furthermore, operational hazards exist in the form of high salinity (300,000 ppm) and presence of H₂S (3.5-12%) and CO₂ (0-6%). The complexities that accompany such type of reservoir have been thoroughly examined in literature.

Sabriyah Field is producing primarily gas condensate of high quality (43° API). The fluid undergoes high pressure of up to 10,000 psi, and is under a temperature of 262 Degree Fahrenheit (KOC PVT Report, 2015). Current production is due to natural depletion, and the area has not been subject to any intervention, such as hydraulic fracturing, or any other stimulation or pressure maintenance job.

Given the tight nature of the carbonate field, most if not all the production is coming from the natural fracture networks within.

1.3 Thesis Organization

This thesis consists of seven chapters. After introducing the research topic, objectives, research location, available data and methodology in Chapter 1, Chapter 2 covers a literature review of the related topics, which includes gas condensate, naturally fractured carbonate reservoirs, hydraulic fracturing in gas condensates, and reservoir simulation.

Chapter 3 details the geology of the Jurassic reservoir to understand the heterogeneity of the carbonate hydrocarbon system, whereas Chapter 4 covers the rock and fluid properties, details of the fluid tests conducted and fluid modeling section.

Chapter 5 contains the PTA and RTA well tests analysis for SA-01. Chapter 6 details the numerical model starting from model construction, and going through base case scenario, history matching, and forecasting scenario. In addition, Chapter 7 demonstrates the conclusions of the study and recommendations going forward.

1.4 Research Location

Well SA-01 is located in south east of Sabriyah field (Figure 1.1). It is part of a six-field cluster in northern Kuwait, which encompasses an area of approximately 1800 sq. km.

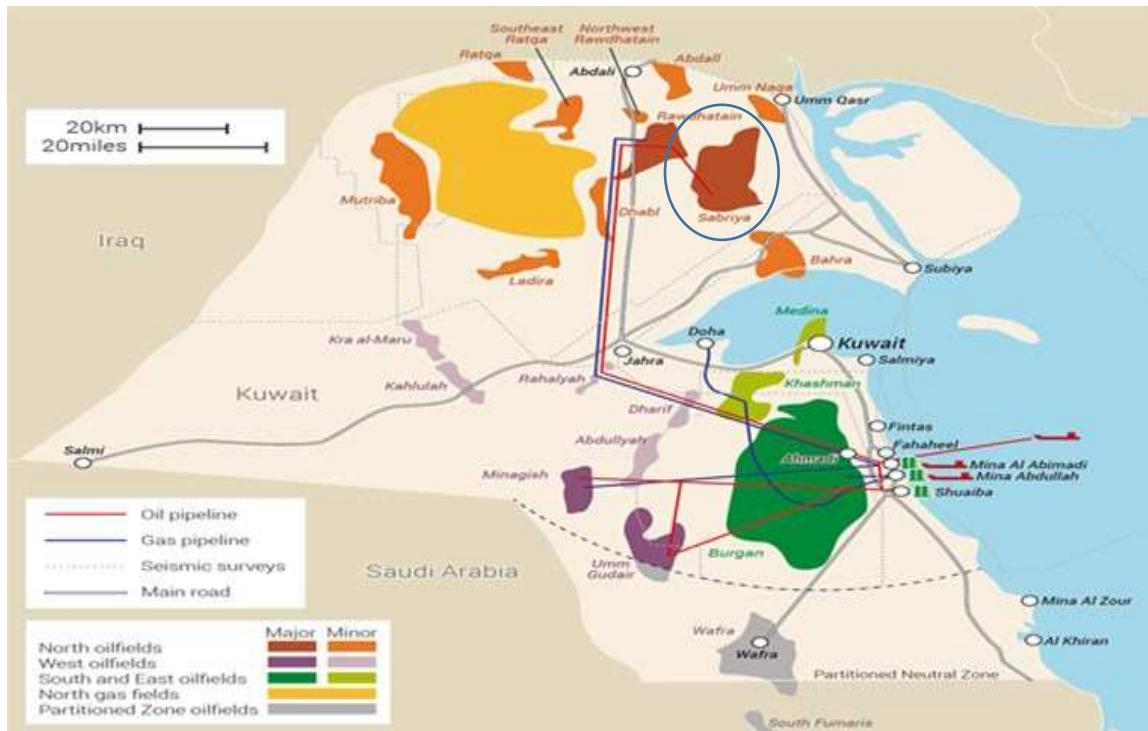


Figure 1.1 Map of Kuwait with field location circled (Rao 2010).

1.5 Research Methodology

1. Review the geological system of Sabriyah field.
2. Review Production data of Sabriyah field.

3. Construct compositional dual porosity model using GEM CMG modeling tool.
4. Validate model by existing related pressure and rate transient data.
5. Perform history matching
6. Examine forecasting scenario for pressure maintenance and production optimization and compare with actual production.

1.6 Available data

Kuwait Oil Company has provided an extensive amount of data to support the study, including full bottomhole sample PVT report, wettability experiment findings, pressure build up test, a built Petrel model with approximate matrix and fracture properties, well trajectory, and three years of production data.

Relative permeability and capillary pressure tables have been modified from a previously generated data in Marathon Center of Excellence for Reservoir Studies (Kazemi, 2017).

CHAPTER 2
LITERATURE REVIEW

This chapter pertains to several key concepts important to the research study—primarily, the theory of gas condensate fluids, naturally fractured carbonate reservoirs, hydraulic fracture stimulation, and reservoir simulation. Thus, in the following, I embark on reporting a thorough review of the relevant literature regarding the above issues.

2.1 Gas Condensate

Gas condensate reservoirs have recently stimulated an immense popular interest in hydrocarbon exploration and production. Gas from gas condensate reservoirs is now a significant percentage of the world’s gas supply. The condensate has a high value in the market place so the economic recovery of the maximum amount of condensate must be a prime consideration to the reservoir engineer.

There are five main types of hydrocarbon reservoirs based on a classification by Cronquist (1979), namely dry gas, wet gas, gas condensate, volatile oil and black oil. A phase envelope for a typical gas condensate is shown in Figure 2-1, which shows that the reservoir temperature lies between the critical point temperature and the cricondentherm. Gas condensates are single-phase gaseous hydrocarbon in the reservoir with considerable liquid hydrocarbon content dissolved in them at a particular reservoir condition. They are generally characterized by straight chain alkanes in the C₂ to C₆₊ range that can condense from gas when the temperature and pressure drop sufficiently low (Table 2.1).

Table 2.1 Gas Condensate Reservoir Characteristics (Terry and Rogers 2014)

Typical primary recovery mechanism	Volumetric gas drive
Initial reservoir conditions	Single phase: Gas
Reservoir behavior as pressure declines	Liquid condenses in the reservoir.
Produced hydrocarbons	Gas and Condensate

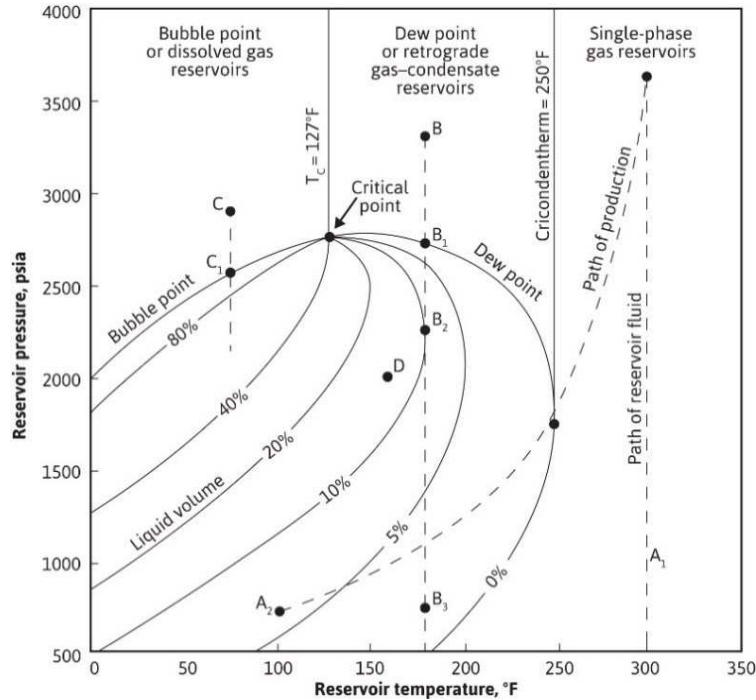


Figure 2.1 Phase diagram of reservoir fluids (Terry and Rogers 2014).

The gas-condensate reservoir is initially gas at the reservoir condition, and as the reservoir pressure decreases below the dew point, liquid condenses from gas and forms a “ring” or “bank” around the producing well in the near-well region. Normally this liquid will not flow until the accumulated condensate saturation exceeds the critical condensate saturation (S_{cc}) due to the relative permeability and capillary pressure effects in the porous medium. Once the reservoir pressure drops below the dew point, a pressure-drop occurs during production, which tends to form condensate banking (also known as the condensate blockage effect) around the well. This causes a loss in productivity. As the reservoir pressure further declines, PVT cell experiments show the liquid begins to re-vaporize in a PVT cell experiment (Shi 2009).

Liquid condensate develops as reservoir pressure declines below the dew point pressure — and the degree to which this occurs depends on many factors such as the composition of the gas, and the reservoir conditions. Liquid condensate will impede the flow of the gas phase, restricting production flowrate and adversely affecting recovery.

2.2 Naturally Fractured Carbonate Reservoirs

Heterogeneity is the norm case for the formation, that is why every reservoir contains fractures, as a result of different types of stress on the earth crust, some reservoirs are more heavily fractured than others. This is an important and beneficial characteristic of a reservoir, which is defined as a plane of discontinuity in rocks, and contributes to reservoir performance in its effect on fluid flow performance. Both carbonates and sandstones can have natural fractures, but more fractures exist in carbonates than in sandstones due to their brittle nature. Since we have established that all hydrocarbon reservoirs are naturally fractured reservoirs to a certain degree (NFR), it can be seen that the uncertainty lies whether or not these fractures form a fracture network that affects the fluid flow properties. Furthermore, the effect of fractures becomes important only when they occur with sufficient length of penetration, connectivity and spacing, as which case it becomes apparent that the difference arises from the two interacting paths (rock matrix and fractures) for fluid flow having totally different properties and communication with each other (Kazemi 2017).

Any change in stress, consequently causes a change in aperture, leading to a change in fracture. Hence, during the life time of a reservoir, when depletion or injection occurs, pressure changes can lead to stress changes that further modify the apertures, and therefore, the permeabilities of the fractures.

Naturally fractured reservoirs contain a significant portion of global hydrocarbon reserves. These reservoirs are characterized by a system of fractures existing within a background rock matrix. Nelson (2001) identified four types of naturally fractured reservoirs. In Type-I reservoirs, fractures provide the essential reservoir storage capacity (porosity) and permeability. In Type-II systems, fractures provide the essential permeability, but the matrix provides the essential porosity. In Type-III reservoirs, the matrix permeability is relatively high, with the fractures acting to further increase flow capacity. In Type-IV fractured reservoirs, the fractures are filled with minerals and provide no additional porosity or permeability. In this case the fractures create significant reservoir anisotropy and tend to form barriers to fluid flow and partition formations into relatively small blocks. In this thesis, we are dealing with Type-I.

Table 2.2 Classification of naturally fractured reservoirs (NFR) (Nelson 2001)

Classification of naturally fractured reservoirs (NFR), modified from Nelson (2001)		
Types of fracture reservoirs		
NFR type	Definition	Examples
Type 1	Fractures provide essential porosity and permeability.	Amal, Libya Edison, California Basement fields, Kansas
Type 2	Fractures provide essential permeability	Agha Jari, Iran Haft Kel, Iran Sooner trend, Oklahoma Spraberry trend area, Texas
Type 3	Fractures provide a permeability assistance	Kirkuk, Iraq Dukhan, Qatar Cottonwood Creek, Wyoming Lacq, France

One of the earliest papers discussing naturally fractured reservoir systems is Warren and Root (1963). Another early paper is Kazemi, et al. (1976). Gilman and Kazemi (1988) refines the formulation of Kazemi et al. (1976), adding additional resolution to the gravity and capillary pressure in the fracture/matrix transfer.

When working with naturally fractured reservoirs, there are a number of important concepts to identify. These are discussed in the following sections.

2.2.1 Dual-Porosity Flow Modeling

The most commonly used flow model for practical simulations of fractured systems is the dual-porosity model. Here the basic idea is to dissociate the flow inside the fracture network and the matrix and to model the exchange between these two media using a transfer function. This concept was first introduced by Barenblatt and Zheltov (1960). These authors already recognized the necessity for two over-lapping media to accurately describe the effect of fractures. Warren and Root (1963) introduced the concept of DP into the reservoir engineering community using their famous sugar cube model (Figure 2.2). In the sugar cube model there are three sets of fractures, but it is also possible to model only one or two sets. In practice, matrix blocks are mostly represented as rectangular cuboids. Sometimes all three sides have the same length (making the matrix block a cube, as in the sugar cube model).

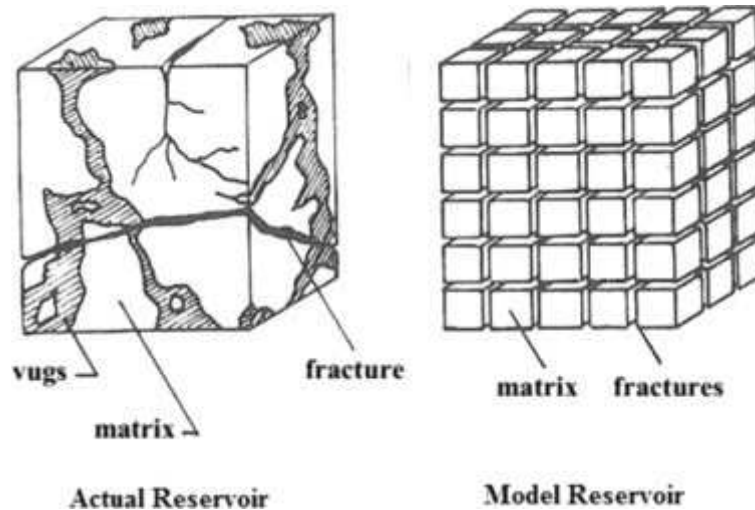


Figure 2.2 Dual porosity Model, taken from Warren and Root (1963).

Initially, the DP was mainly used for the interpretation of well tests (Warren and Root 1963; Kazemi 1969), but soon scientists started to use the concept for reservoir simulation. Kazemi et al. (1976) were the first that programmed a simulator that was able to handle three-dimensional, three-phase multiple-well scenarios.

2.2.2 Fracture Porosity

Fracture Porosity is a type of secondary porosity produced by the tectonic fracturing of rock. Fractures themselves typically do not have much volume, but by joining preexisting pores, they enhance permeability significantly.

It can also be defined as the ratio of the void space within fractures divided by the total rock volume. Fracture porosity is very difficult to determine, but we put a number to it using idealized models of fracture morphology. For instance, one can calculate fracture porosity from the volume of a discrete fracture network (DFN) model of the drainage volume of the reservoir. The DFN porosities are typically too large and should be considered the upper limit of porosity. Fracture porosity can be estimated from field-measured permeability using the pressure-time behavior of the producing wells (Kazemi 2017).

Fracture porosity is typically a small number such as 0.0001 to 0.001 for many reservoirs, or 0.004 for Yates field which probably includes contributions from some fracture-intersecting

vugs and caverns. In Cantarell field fracture porosity is probably is about 0.02 which definitely includes contributions from fracture-intersecting vugs (Kazemi 2017).

2.2.3 Fracture Permeability

Fracture Permeability is the measure of connectivity between pore spaces and the ease with which fluids flow through the connecting pore spaces of a rock with naturally occurring fractures in the formation. In these pore spaces, the hydrocarbon fluids can be trapped naturally. Fracture Permeability is an important measure to understand a reservoir's production capability or recovery of hydrocarbon from a reservoir. The unit of measurement of Permeability is Darcy or milli Darcy.

Fracture Permeability depends on various factors of the rock formations such as:

- The grain size, shape and its distribution.
- The type of formation.
- Porosity of the formation.
- Pressure and type of fluid in formation.

2.2.4 Effective Fracture Permeability

To include the effect of fracture porosity and tortuosity on fracture flow, we multiply fracture permeability by fracture porosity;

$$k_{f,\text{eff}} = k_f \phi_f / \tau_f \quad (2.1)$$

but we assume that fracture tortuosity is one. The result is called effective fracture permeability as shown below;

$$k_{f,\text{eff}} = k_f \phi_f \quad (2.2)$$

Thus, the fracture effective permeability can be considered the *reservoir excess permeability* due to the presence of interconnected fractures (Kazemi 2017).

2.2.5 Shape Factor

In order to better understand the optimal recovery mechanisms, numerical simulation models require an adequate transfer function (shape factor) for the fracture networks and matrix blocks. The shape factor considers the fracture-matrix geometry and is defined as a cross-sectional area for the fluid transfer per unit volume divided by fracture spacing. It can also be described as a geometrical factor that partially governs the flow behavior between the fractures and the matrix blocks.

Shape factor reflects the geometry of the matrix and represents flow between the two continua in the NFR. Warren and Root define shape factor as follows:

$$\sigma_{WR} = \frac{20}{30} \left(\frac{1}{L_x^2} + \frac{1}{L_y^2} + \frac{1}{L_z^2} \right) \quad (2.3)$$

Kazemi et al. (1976) extended Warrant and Root's formulation for two phases and three dimensional NFR systems. In their study, they define their shape factor as the following expression:

$$\sigma_K = 4 \left(\frac{1}{L_x^2} + \frac{1}{L_y^2} + \frac{1}{L_z^2} \right) \quad (2.4)$$

They derived it from a finite-difference formulation where L is defined as the width of the matrix block in the three directions. And the latter is the shape factor equation used in our model.

2.3 Hydraulic fracturing

Hydraulic fracturing is defined as the technique that makes use of a fluid to fracture reservoir rock. It is pumped at a rate enough to achieve a pressure that exceeds the strength of the rock. This increases the conductivity of flow path of fluid to the wellbore. Hydraulic fracturing is considered a stimulation technique, and along with horizontal wells, helps recover more of the untapped hydrocarbons in tight formations.

The key advantages of this technique are:

- Increase reservoir contact.
- Boost production rate: larger reservoir contact area is the reason why stimulated reservoir has a much better production profile; single well economic performance is largely depending on the production rate.
- Provide better access to reserves: a single hydraulically stimulated well could have larger drainage volume; therefore, the number of wells needed to drain a unit area is reduced resulting in lower overall drilling and completion cost.

For the purpose of this study, three stage hydraulic fracturing is implemented, the combination of hydraulic fractures and natural fractures provides the required conduits to access a much bigger matrix contact area.

2.4 Reservoir Simulation

Reservoir simulation is a process of establishing and operating a model that reflects the behavior of an actual reservoir. Reservoir simulators use numerical methods and computers to model multidimensional fluid flow in reservoir rock (Mattax and Dalton 1990). The main purpose of reservoir simulation according to (Odeh 1969) is to predict the recovery rate of hydrocarbon fluids for various field operations. Also, the accuracy of reservoirs' performance depends on adequate field data availability. Coats (1987) sees the purpose of the simulation as the estimation of field performance under various production scenarios and selecting the optimal plan for the field's future development. Hence, numerical reservoir simulation helps us understand actual performance and forecast future performance of fluid flow in reservoirs while giving opportunity to understand the sensitivity of different parameters.

CMG (Computer Modelling Group Ltd.) commercial simulation software is used for this study. The programs used include WinProp, Builder, GEM, Results 3D and Results Graph:

2.4.1 WinProp

WinProp is CMG's phase behavior module, which allows to construct the fluid model, allow for component lumping, PVT matching, and modeling of laboratory experiments.

2.4.2 Builder

The Builder module is the framework on which the model is built, and the WinProp generated model is integrated, it includes a set of applications that allows for building model from scratch, as well as incorporating other forms of data, such as geological built models from Petrel software, actual production data, actual relative permeabilities, well trajectory, etc.

2.4.3 GEM

GEM is CMG's general equation-of-state (EOS) based compositional reservoir simulator for modeling the flow of three-phase, multi-component fluids. GEM is described as a robust, fully compositional simulator used to model any type of reservoir where the importance of the fluid composition and their interactions are essential to the understanding of the recovery process. For our case, GEM is the adequate module for gas condensate reservoirs.

2.4.4 Results Modules

Results and Results 3D are the modules responsible for generating the results, and can efficiently analyze the output from CMG simulators, in various informative graphs and tables.

CHAPTER 3

GEOLOGY OF THE SABRIYAH JURASSIC RESERVOIR

North Kuwait is a challenging exploration and development environment that consists of highly complex compartments and heterogeneous reservoirs where natural fractures contribute significantly to the well productivity. The North Kuwait Jurassic Complex (NKJC) consists of six fields with four potential reservoirs in the Jurassic age naturally fractured carbonate formation (Najmah/Sargelu, Upper Marrat, Middle Marrat, Lower Marrat).

Complexities in the North Kuwait Jurassic fields include– deep wells with depth in the range of 14000’-16500’ associated with high pressure (10000+ psi) and high temperatures (~280° F) presence of H₂S: 3.5% - 12% and CO₂: 0-6%; highly heterogeneous reservoirs with low porosity (range 0-22%, Avg. ~2%) and low permeability (Avg. ~ 0.1 md); different rock types; different fluid types: Free gas / condensate/ volatile oil/ near critical fluid; and poor seismic resolution. Geological and petrophysical data and production tests have shown that fractures play the primary role in attaining sustainable production from Najmah-Sargelu formations (Al-Eidan et al. 2010).

To achieve and sustain the production target of 1Bcf/d from the NK Jurassic fields requires significant contribution from Najmah-Sargelu, Lower and Upper Marrat reservoirs in addition to the bulk of the production from Middle Marrat.

The study focuses on a well penetrating Najmah-Sarelu formation (Figure 3.1), which is a purely fracture driven tight carbonate reservoir with average porosity less than 2 pu, average permeability less than 0.1 md and only sub-vertical fractures contributing to the production.

The primary driver for successful field development of such tight fractured carbonate reservoirs is optimal wellbore design maximizing reservoir contact which intersects open fractures. This necessitates appropriately designed horizontal drain holes, as horizontal drilling effectively increases wellbore-formation contact surface area. The well under study, SA-01, is a horizontal well, drilled along the crestal part of Sabriyah field in the North Kuwait Jurassic complex, targeted on the challenging (over 13000 ft depth, HPHT), on the deep Najmah MFS tight fractured carbonate reservoir which is sandwiched between Najmah Kerogen and Sargelu, and the well encountered all scales of fractures.

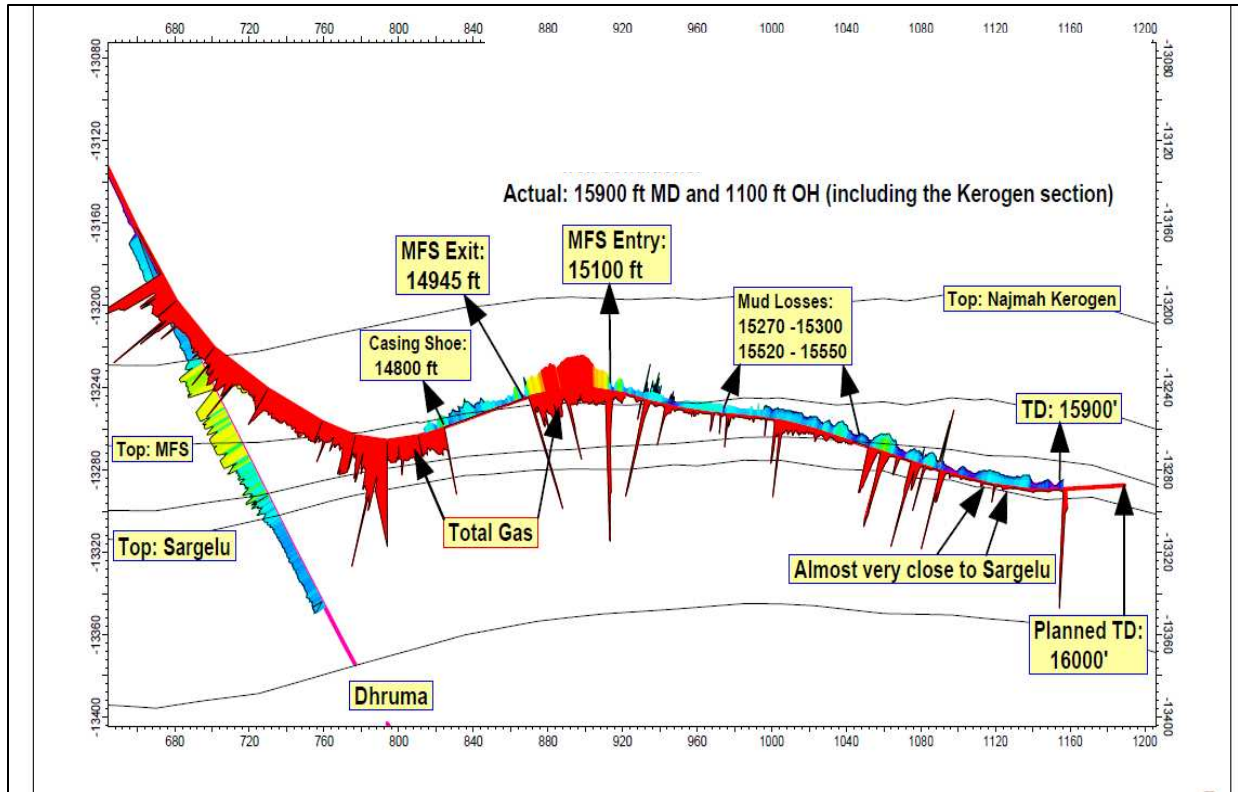


Figure 3.1 SA-01 horizontal well in Sabriyah (Narhari et al. 2012).

The reservoir section of interest is within the Najmah formation; which is a world-class source rock that has high TOC content with an average thickness of 85 ft (50 ft of Najmah Kerogen and 35 ft of Lower Najmah Kerogen that is also called MFS). Najmah MFS (Maximum Flooding Surface) is a relatively thin (with foot scale alternating organic rich layers and tight limestone (2pu rock with 0.01 md). Figure 3.2 details the stratigraphic column including the formation of interest.

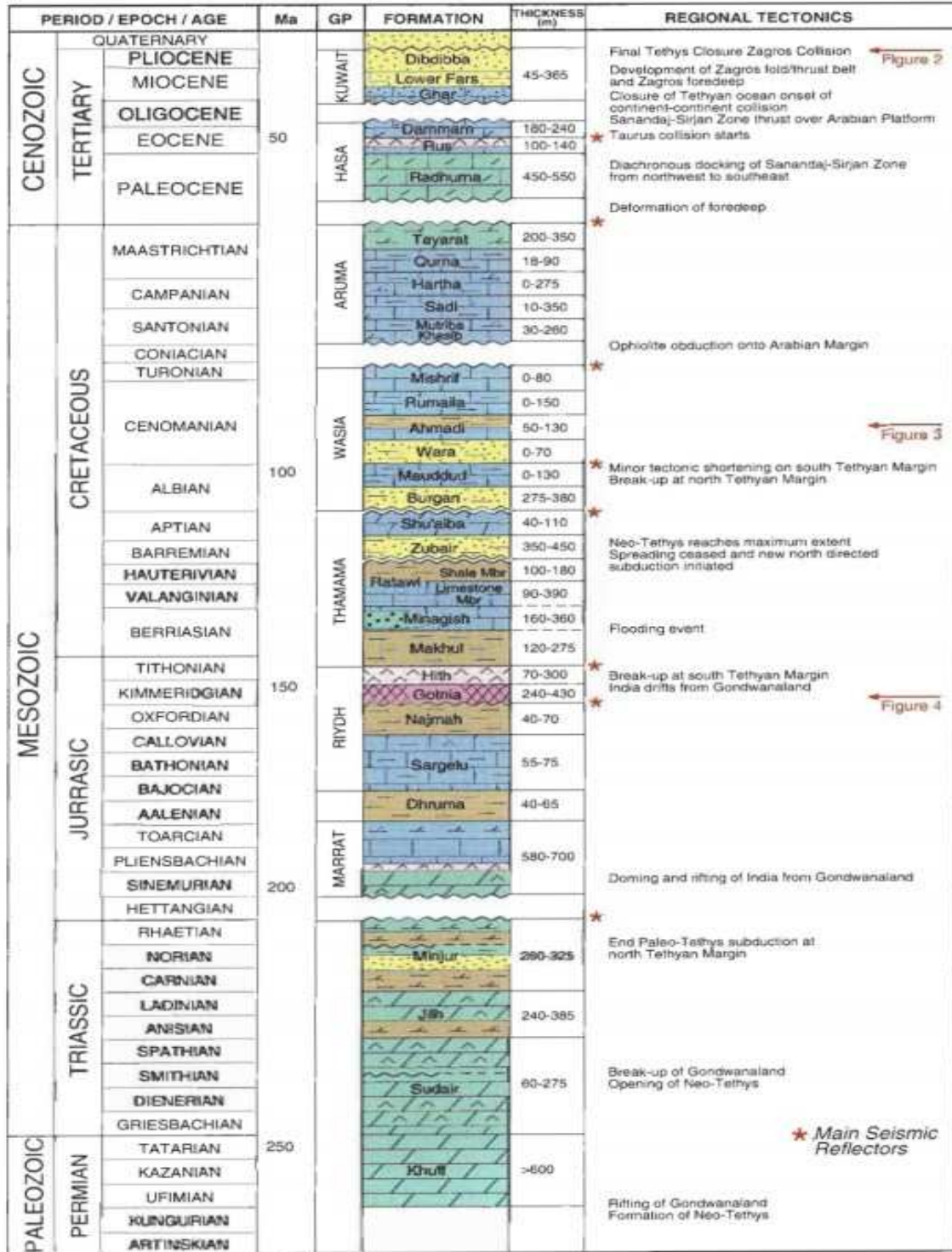


Figure 3.2 Stratigraphic section of Kuwait (Carman 1996).

CHAPTER 4
RESERVOIR ROCK AND FLUID PROPERTIES

4.1 Sabriyah Jurassic Rock Properties

The Sabriyah Jurassic reservoir has a variable range for rock properties as described in Table 4-1. The matrix permeability is small ranging between 0.001 md to 0.2 md, the fracture permeability however has even more variant range (0-300 md) populated throughout the reservoir and demonstrated accordingly in the static model. It is understood from rock description that the hydrocarbons are primarily being fed by the fractures.

Table 4.1 Grid Properties

Property	Petrel Model Values
$k_{m,i}, k_{m,j}$ (md)	variant, range: 0.001-0.2
$k_{m,k}$ (md)	variant, range: 0.001-0.2
$k_{f,i}$ (md)	variant, range: 0-150
$k_{f,j}$ (md)	variant, range: 100-300
$k_{f,k}$ (md)	variant, range: 0-350
$k_{f,eff,(i,j,k)}$ (md)	Calculated internally
ϕ_m	variant, range: 0.0102-0.0712
ϕ_f	variant, range: 0 -0.17
S_w	variant, range: 0.129-1
$c_{r,m} c_{r,f}$ (1/psi)	7.30E-06
$L_i L_j$ (ft)	variant, range: 0-75
L_k (ft)	variant, range: 0-75

4.2 Fluid Description

The PVT bottom hole sample has been taken at a reservoir of 11000 psia, and 262 °F, at a depth of 13689 ft. The molar mass of reservoir fluid is 38 g/mol, with a single stage flash GOR of 4933 SCF/STB. The API gravity is measured as 47.7° and the Saturation Pressure (dew point

pressure) is 5341 psia. Below are summary tables (Table 4.2 and Table 4.3) for flash data and the compositional summary.

Table 4.2 Flash Data for bottom hole sample of SA-01

CGR (STB/MMSCF)	GLR (SCF/BBL)	Density (gm/cm ³)	Gas Specific Gravity
202.69	4934	0.789	0.774

Table 4.3 Compositional Summary for the bottom hole sample of SA-01

C1 (mole %)	C7+ (mole%)	C1/C7+(ratio)	H ₂ S (mole%)	CO ₂ (mole%)	N ₂ (mole%)
65.57	10.24	6.4	2.52	1.43	0.09

For the purpose of this study, the initial conditions of the reservoir and fluid properties are provided based on field measurements in Table 4.4.

Table 4.4 General reservoir conditions and fluid properties

Reservoir Temperature	262	°F
Saturation Pressure	5241	Psia
GOR	4934	SCF/STB
API Gravity	47.7	°API
Depth	13,500	Ft
Initial Formation Pressure	9,690	Psia

The PVT tests on SA-01 included constant composition expansion (CCE), constant volume depletion (CVD) tests. Outputs for CCE experiments are shown in Figures 4.1 to 4.5.

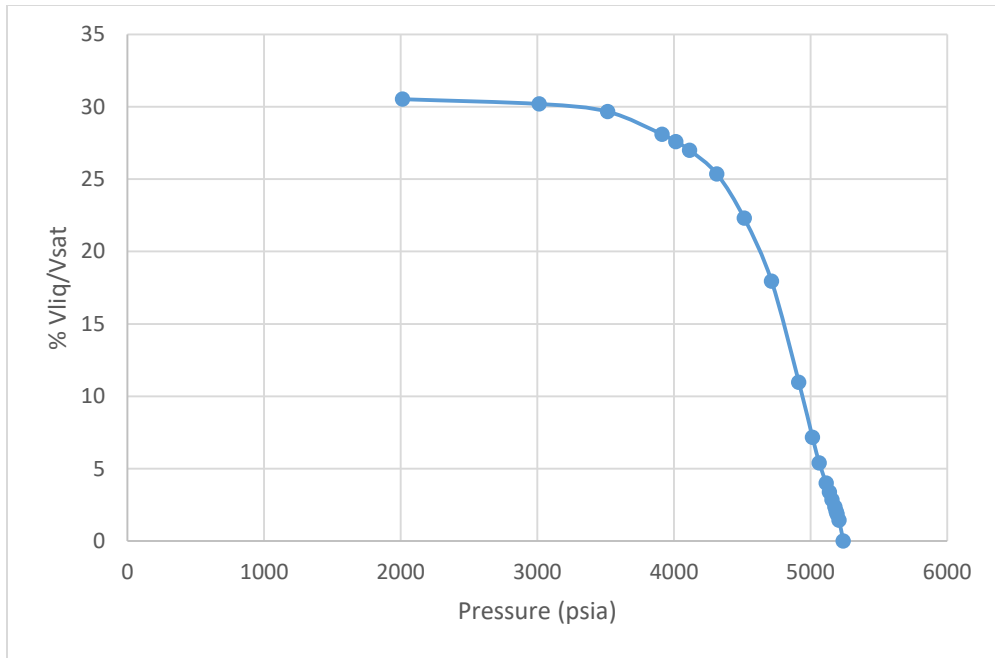


Figure 4.1 SA-01 percentage of V^{liq}/V^{sat} .

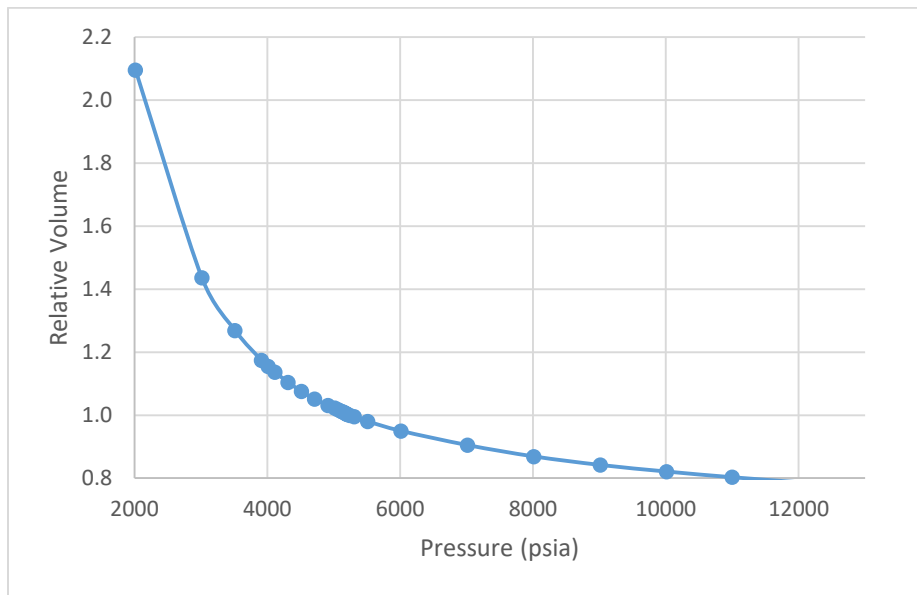


Figure 4.2 Relative Volume for SA-01.

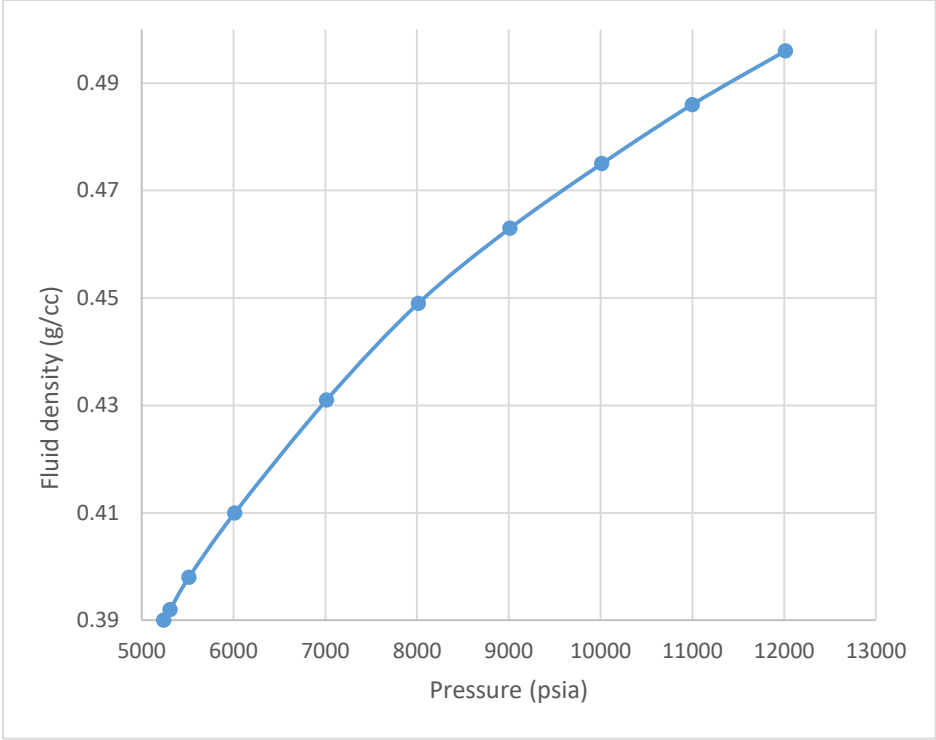


Figure 4.3 SA-01 Fluid density.

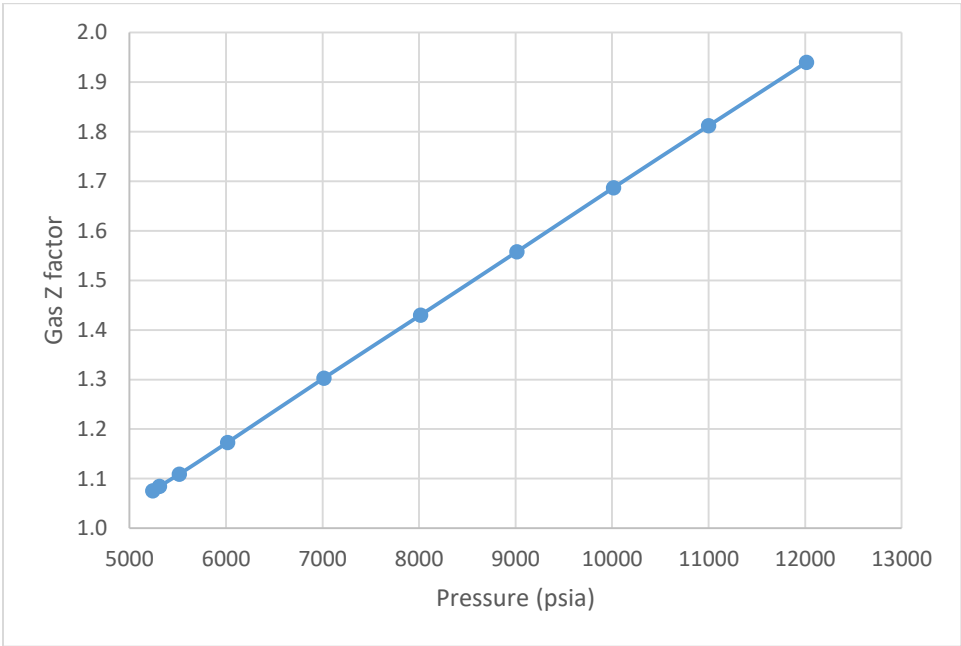


Figure 4.4 Z factor Constant Composition Expansion output for SA-01.

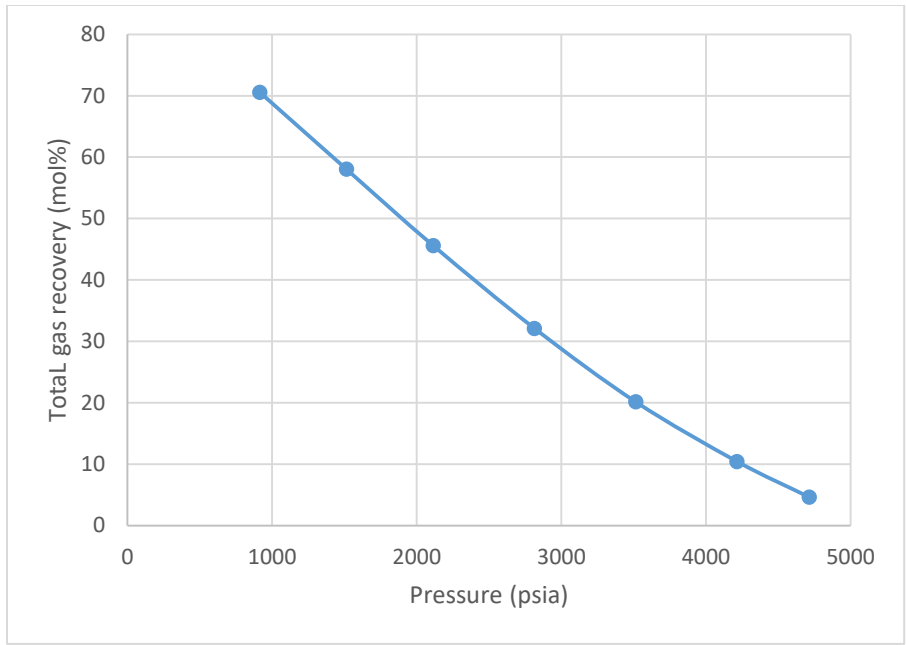


Figure 4.5 SA-01 Total gas recovery.

Outputs for CVD experiments are shown in Figures 4-6 to 4-8.

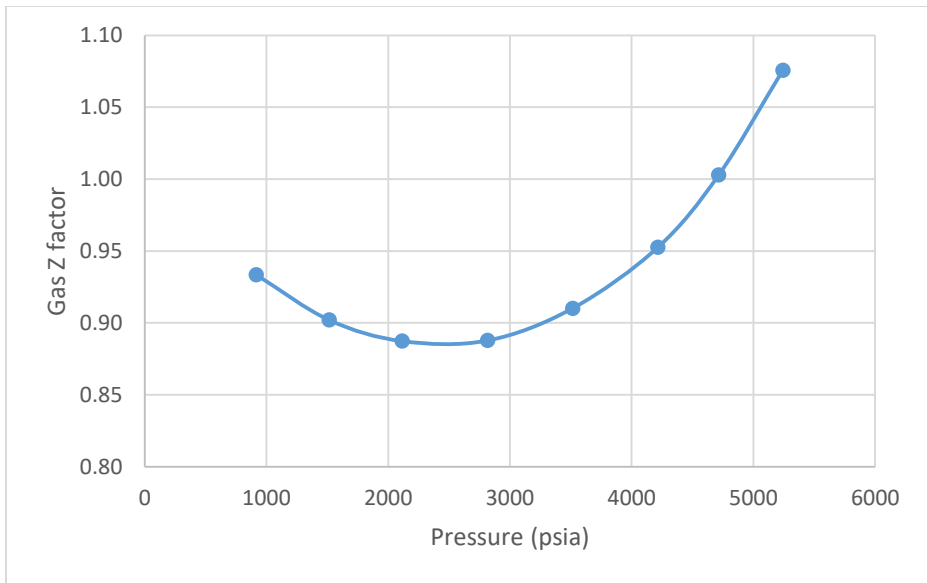


Figure 4.6 SA-01 Z factor from CVD.

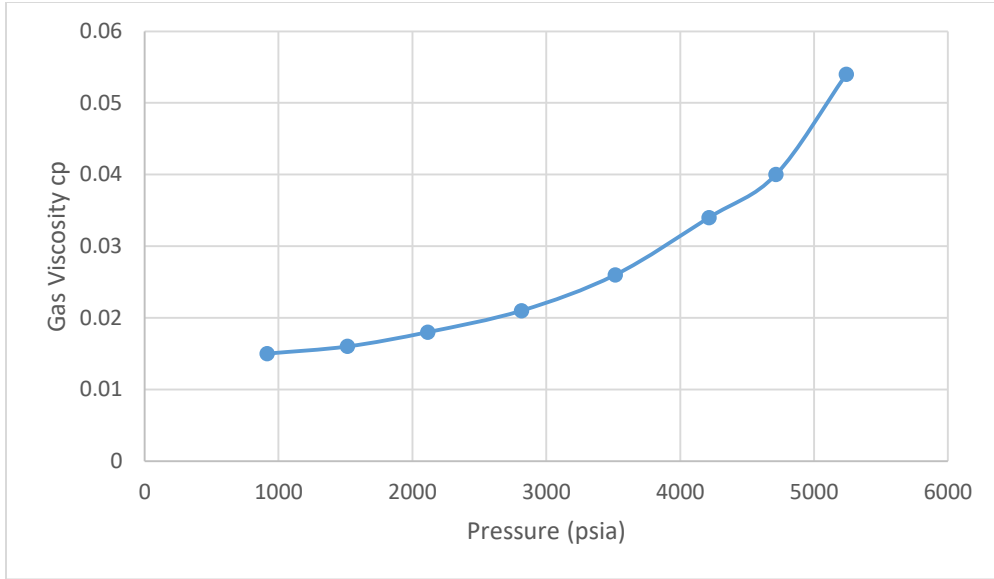


Figure 4.7 SA-01 Gas Viscosity from CVD.

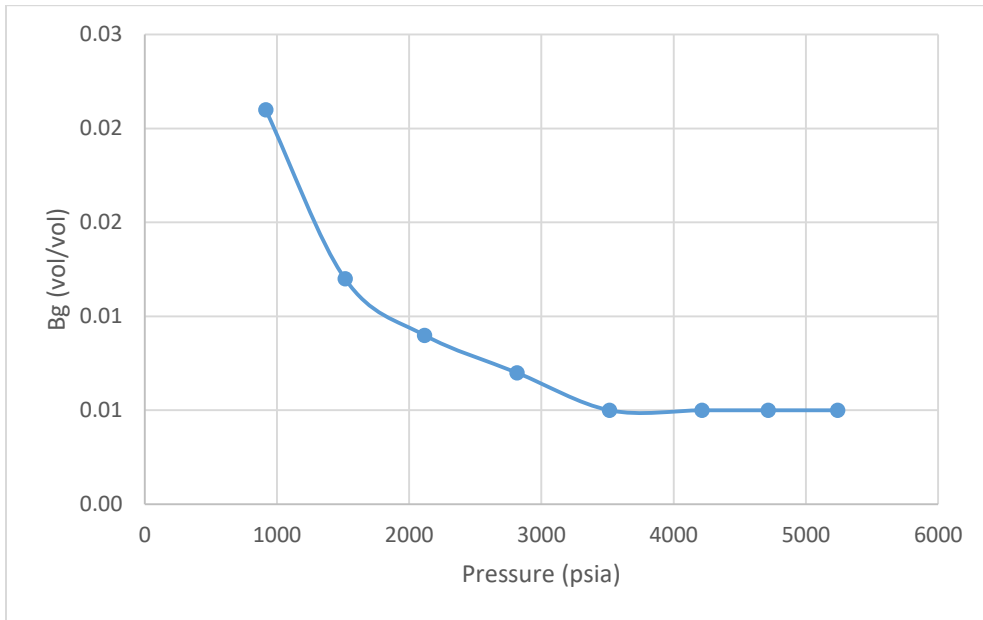


Figure 4.8 Gas Formation Volume Factor from CVD for SA-01.

In addition to the pressurized PVT sample, a stock tank oil has also been collected from the well, and the characteristics of the crude are described in Table 4.5.

Table 4.5 Crude Oil Assay for SA-01

Test	Method	Unit	Result
Specified Gravity @ 60/60 deg F			0.797
Total Acidity	ASTM D664	mgKOH/g	0.35
Ash Content	ASTM D482	% wt	0.002
Asphaltene		% wt	<0.5
Sulphur Content	ASTM D4294	% wt	0.412
Carbon Residue	ASTM D189	% wt	0.06
Water Content	ASTM D6304	Ppm	0.17
Sediment by extraction	ASTM D473	% wt	<0.01
Salt Content	ASTM D3230	Ptb	5.9
Pour point	ASTM D97	° C	-36
Flash point	ASTM D93	° C	below 0
Reid vapour pressure	ASTM D323	Psi	6.4
Wax content	UOP 46	% wt	<5
Kinematic viscosity @ 70 deg F	IP 71	cSt	2.574
Kinematic viscosity @ 100 deg F	IP 71	cSt	2.016
Kinematic viscosity @ 120 deg F	IP 71	cSt	1.706
Kinematic viscosity @ 150 deg F	IP 71	cSt	1.366
Kinematic viscosity @ 287 deg F	IP 71	cSt	0.825
Distillation	ASTM D86		not possible due to H ₂ S

4.3 EOS Modeling and Tuning

When it comes to reservoir simulation, one must mathematically express reservoir fluid properties. A common practice is to use Equation-Of-State (EOS) to describe reservoir fluid properties and reservoir phase behaviors. In this study, Peng-Robinson EOS was used to model

fluid properties and phase behaviors. The mathematical expression of Peng-Robinson cubic EOS (Peng and Robinson 1976) is expressed as:

$$p = \frac{RT}{v-b} + \frac{a}{v(v+b)+b(v-b)} \quad (4-1)$$

Where:

p = pressure, psia

R = gas constant, $\frac{\text{ft}^3 \cdot \text{psia}}{\text{R} \cdot \text{lb-mole}}$

T = temperature, °R

v = specific volume, $\frac{\text{ft}^3}{\text{mole}}$

a = attraction parameter

b = repulsion parameter

A proper tuning of EOS model is required to ensure a match between EOS model and PVT experimental data used for the reservoir fluid. It can be achieved by adjusting EOS model parameters such as molecular weights of the plus fractions, volume shift parameters, binary interaction coefficients, among others. It is important to note this is an iterative process with no clear cut path (Liu 2008).

To perform this, a process in WinProp module called regression is used. However, since this is a simulation method, and will require increased computing time as there are thousands of individual hydrocarbon components in reservoir fluids. The first step ahead of EOS tuning is component lumping, where reservoir fluid components are grouped into a few pseudo-components.

Figure 4.9 displays the full range of fluid compositions. To avoid time consuming in compositional simulation, and for the purpose of this study, six pseudo-component lumping scheme was applied, and the fraction of lumped pseudo-components are displayed in Figure 4-10.

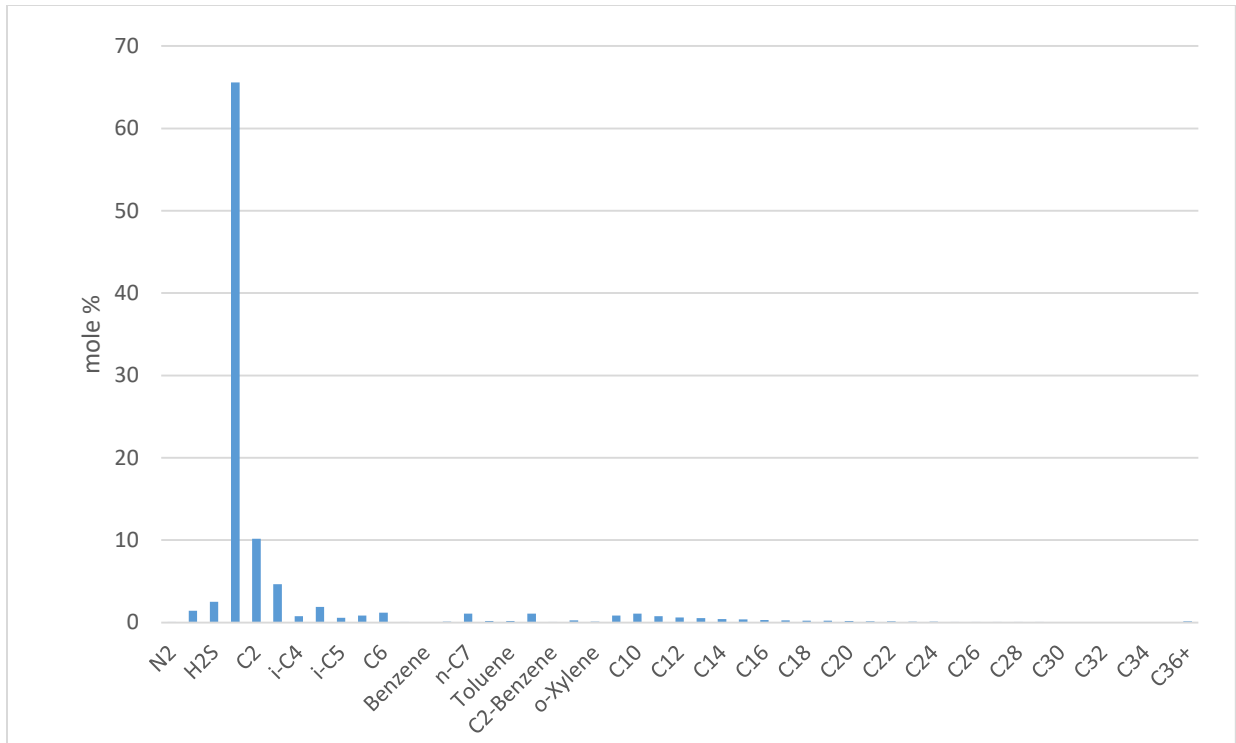


Figure 4.9 SA-01 fluid composition in mole %.

Tables 4.6 and 4.7 show fluid composition details.

Table 4.6 SA-01 Compositional Analysis

Component	MW	Flashed Gas		Flashed Liquid		Reservoir Fluid	
	g/mol	wt%	mole%	wt%	mole%	wt%	mole%
N2	28.01	0.131	0.106	0	0	0.068	0.094
CO2	44.01	3.191	1.635	0	0	1.642	1.448
H2S	34.08	4.114	2.723	0	0	2.116	2.410
C1	16.04	52.53	73.862	0	0	27.023	65.375
C2	30.07	15.286	11.467	0	0	7.864	10.150
C3	44.10	10.200	5.218	0.072	0.268	5.282	4.649
i-C4	58.12	2.228	0.865	0.047	0.134	1.169	0.781
n-C4	58.12	5.533	2.147	0.192	0.541	2.940	1.963
i-C5	72.15	1.868	0.584	0.330	0.750	1.121	0.603
n-C5	72.15	2.414	0.755	0.813	1.849	1.637	0.880
C6	84.00	1.620	0.435	3.710	7.246	2.635	1.217

Table 4.6 Continued

C7	Mcyclo-C5	84.16	0.072	0.019	0.285	0.556	0.176	0.081
	Benzene	78.11	0.023	0.007	0.074	0.156	0.048	0.024
	Cyclo-C6	84.16	0.087	0.023	0.383	0.746	0.230	0.106
	n-C7	98.39	0.402	0.092	5.351	8.922	2.805	1.106
C8	Mcyclo-C6	98.19	0.062	0.014	1.025	1.712	0.529	0.209
	Toluene	92.14	0.042	0.010	0.798	1.421	0.409	0.172
	n-C8	112.22	0.121	0.024	6.611	9.666	3.272	1.132
C9	C2-Benzene	106.17	0.007	0.002	0.329	0.509	0.164	0.060
	m&p-Xylene	106.17	0.015	0.003	1.621	2.505	0.795	0.291
	o-Xylene	106.17	0.004	0.001	0.546	0.844	0.267	0.098
	n-C9	128.26	0.036	0.006	6.065	7.758	2.963	0.897
C10	134.00	0.014	0.002	7.920	9.699	3.853	1.116	
C11	147.00	0	0	6.317	7.050	3.067	0.810	
C12	161.00	0	0	5.545	5.650	2.692	0.649	
C13	175.00	0	0	4.971	4.660	2.414	0.535	
C14	190.00	0	0	4.363	3.767	2.118	0.433	
C15	206.00	0	0	4.204	3.348	2.041	0.385	
C16	222.00	0	0	3.687	2.725	1.790	0.313	
C17	237.00	0	0	3.245	2.246	1.576	0.258	
C18	251.00	0	0	2.910	1.902	1.413	0.218	
C19	263.00	0	0	2.87	1.791	1.394	0.206	
C20	275.00	0	0	2.64	1.576	1.282	0.181	
C21	291.00	0	0	2.319	1.307	1.126	0.150	
C22	305.00	0	0	2.133	1.147	1.036	0.132	
C23	318.00	0	0	1.867	0.963	0.907	0.111	
C24	331.00	0	0	1.366	0.810	0.793	0.093	
C25	345.00	0	0	1.479	0.703	0.718	0.081	
C26	359.00	0	0	1.376	0.629	0.668	0.072	
C27	374.00	0	0	1.302	0.571	0.632	0.066	
C28	388.00	0	0	1.211	0.512	0.588	0.059	
C29	402.00	0	0	1.062	0.433	0.516	0.050	
C30	416.00	0	0	0.982	0.387	0.477	0.044	
C31	430.00	0	0	0.905	0.345	0.440	0.040	
C32	444.00	0	0	0.801	0.296	0.389	0.034	
C33	458.00	0	0	0.719	0.258	0.349	0.030	
C34	472.00	0	0	0.678	0.236	0.329	0.027	
C35	486.00	0	0	0.623	0.210	0.302	0.024	
C36+	546.75	0	0	3.985	1.196	1.935	0.137	

Table 4.6 continued

Calculated MW		22.5600		164.06		38.810	
Mole Ratio		0.8851		0.1149			

Table 4.7 Lumped Components Composition for SA-01

Component	Composition (Mole fraction)
N2 to CH4	0.68181
CO2 to IC4	0.17038
NC4 to C6	0.04540
C7 to C12	0.06517
C13 to C19	0.02347
C20 to C36	0.01377
Sum	1

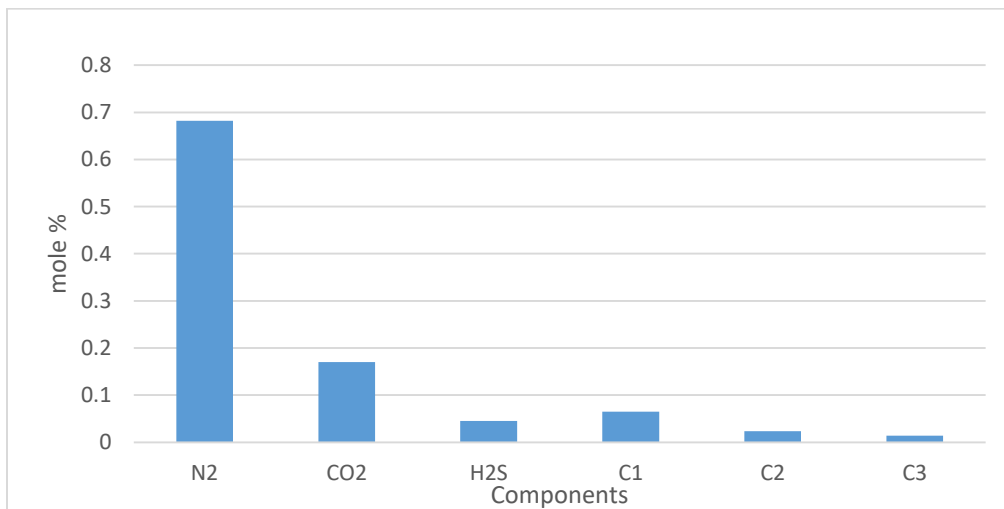


Figure 4.10 SA-01 lumped component composition in mole fraction.

The tuning / regression process is a trial and error process and the matching is achieved by continuous adjusting of tuning parameters, and performing regression using CMG WinProp.

Figures 4-11 to 4-17 show simulation match with experimental PVT data of different hydrocarbon properties from CCE and CVD tests.

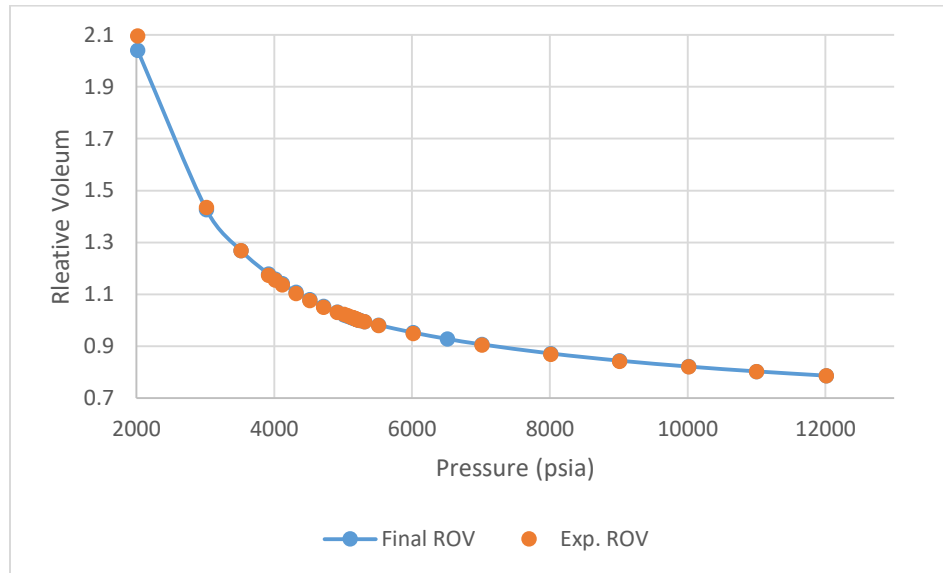


Figure 4.11 SA-01 CCE ROV experimental vs. final simulated data after tuning.

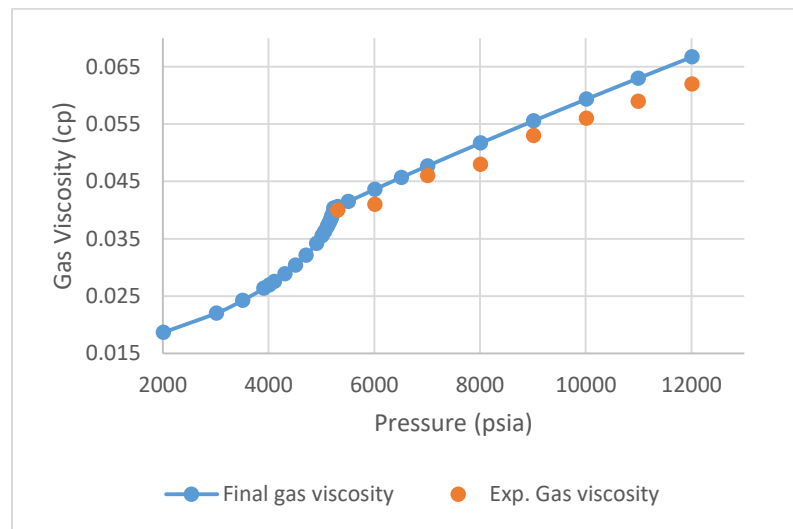


Figure 4.12 SA-01 gas viscosity experimental vs. tuned simulated data.

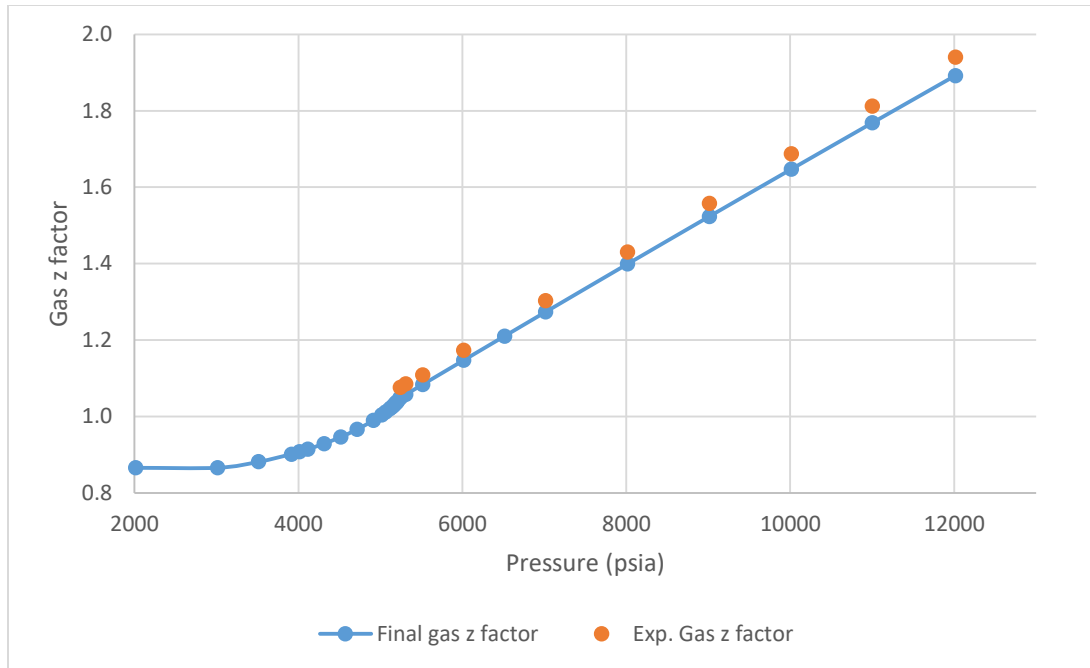


Figure 4.13 SA-01 Gas z factor experimental vs. tuned simulated data.

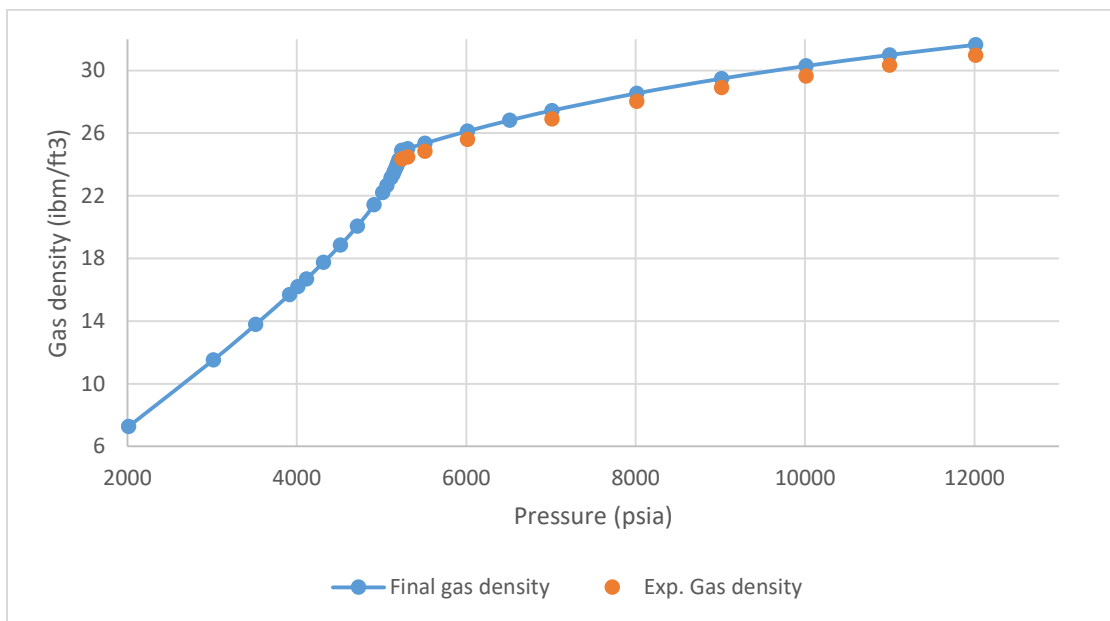


Figure 4.14 SA-01 Gas density experimental vs. tuned simulated data.

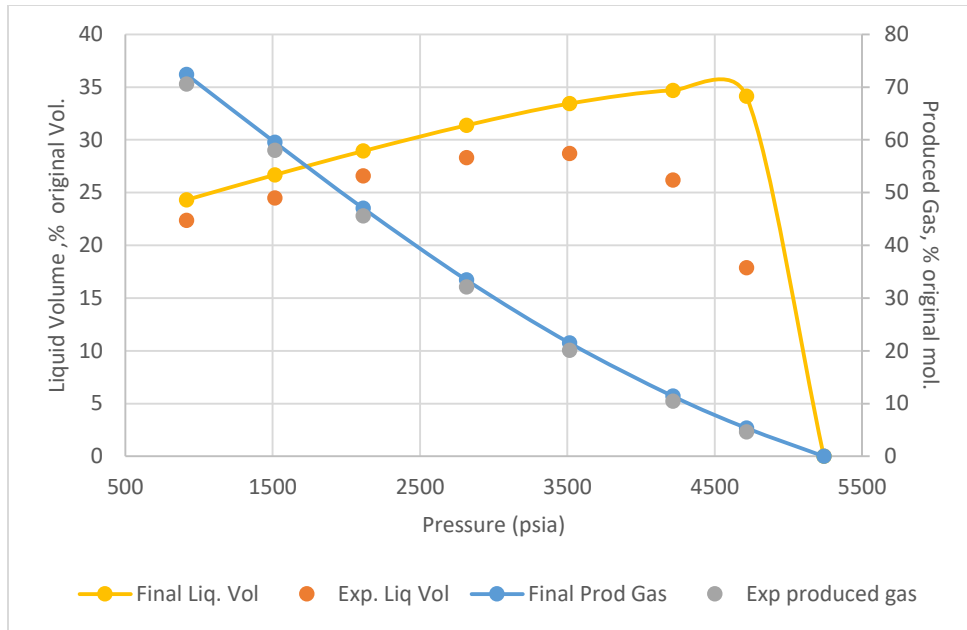


Figure 4.15 SA-01 Liquid and produced gas experimental vs. tuned simulated data.

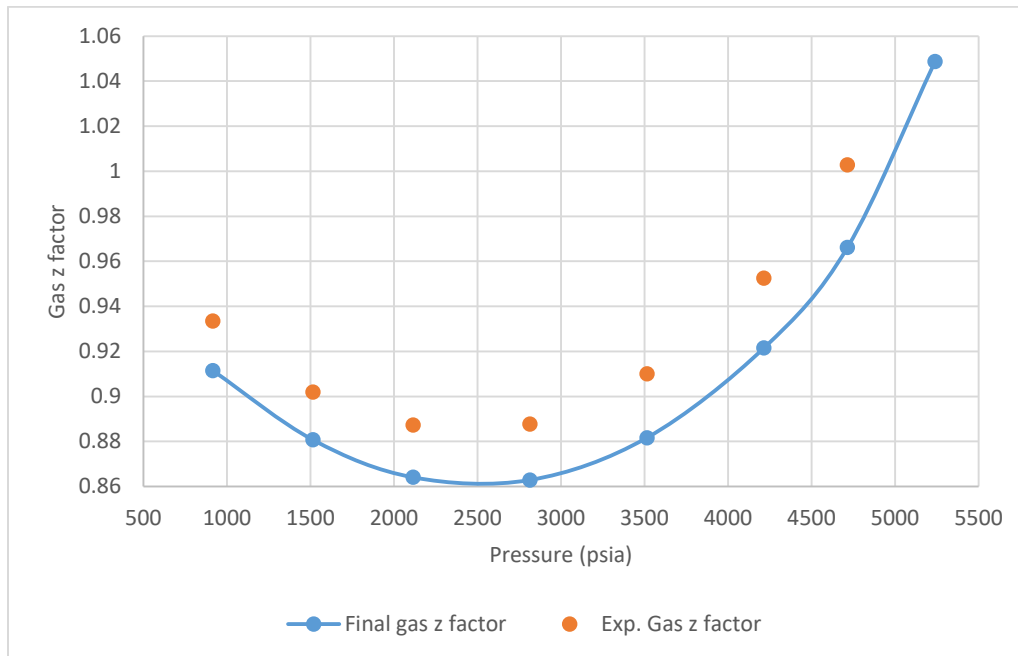


Figure 4.16 SA-01 Gas z factor experimental vs. tuned simulated data.

For an overall overview understanding of fluid path in Well SA-01, Figure 4-17 shows path from initial pressure of 11,000 psi at a reservoir temperature of 262 degree F.

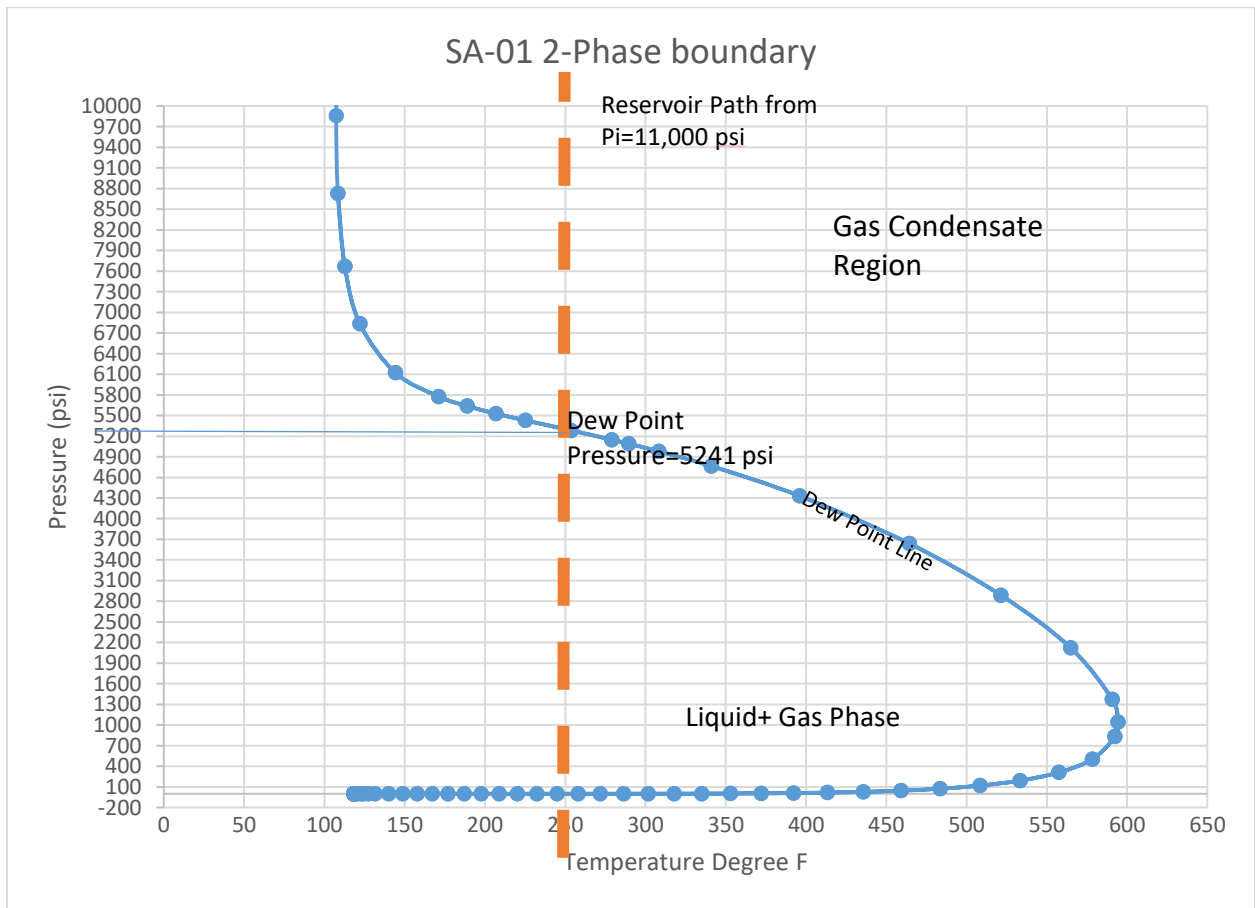


Figure 4.17 SA-01 Two phase envelope.

CHAPTER 5

RESERVOIR CHARACTERIZATION BY WELL TEST

5.1 Pressure Transient Analysis

Pressure transient analysis (PTA) is a helpful tool in evaluating reservoir pressure, fluid, and properties. It can help us understand the productive capacity of the well, the current average reservoir pressure, and specific reservoir properties.

The input data used for the PTA are:

- pressure buildup test (PBT).
- Surface flow rates.
- Fluid properties such as FVF, viscosity, compressibility, etc.
- Reservoir properties such as thickness, porosity, compressibility.

Pressure build up test for SA-01 was analyzed through pressure transient tests, with the primary objective of complementing the geoscientific model with a dynamic behavior and flow movement. As it is well known that in any fractured reservoir, flow occurs through the primary porosity, i.e., fracture system, whereas the second porosity, i.e., matrix, contains the bulk of the reserves in-place. This latter, may or may not supply fluid to the depleted fracture system, depending on the rock conductivity and size. When it does, this behavior can be observed in a pressure test, which normally shows three flow regimes: the fracture flow, matrix-to-fracture flow, and finally matrix and fracture flow concurrently. The analysis of the double-porosity behavior yields values for storativity of the matrix and the transfer coefficient between the matrix and the fracture (Fawzi et al 2005).

5.1.1 Pressure Transient Analysis Theory

This section goes through the equations used to deliver the diagnostic plots for PTA (Kazemi 2017).

First, the early definition of dimensionless pressure and wellbore skin for radial flow is explained as:

In absence of skin:

$$p_{Dw}(t_{Dw}) = \frac{2\pi kh}{qB\mu} \underbrace{[\dots]}_{\Delta p} \quad (5.1)$$

In presence of wellbore skin:

$$p_{Dw}(t_{Dw}) + s_d = \frac{2\pi kh}{qB\mu} [p_i - p_{wf}(t)] \quad (5.2)$$

Where,

$$p_{wf}(t)|_{with\ skin} = p_{wf}(t)|_{without\ skin} + \Delta p_{skin} \quad (5.3)$$

In the case of horizontal wells, early linear flow equation:

$$\Delta p = \frac{qB\mu}{2\pi kh} (p_{wD}) \quad (5.4)$$

The dimensionless pressure of the horizontal well is Ozkan et al. (2009):

$$p_{wD} \approx \sqrt{\frac{k}{k_y}} \left[\sqrt{\pi t_D} + \frac{1}{2L_D} (s_c + s_d) \right] \quad (5.5)$$

Where,

$$t_D = \frac{0.0002637k}{\phi c_t \mu (L/2)^2} t \quad (5.6)$$

$$L_D = \frac{L_w}{2h} \sqrt{\frac{k_z}{k}} \quad (5.7)$$

$$k = \sqrt[3]{k_x k_y k_z} \quad (5.8)$$

Substituting Equation 5.6 and Equation 5.7 in Equation 5.5,

$$p_{wD} \approx \sqrt{\frac{k}{k_y}} \left[\sqrt{\pi \frac{0.0002637k}{\phi c_t \mu (L_w/2)^2} t} + \frac{1}{2 \frac{L_w}{2h} \sqrt{\frac{k_z}{k}}} (s_c + s_d) \right]$$

(5.9)

Rearrange Equation 5.9:

$$p_{wD} \approx \frac{k}{L_w} \sqrt{4\pi(0.0002637)} \sqrt{\frac{1}{k_y \phi c_t \mu}} \sqrt{t} + \frac{kh}{L_w \sqrt{k_y k_z}} (s_c + s_d) \quad (5.10)$$

Substituting Equation. 5.10 in Equation. 5.4,

$$\Delta p = \frac{qB\mu}{2\pi kh} \left[\frac{k}{L_w} \sqrt{4\pi(0.0002637)} \sqrt{\frac{1}{k_y \phi c_t \mu}} \sqrt{t} + \frac{kh}{L_w \sqrt{k_y k_z}} (s_c + s_d) \right] \quad (5.11)$$

Rearrange Equation 5.11,

$$p_i - p_{wf}(t) = \frac{8.128qB}{L_w h} \sqrt{\frac{\mu}{k_y \phi c_t}} \sqrt{t} + \frac{141.2qB\mu}{L_w \sqrt{k_y k_z}} (s_d + s_c) \quad (5.12)$$

To check the existence of the radial flow regime, the time for the beginning of radial flow was calculated using the following theoretical equation from E. Ozkan (2009):

$$t \geq \max \left\{ \frac{988\phi c_t \mu L_w^2}{k_x}, \frac{2515\phi c_t \mu h^2}{k_z} \right\} \quad (5.13)$$

Using data from the pressure build-up test that will be reported later, the beginning of the radial flow was calculated to be 2.7 hours based on the above constraint: $t \geq \max \{2.7; 0.029\}$.

The build test for the well SA-01 was conducted for around one-day. To identify the flow regimes first diagnostic plot, a log-log plot of pressure drop during shut-in versus time, was studied for the build-up test (Figure 5.1). Linear flow regime followed by a radial flow regime was identified.

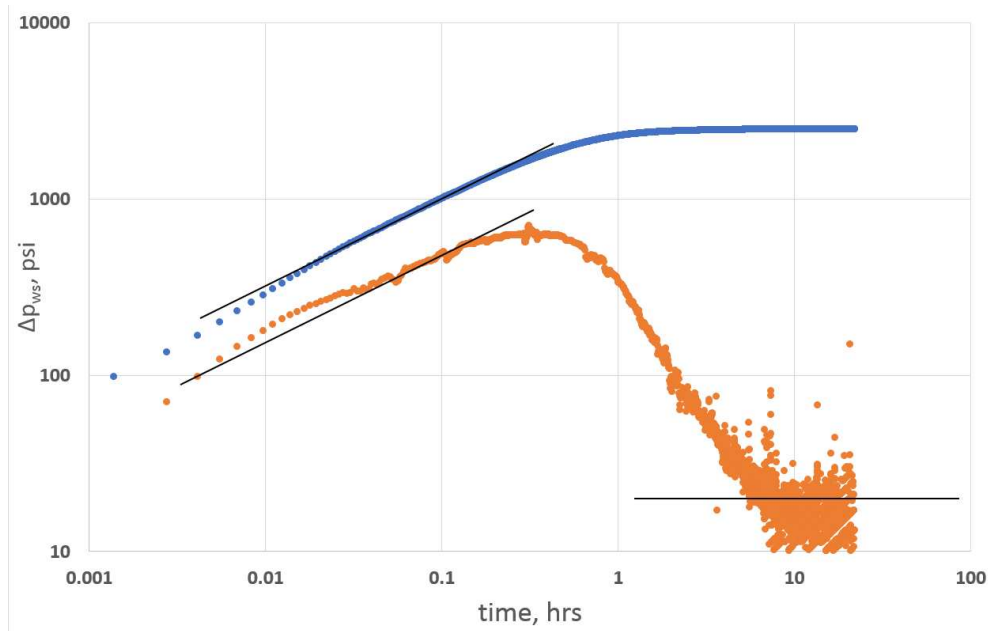


Figure 5.1 Diagnostic plot for SA-01 PTA.

First, radial flow regime was identified to calculate the reservoir permeability. From the semi-log plot of pressure drop during shut-in versus Horner time (Figure 5.2), the reservoir permeability was calculated to be 0.6 md. Also, the skin s_d was calculated to be 9.39 using the following equation:

$$p_i - p_{wf}(t) = \frac{162.6qB\mu}{\sqrt{k_{f,eff,x}k_{f,eff,z}L_w}} \left[\log \left(\frac{\sqrt{k_{f,eff,x}k_{f,eff,z}}}{\phi\mu c_t r_w^2} \right) + \log(t) - 3.227 + 0.868s_d \right] \quad (5.15)$$

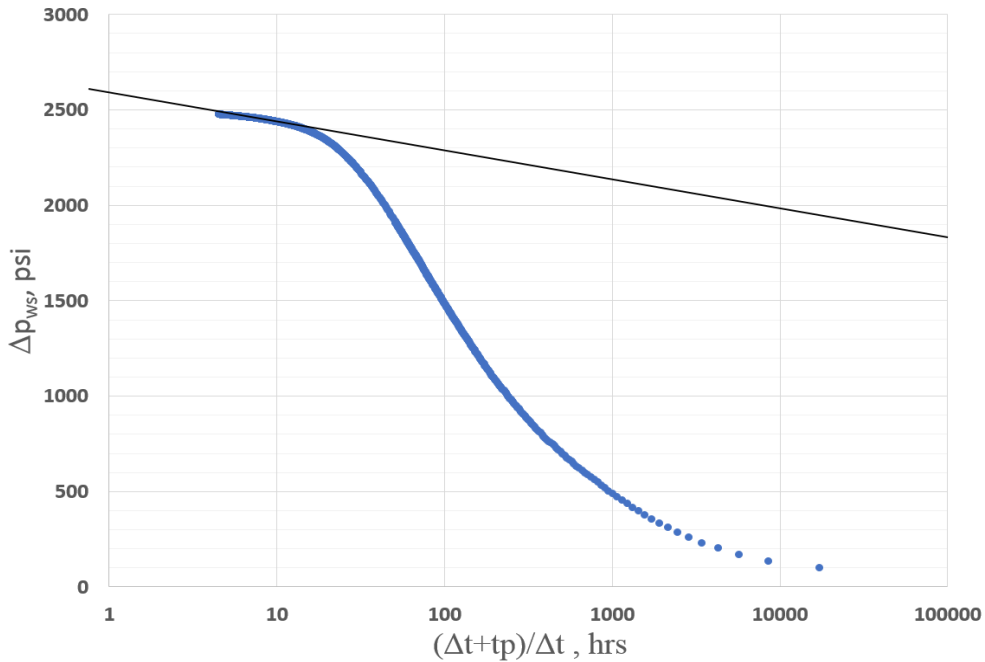


Figure 5.2 Radial flow analysis for SA-01.

To check the validity of the radial flow analysis, linear flow analysis was also performed. Pressure drop during shut-in versus square root of time was plotted (Figure 5.3). Using Equation 5.12, the reservoir permeability was calculated as 0.52 md. Similarly, the skin, resulting from wellbore damage and completion practice, was calculated as $s_d + s_c = 46.3$ using the following equation:

$$p_i - p_{wf}(t) = \frac{8.128qB}{hL_w} \sqrt{\frac{\mu t}{k_v \phi c_t} + \frac{141.2qB\mu}{L_w \sqrt{k_x k_z}} (S_d + S_c)} \quad (5.15)$$

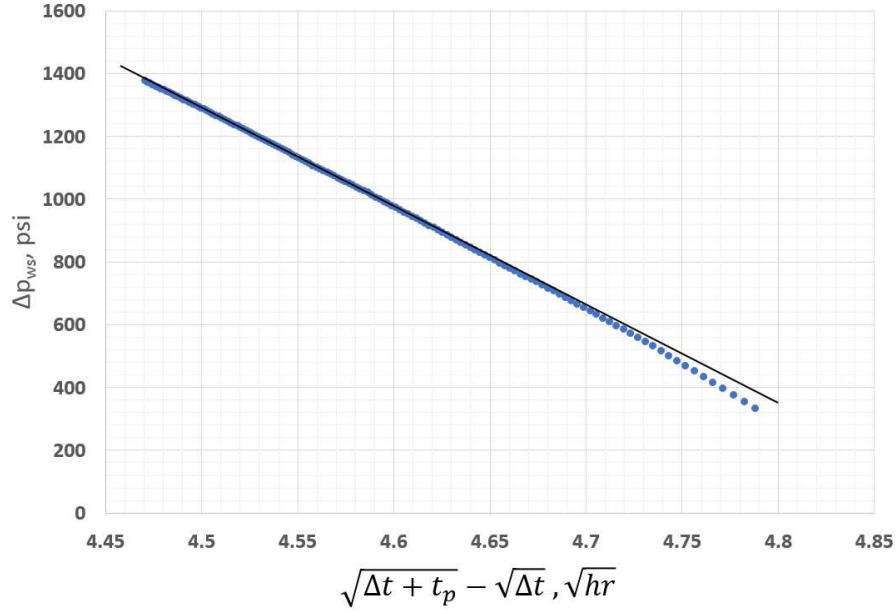


Figure 5.3 Linear flow analysis for SA-01.

Thus, it was concluded that the reservoir permeability should be taken around 0.5 – 0.6 md for the simulation runs.

5.2 Rate Transient Analysis (RTA)

In reservoir evaluation of unconventional reservoirs, engineers use rate transient analysis (RTA) to assess the performance of hydraulically fractured horizontal wells. This technique consists of plotting rate-normalized pressure drop at the well sandface versus square root of time (i.e., linear flow) to calculate the reservoir effective permeability.

Winestock and Colpitts (1965) used rate transient analysis of production data from vertical wells in conventional reservoirs. In their approach the flow toward the well was radial. Thus their rate-transient analysis has a radial form:

$$\frac{\Delta p_{wf}(t)}{q(t)} = 141.2 \frac{\mu}{kh} \left[\frac{1}{2} (\ln t_D + 0.809) + s \right] \quad (5.13)$$

Where, $\Delta p_{wf}(t)$ is the bottom-hole flowing pressure drop, $q(t)$ flow rate, μ viscosity, k formation permeability, h formation thickness, t_D dimensionless time, and s skin factor.

Similarly, Wattenbarger et al. (1998) and Bello and Wattenbarger (2008) presented the rate-transient analysis for unconventional reservoirs using the analytical solution for the linear flow

regime in dual-porosity systems. The following equation represents the main contribution of their work:

$$A_{SRV} \sqrt{k_{f,eff}} = \frac{1262}{\sqrt{\phi \mu c_t}} \frac{T}{m_l} \quad (5.14)$$

Where, A_{SRV} is the areal extent of the stimulated reservoir volume, $k_{f,eff}$ effective permeability, ϕ porosity, μ viscosity, c_t total compressibility, T temperature, and m_l slope of $\frac{\Delta p_{wf}(t)}{q_{total}(t)}$, vs. $t^{1/2}$.

Wattenbarger et al. (1998) provided the following equation for the end-of linear flow in single-phase case for constant production flow rate:

$$t_{D,elf} = \frac{0.006328kt_{elf}}{\phi\mu c_t L_e^2} = 0.5 \quad (5.15)$$

Where, $t_{D,elf}$ is the dimensionless time at the end-of linear flow regime, t_{elf} time of the end of linear flow regime in days, and L_e the no-flow boundary between fracture stages; thus, the distance to the no-flow boundary between fracture stages, is:

$$L_e = 0.113 \sqrt{\frac{k t_{elf}}{\phi\mu c_t}} \quad (5.16)$$

According to Wattenbarger et al. (1998), for constant bottom-hole pressure, 0.5 should be replaced by 0.25, and 0.113 should be replaced by 0.159, respectively. The following equations reflect these suggestions, which we invariably use in our rate transient analyses.

$$t_{D,elf} = \frac{0.006328kt_{elf}}{\phi\mu c_t L_e^2} = 0.25 \quad (5.17)$$

$$L_e = 0.159 \sqrt{\frac{k t_{elf}}{\phi\mu c_t}} \quad (5.18)$$

Nobakht and Clarkson (2012) studied linear gas flow in shale reservoirs which included gas adsorption and slippage. Tivayanonda (2012) presented results for linear and bilinear flow in fractured horizontal wells for unconventional shale oil and gas reservoirs using a triple-porosity model.

Kazemi et al. (2014), Uzun et al. (2016), and Uzun et al. (2017) presented both the single- and multi-phase flow for multi-stage hydraulically fractured, low-permeability, dual-porosity

shale reservoirs. The rate-normalized pressure drop equations for single- and multi-phase flow are presented in the following two equations, respectively.

$$\frac{\Delta p_{wf}(t)}{q(t)B} = 4.064 \frac{\mu}{\sqrt{k_{f,eff}} (n_{hf} h y_{hf})} \left[\left(\frac{1}{(\phi c_t)_{f+m} \mu} \right)^{1/2} \sqrt{t} \right] + 141.2 \frac{\mu}{k_{f,eff} h} S \quad (5.19)$$

$$\frac{\Delta p_{wf}(t)}{q_{total}(t)} = \frac{4.064 \sqrt{24} (\pi/2) \lambda_i^{-1}}{\sqrt{k_{f,eff}} (h n_{hf} y_{hf})} \left[\left(\frac{\lambda_i}{(\phi c_t)_{f+m}} \right)^{1/2} \right] \sqrt{t} + \frac{141.2 \lambda_i^{-1}}{k_{f,eff} h n_{hf}} S_{hf}^{face} \quad (5.20)$$

Gannaway and Ibrahim (2016) implemented the multi-phase approach of Equation 5.6 for water-oil flow in Wolfcamp and Bone Spring formations. These formations produce substantial amounts of water. Finally, Qanbari and Clarkson (2016) presented a time-varying drainage area in the RTA equation, which also incorporates the dependence of rock and fluid properties on pore pressure.

To verify the simulation results for the initial case where only 535 ft of perforation was created, rate-transient analysis was conducted. The first step for the RTA is to identify the flow regimes via plotting rate-normalized pressure drop versus time on a log-log scale (Figure 5.4).

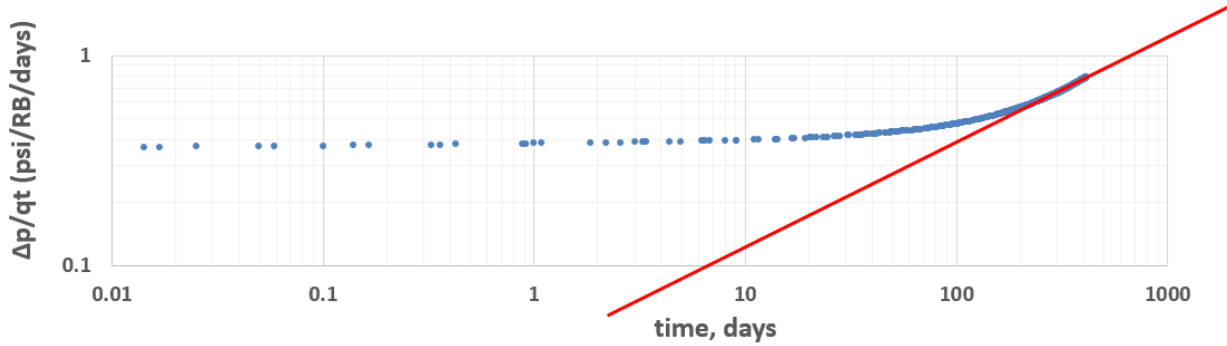


Figure 5.4 Diagnostic plot for SA-01 RTA.

From the diagnostic plot, linear slope with a half-slope was identified. To analyze the linear flow analysis, rate-normalized pressure drop versus square root of time was plotted (Figure 5.5).

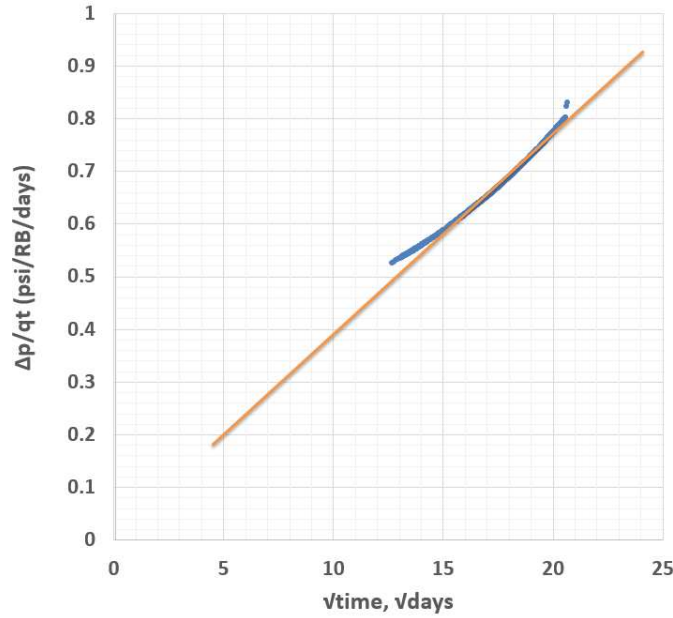


Figure 5.5 Linear flow analysis for SA-01 using RTA.

Using the slope obtained from the linear flow analysis and the Equation 5.21, the product of effective reservoir permeability and total mobility $k_{f,eff} \lambda_t$ was calculated as 8.92 md/cp. The mobility was then calculated as 25.2 1/cp during the linear flow. Thus, the $k_{f,eff}$ was back calculated as 0.35 md.

$$\frac{\Delta p_{wf}(t)}{q(t)B} = 8.128 \frac{(\pi/2)\lambda_t}{\sqrt{k_{f,eff}}(hL)} \left[\left(\frac{1}{(\phi c_t)_{f+m} \lambda_t} \right)^{1/2} \sqrt{t} \right] + 141.2 \frac{\mu}{k_{f,eff} h} s \quad (5.21)$$

Next, three hydraulic fractures with 150 ft of half-length were created inside the perforated area. Similarly, RTA was conducted to verify the simulation results. First, log-log plot of rate-normalized pressure drop versus time was obtained to identify the flow regimes (Figure 5.6).

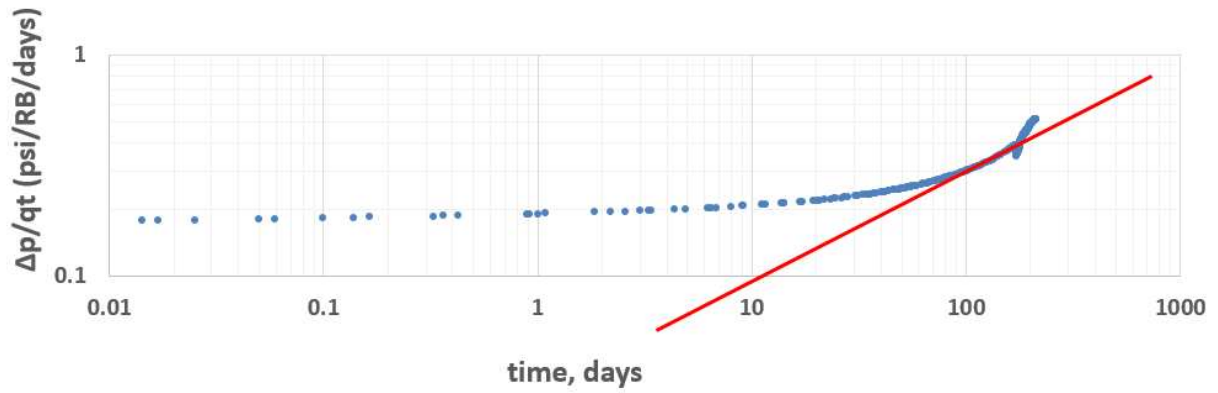


Figure 5.6 Diagnostic plot for SA-01 RTA.

The linear flow was identified from the diagnostic plot and linear flow analysis using the slope of rate-normalized pressure drop versus square root of time (Figure 5.7).

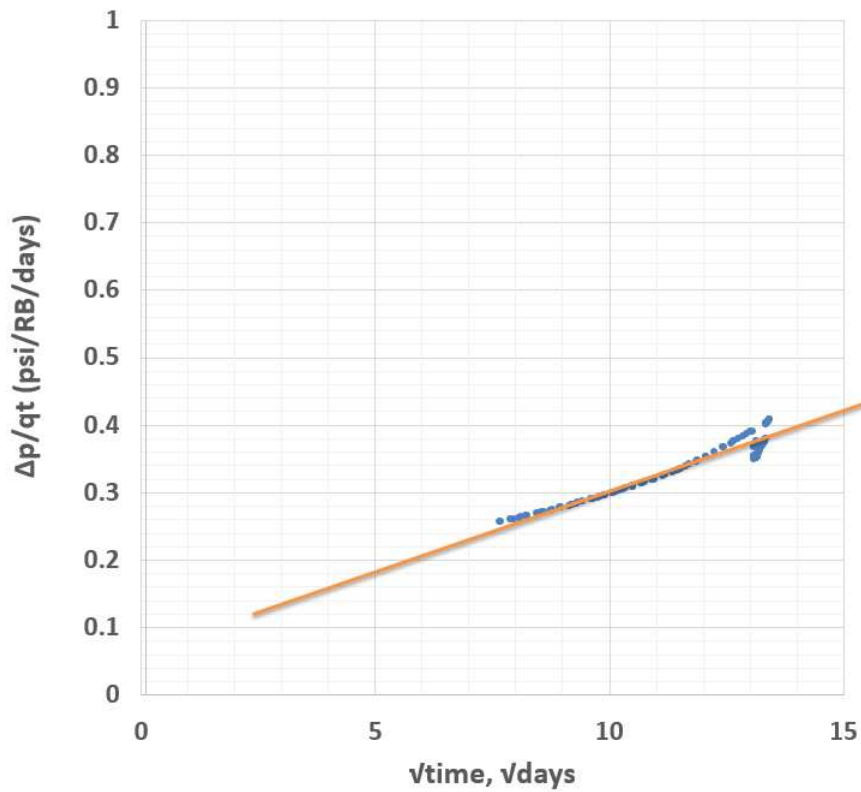


Figure 5.7 Linear flow analysis for SA-01 using RTA.

Using the Equation 5.20 and the slope obtained from Figure 5.7, the product of effective reservoir permeability and total mobility $k_{f,eff} \lambda_t$ was calculated as 11.28 md/cp. The mobility was then calculated as 25.7 1/cP during the linear flow. Thus, the $k_{f,eff}$ was back calculated as 0.44 md.

CHAPTER 6
NUMERICAL MODELING

6.1 Model Construction

The static reservoir model was created using Schlumberger’s Petrel; it consists of a structural framework that is populated with representative /modeled matrix and fracture properties. It was constructed by integrating all the available geological, geophysical, petrophysical and engineering data from the North Kuwait Jurassic fields. The main building blocks of the static reservoir model include structure, sedimentology and stratigraphy, petrophysics, and fracture characterization. The model contained numerous uncertainties, mainly in: structural uncertainty, FWL uncertainty, facies modeling uncertainty, and porosity uncertainty.

The modeled volume is 3614 ft in length (x-direction) by 8364 ft in width (y-direction) by 85 ft in thickness (z-direction). The model has grid dimensions of 24 (x-direction) × 39 (y-direction) × 24 (z-direction) with local refinement around the well area. The general gridding scheme is shown in Figures 6.1 to 6.4.

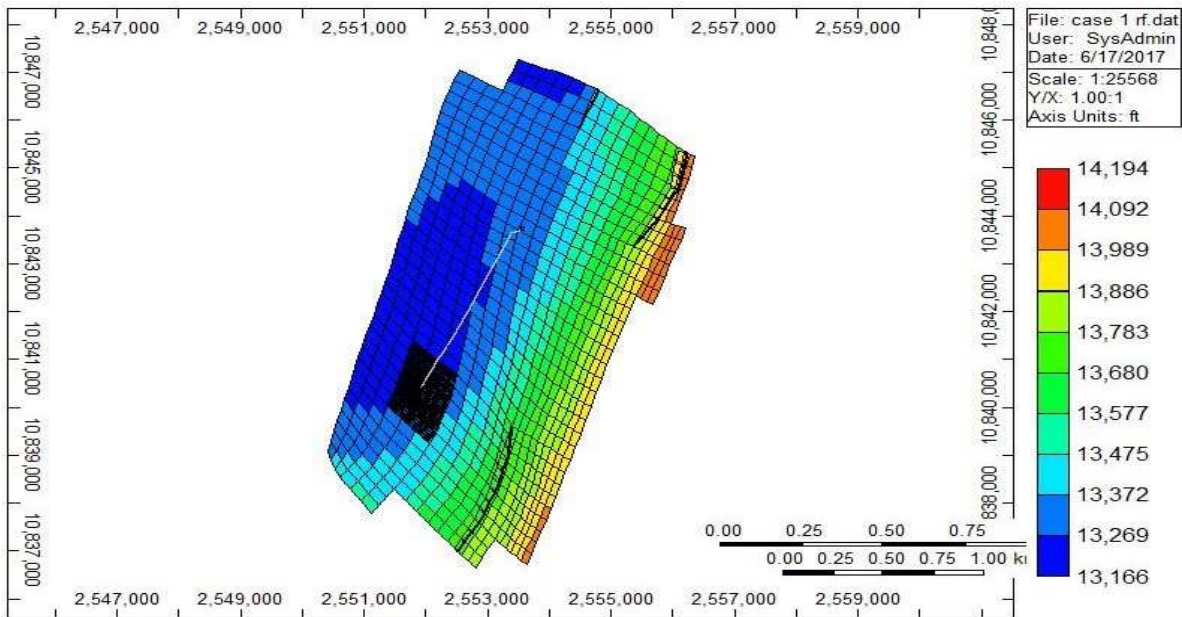


Figure 6.1 Sector Model 2D I-J view.

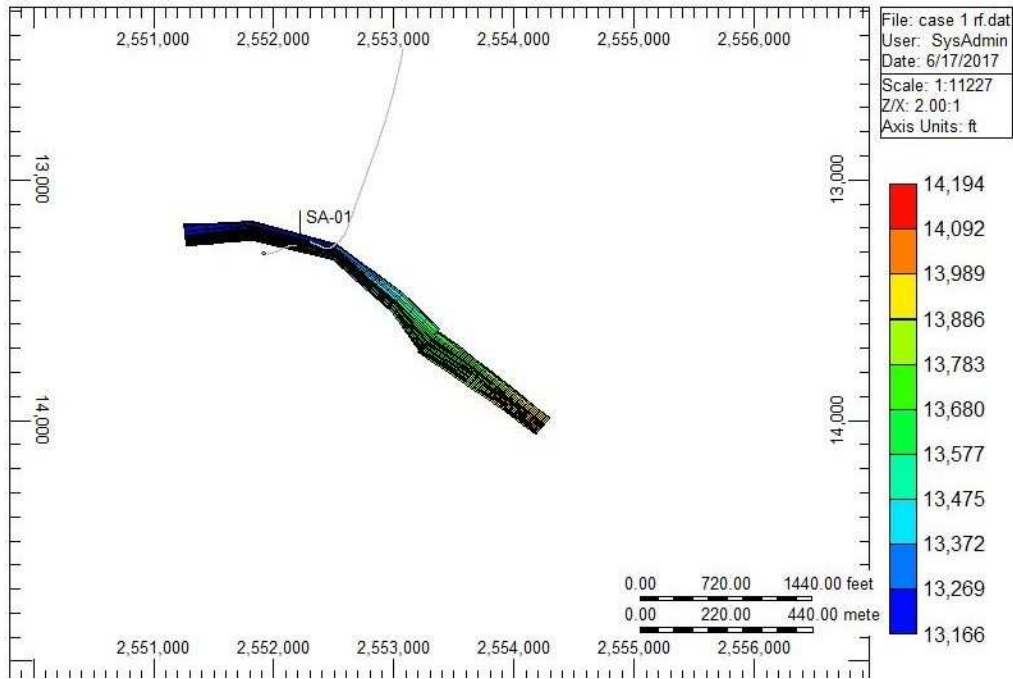


Figure 6.2 Sector Model 2D I-K view.

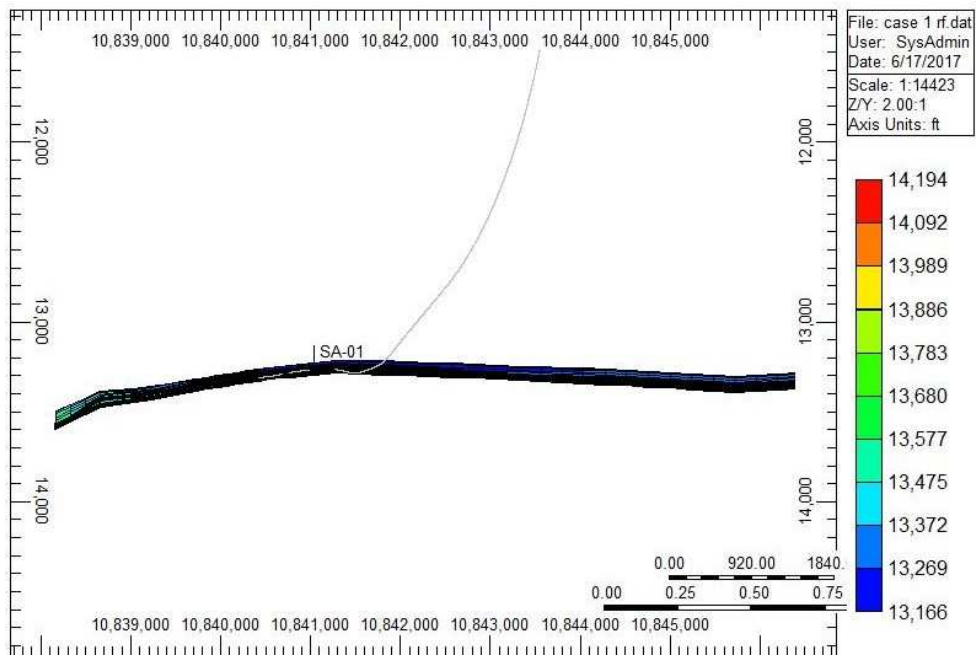


Figure 6.3 Sector Model 2D J-K view.

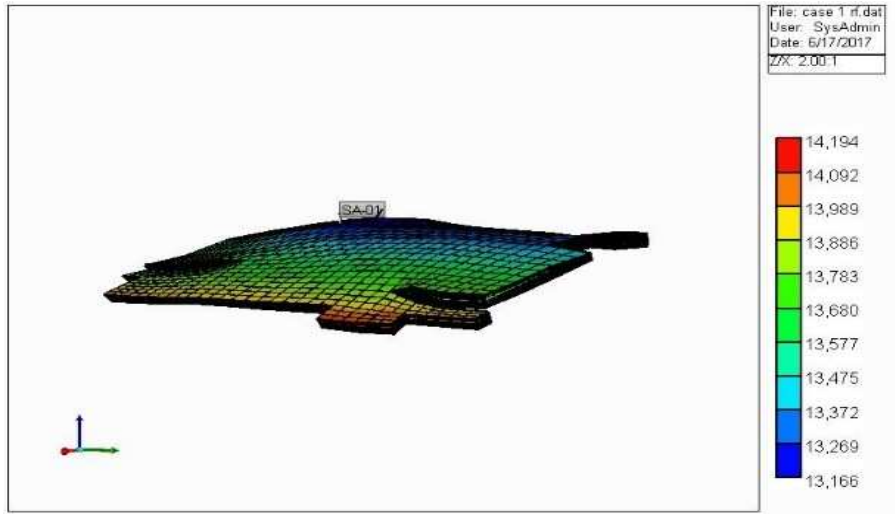


Figure 6.4 Sector Model 3D view.

The deviated well SA-01 is perforating in layers 11-20 in z direction, with a perforated section of less than 600 ft as shown in Figure 6.5 and Figure 6.6.

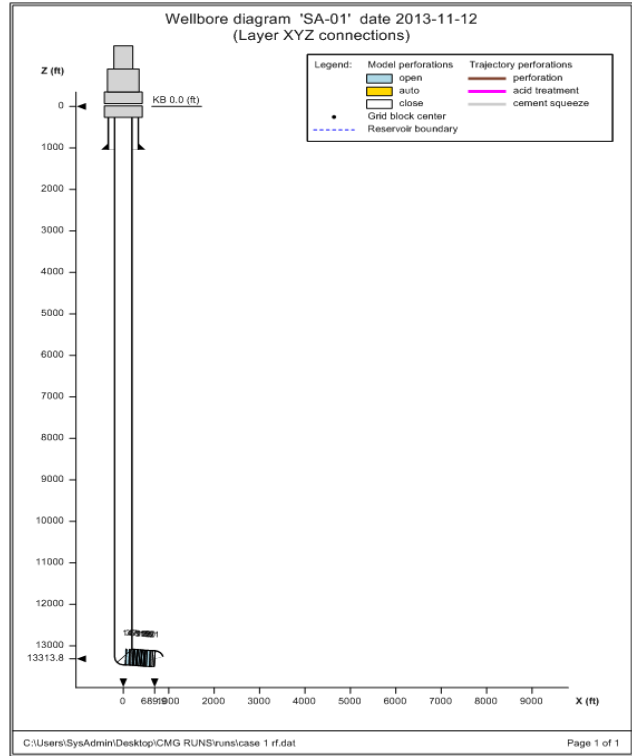


Figure 6.5 SA-01 well diagram.

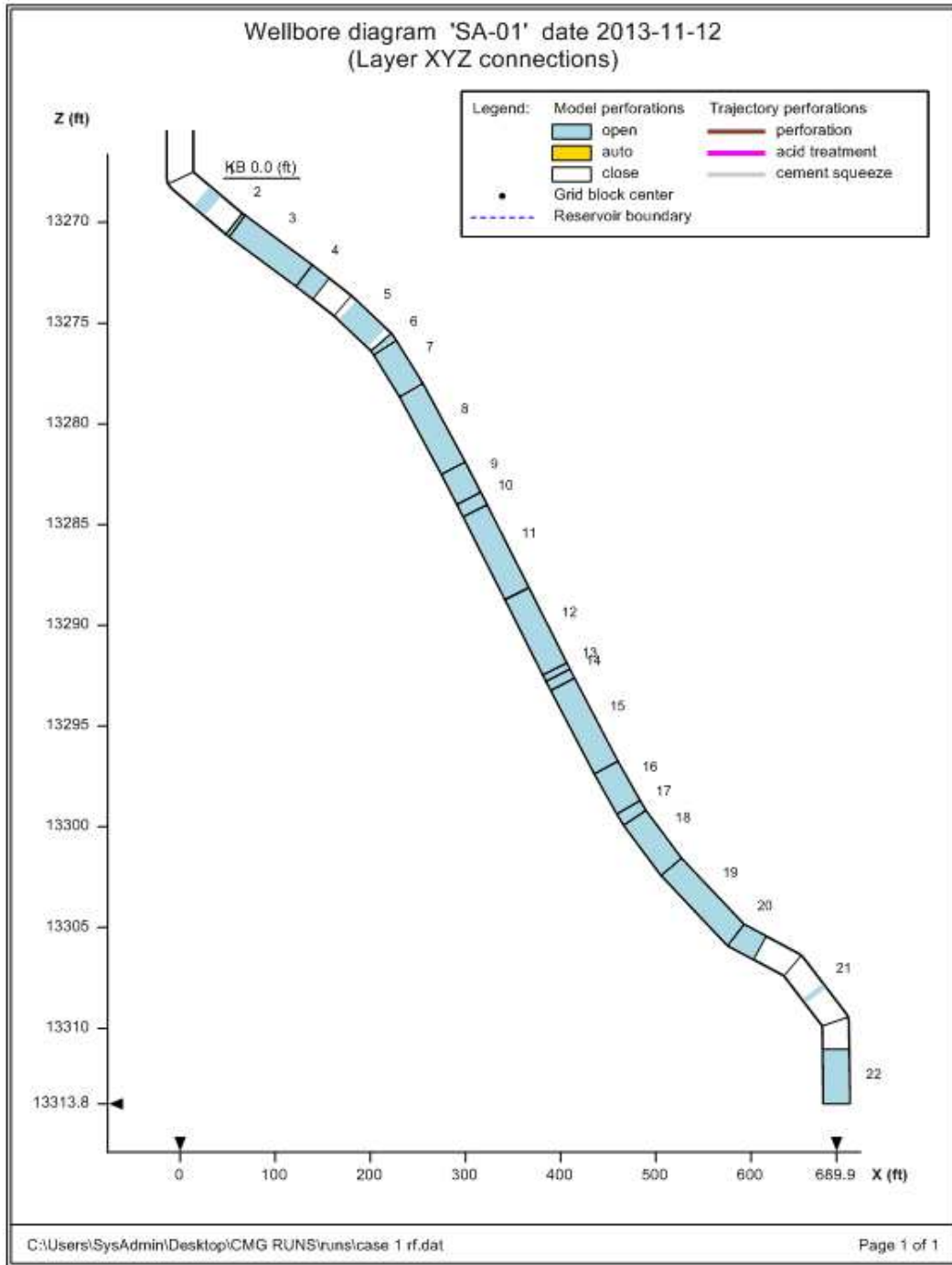


Figure 6.6 Zoomed diagram of perforated section.

Once the fluid models were obtained, a number of reservoir simulations were executed with CMG GEM Module (composition model). For primary recovery case and for primary recovery followed by hydraulic fracturing case, the reservoir model was simulated for 7 years, of

which 3 are beyond actual production data, namely from November 11th, 2013 to February 1st, 2020. The study ran for 6 cases as described in Table 6.1.

Table 6.1 Model cases description for SA-01

Case No.	Constraint	Water Saturation
1	Constant rate: 2.7 MMscf/day	variant
2	Constant rate: 2.7 MMscf/day	irreducible
3	Constant rate: 4 MMscf/day	variant
4	Constant rate: 4 MMscf/day	irreducible
5	Constant rate: 2.7 MMscf/day	variant
6	Constant rate: 2.7 MMscf/day	irreducible

6.1.1 Base Case Scenario

The data obtained for this study has been provided by Kuwait Oil Company (KOC), which is a national oil company located in the city of Ahmadi in South Kuwait. There are 8 producing wells in Sabriyah field, only two are producing from MFS formation, and one of those two is the horizontal well of SA-01. Information on the well tops, well logs, structure map, well trajectory and production history are all available for the well. The static grid system has been internally built in KOC with Schlumberger Petrel software, and imported into CMG Builder as a rescue file, feeding the simulator with information about reservoir boundary, grid tops and dimensions, and petrophysical properties. The WinProp fluid model was also imported to provide the fluid properties of the system. Given that the system is highly fractured, a dual porosity approach was chosen to best describe and represent the heterogeneity of the reservoir, with the start date of the simulation as November 11th, 2013 coinciding with the well's first production date.

Table 6.2 shows the properties considered in the base case scenario. It is important to note here the model contained large uncertainties in terms of fracture permeability values, fracture porosity, shape factor representation, and water saturation. Those parameters were used as tuning parameters for history matching.

Table 6.2 Grid Properties

Property	Petrel Model Values
$k_{m,i}, k_{m,j}$ (md)	variant, range: 0.001-0.2
$k_{m,k}$ (md)	variant, range: 0.001-0.2
$k_{f,i}$ (md)	variant, range: 0-150
$k_{f,j}$ (md)	variant, range: 100-300
$k_{f,k}$ (md)	variant, range: 0-350
$k_{f,eff,(i,j,k)}$ (md)	Calculated internally
ϕ_m	variant, range: 0.0102-0.0712
ϕ_f	variant, range: 0 -0.17
S_w	variant, range: 0.129-1
$c_{r,m} c_{r,f}$ (1/psi)	7.30E-06
$L_i L_j$ (ft)	variant, range: 0-75
L_k (ft)	variant, range: 0-75

6.1.2 Grid Size Sensitivity

Initially the gridding system imported from petrel had large grid size blocks. The block sizes are variant in all three directions across the sector. However, they are very large. In order to better represent the reservoir and well performance, a sensitivity analysis of grid system was considered, Figure 6.7 shows the original grid system as taken from petrel, the block size is large with typical dimensions of (844 ft in x-direction, 759 ft in y-direction, 2.2 ft in z-direction). The overall grid system was refined in x and y direction, and kept as is in z direction as it was already fairly small, as can be seen in Figure 6.8 with typical dimensions of (288 ft in x-direction, 253 ft in y-direction, 2.2 ft in z-direction). Figure 6.9 shows an additional considered refinement, this time only around the well area, with typical dimensions of (19.3 ft in x-direction, 125.4 ft in y-direction, 1.8 ft in z-direction).

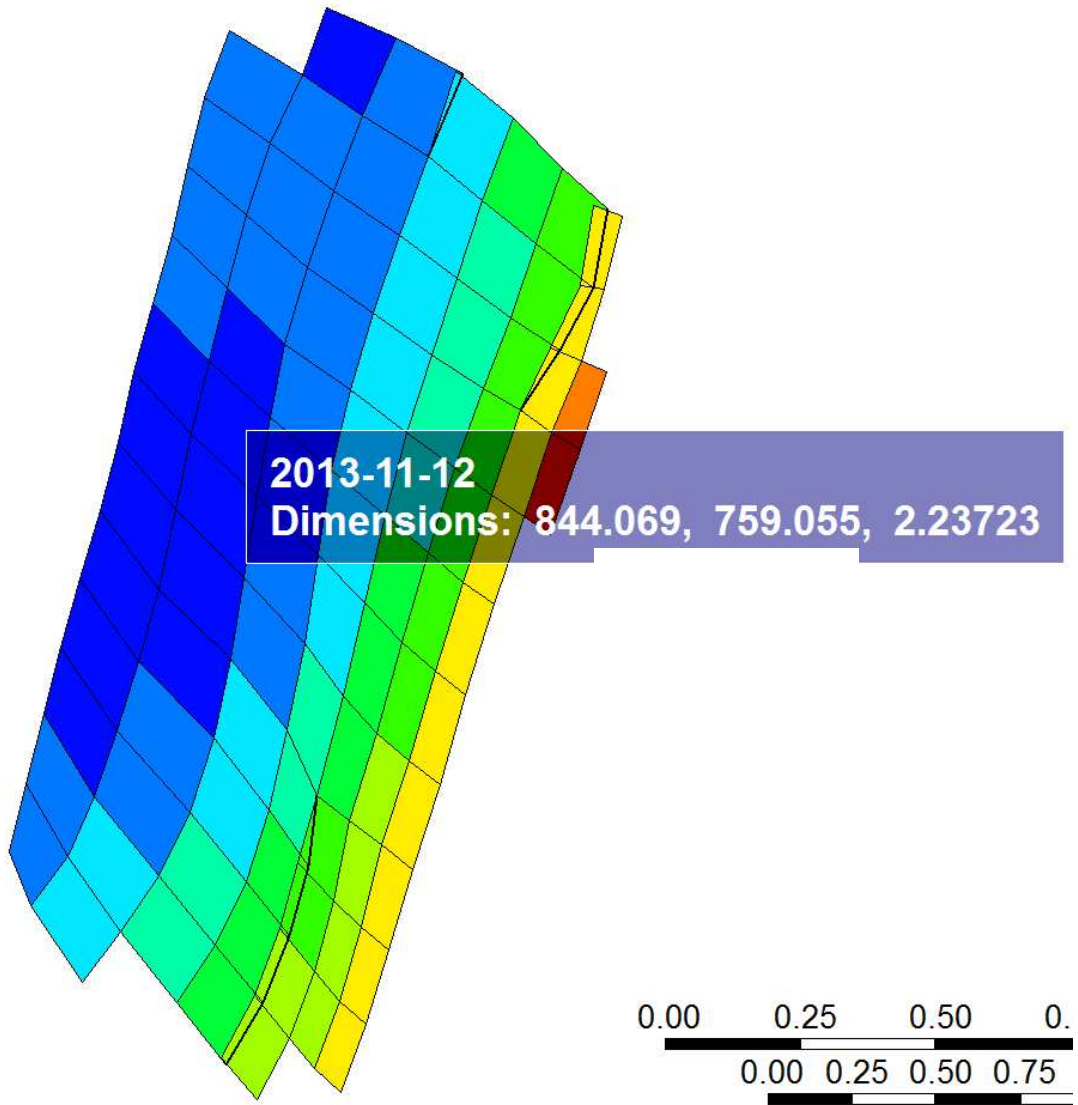


Figure 6.7 Original Petrel sector model with large block dimensions in ft.

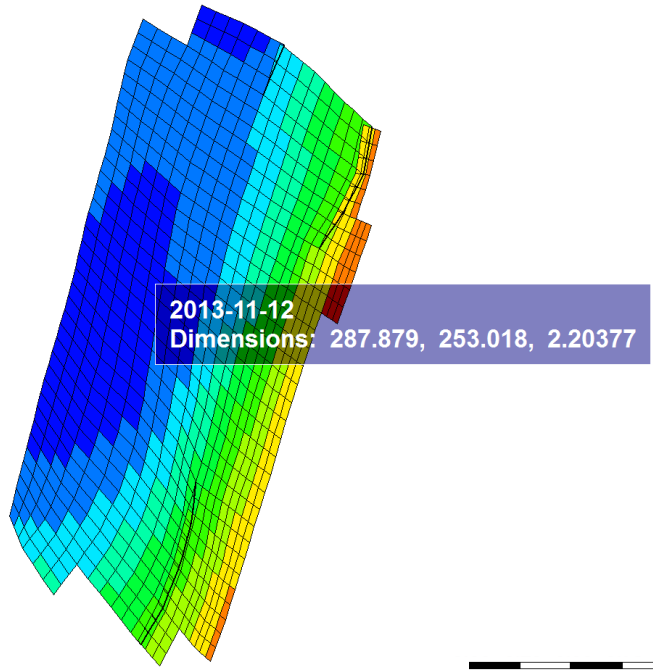


Figure 6.8 Refined version of sector model with block dimensions in ft.

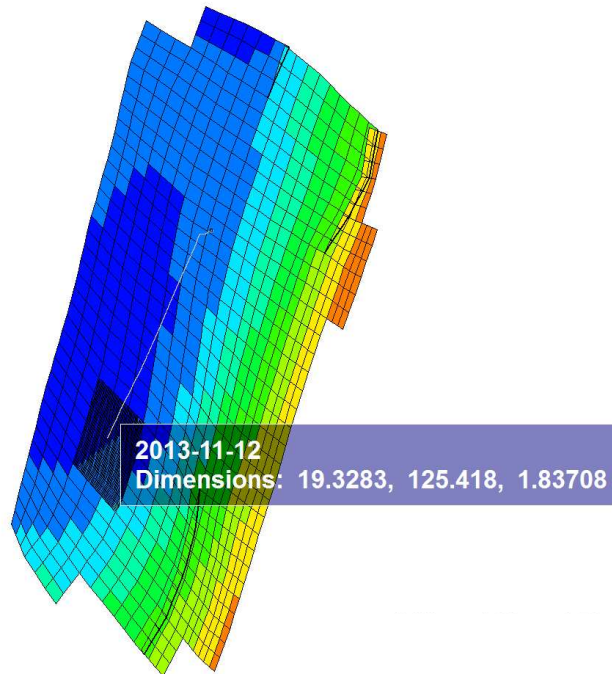


Figure 6.9 Additional Local refinement for the sector model with dimensions in ft.

6.1.3 Relative Permeability and Capillary Pressure Data

There were no measured relative permeability data that could be used in the model. Instead, several versions of relative permeability data (Cho et al., 2016) were used along with measured capillary pressure data, and inserted in rock-fluid properties in CMG Builder. Nevertheless, the data were later tuned in history matching process to acquire the best representation of the actual fluid production. Figures 6.10 to 6.15 describe the relative permeability and capillary pressure data considered for the history matched model.

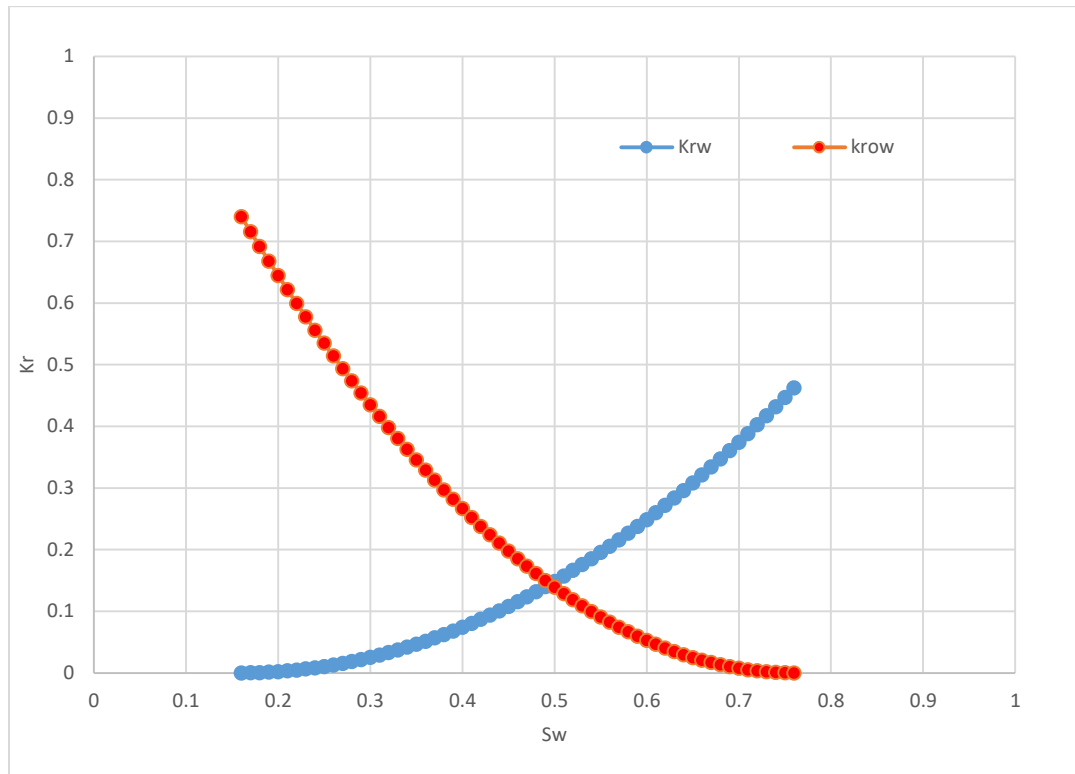


Figure 6.10 W-O Relative permeability curve for matrix rock SA-01.

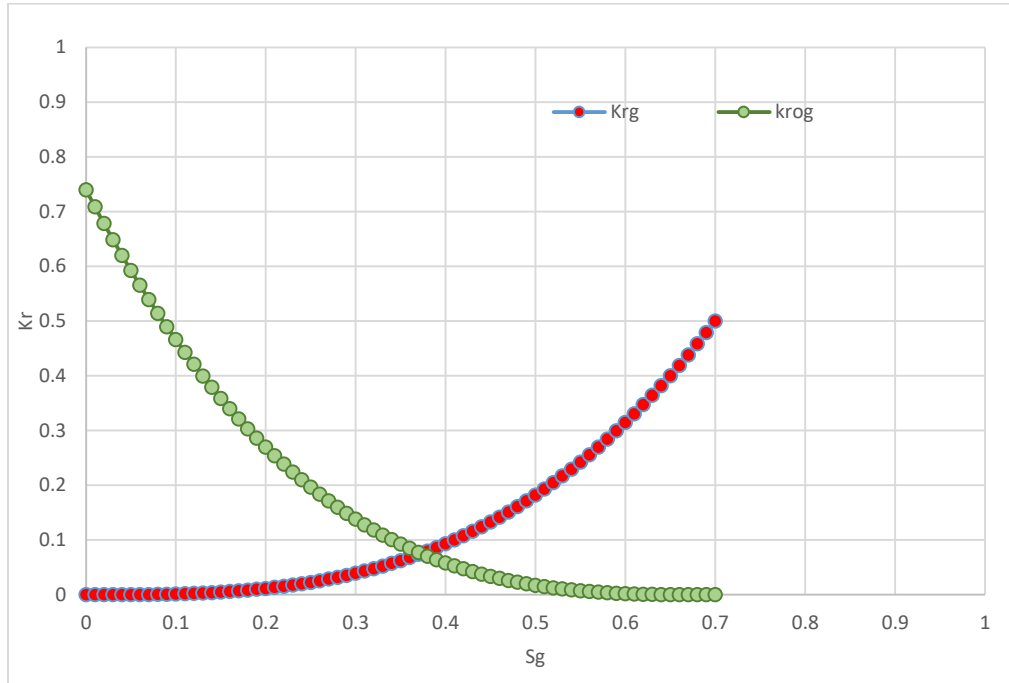


Figure 6.11 G-O Relative permeability curve for matrix rock of SA-01.

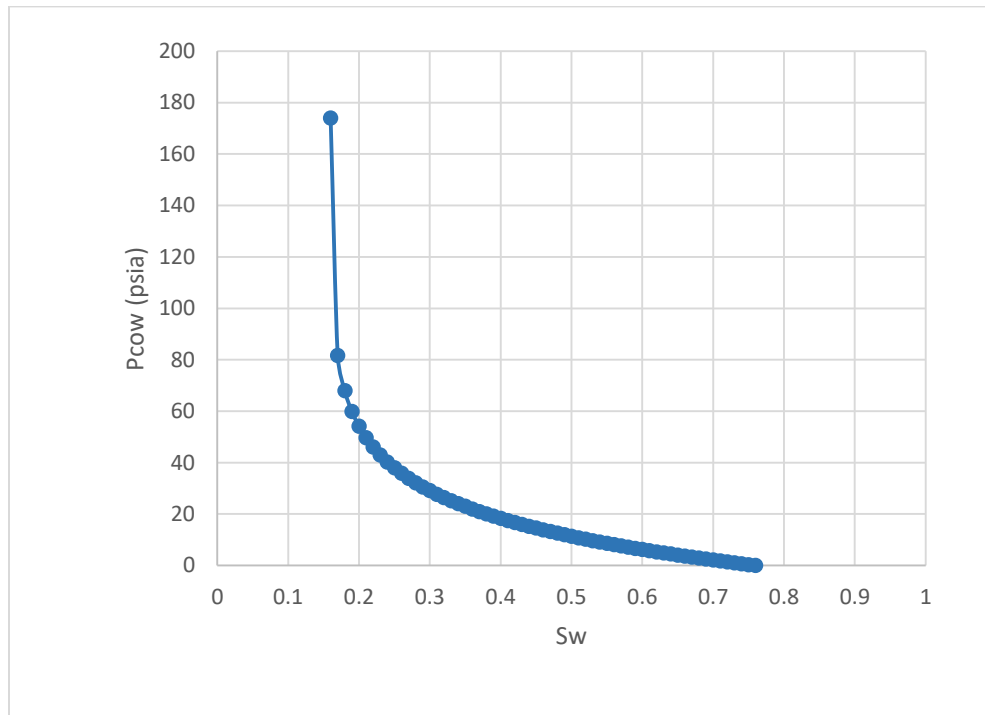


Figure 6.12 Matrix Capillary Pressure Data (Oil-Water) for SA-01.

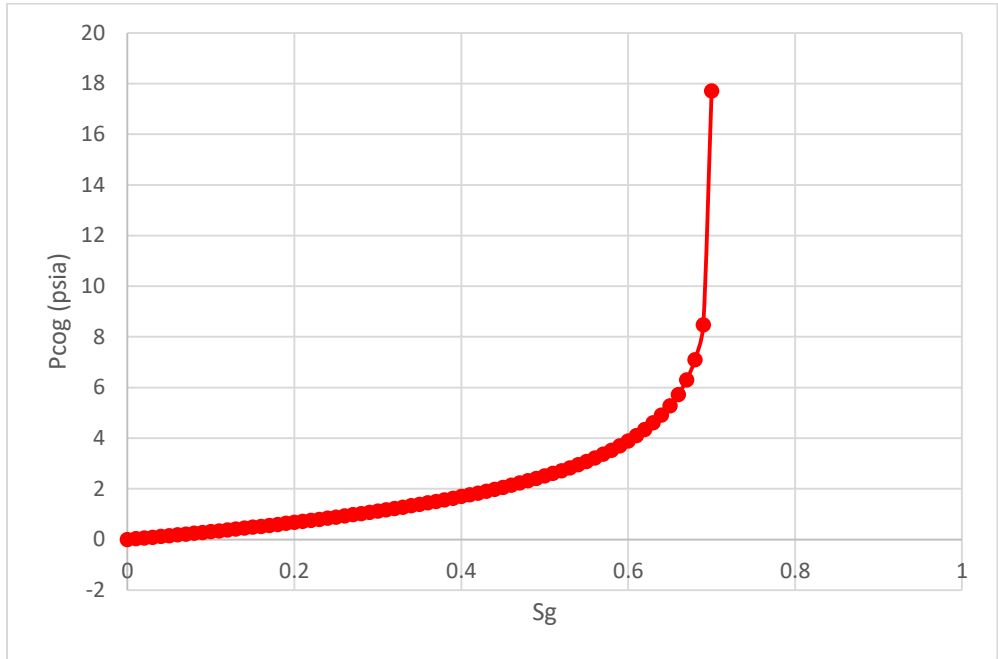


Figure 6.13 Matrix Capillary pressure curve for Oil-Gas of matrix rock of SA-01.

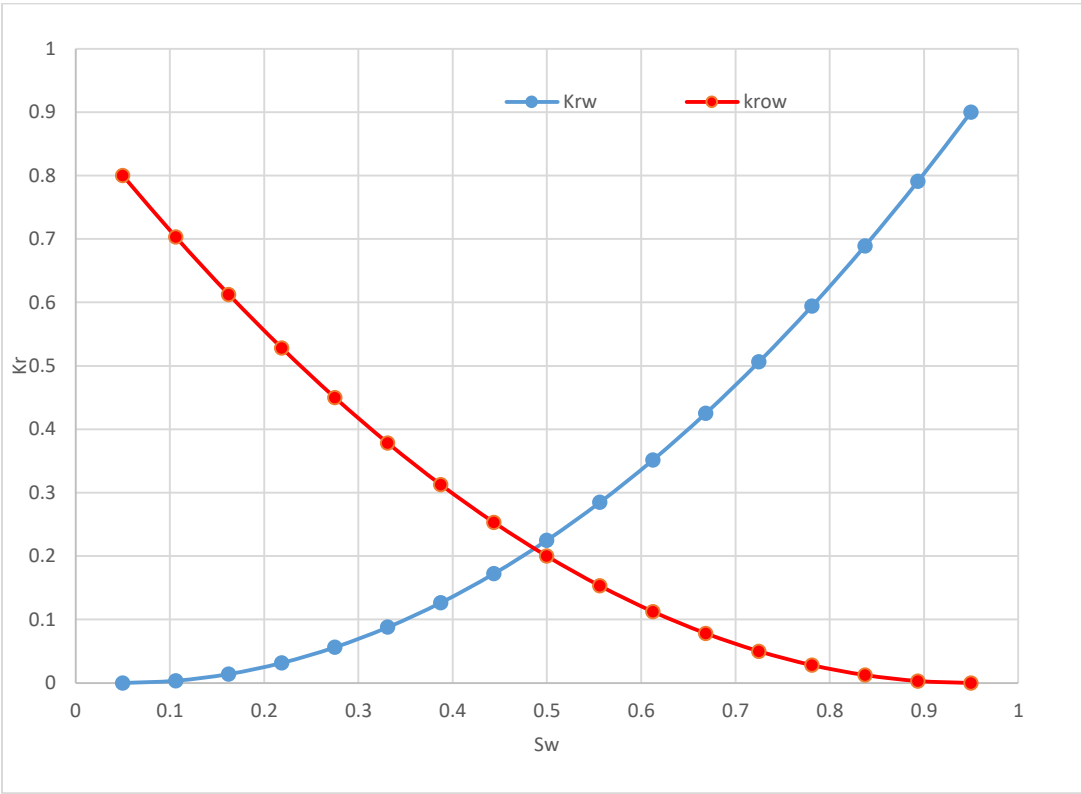


Figure 6.14 Fracture Relative Permeability Data (Oil-Water).

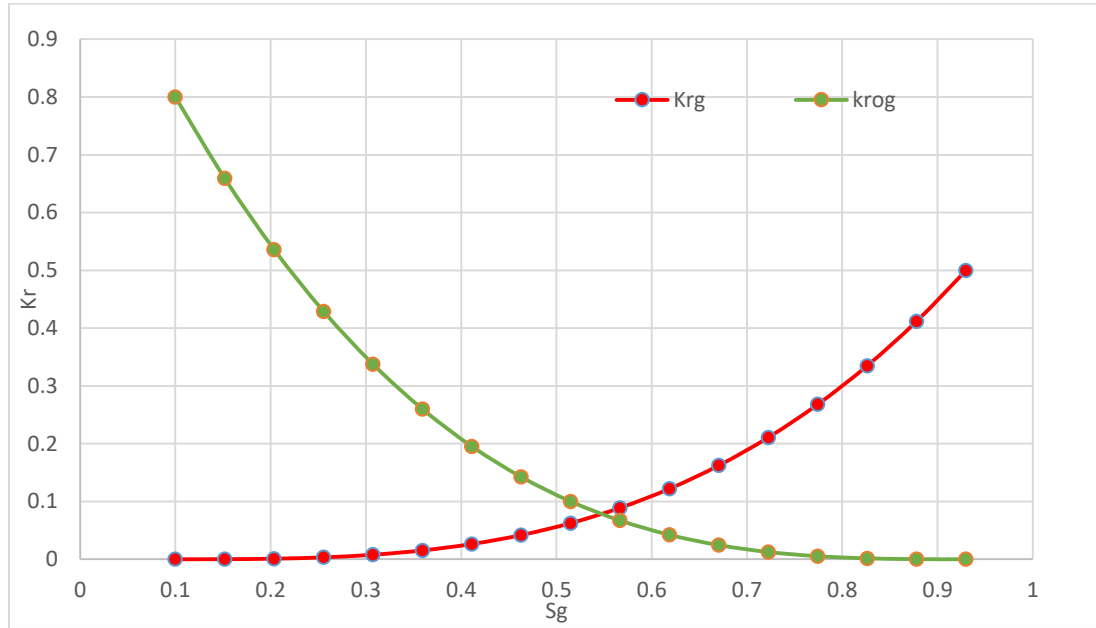


Figure 6.15 Fracture Relative Permeability Data (Oil-Gas).

6.1.4 Well Trajectory and Completion.

Well trajectory values were imported to CMG, along with completion data as can be seen in Figure 6.16 and Table 6.3.

Table 6.3 SA-01 Well Data

Well Name	SA-01
Production Date	11th November 2013
Well Profile	Horizontal Well
Total Drilled Depth	15,900 ft
Total Vertical Depth	13,504.5 ft
Formation	Najmah MFS
Perforations	15,850 ft – 15,275ft (575ft)

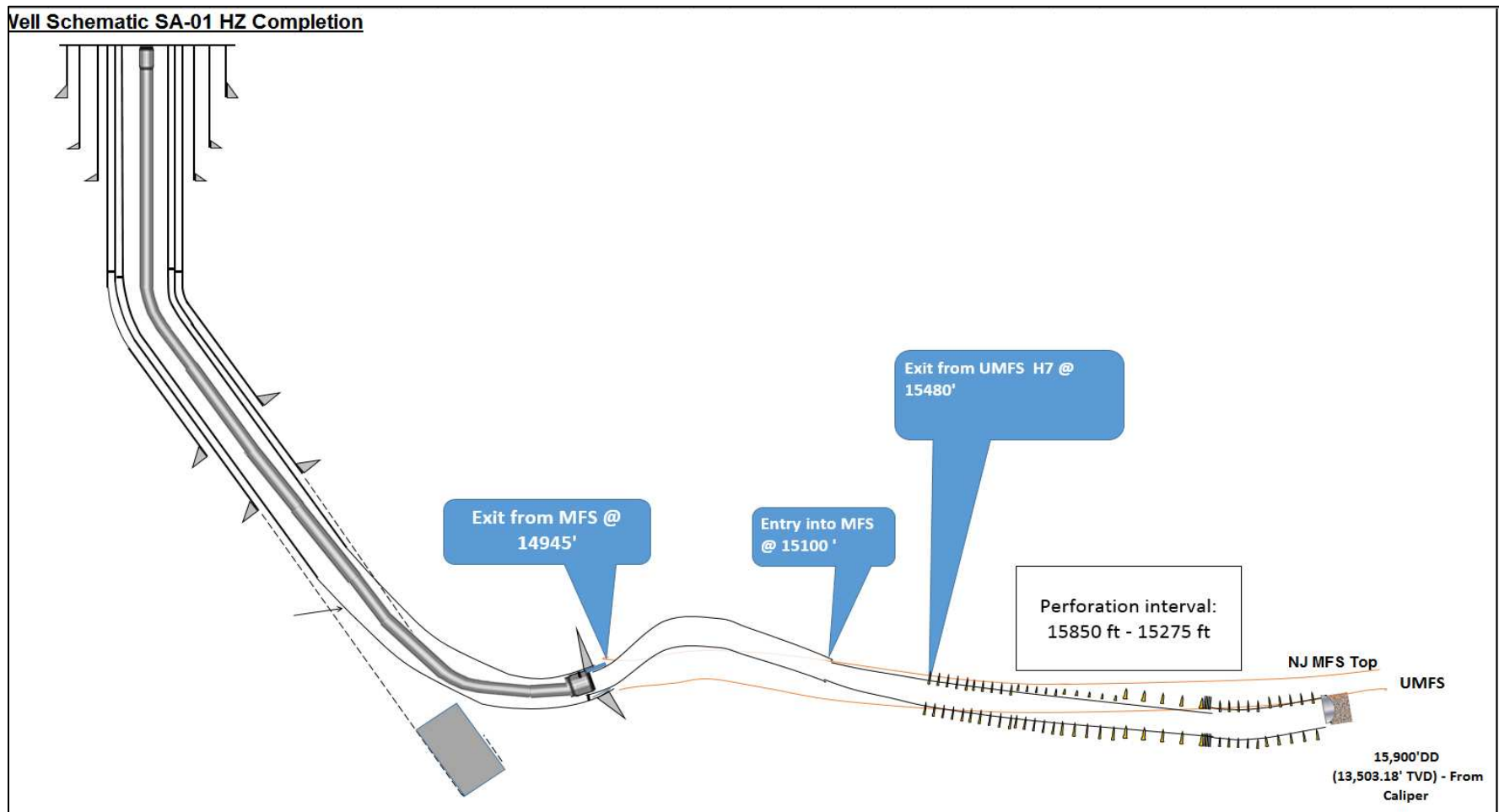


Figure 6.16 SA-01 Well Schematic.

The well was drilled in a deviated matter, and having two types of completion, cemented until perforation section, when it is switched to open hole completion. Figure 6.17 shows path of well along formations.

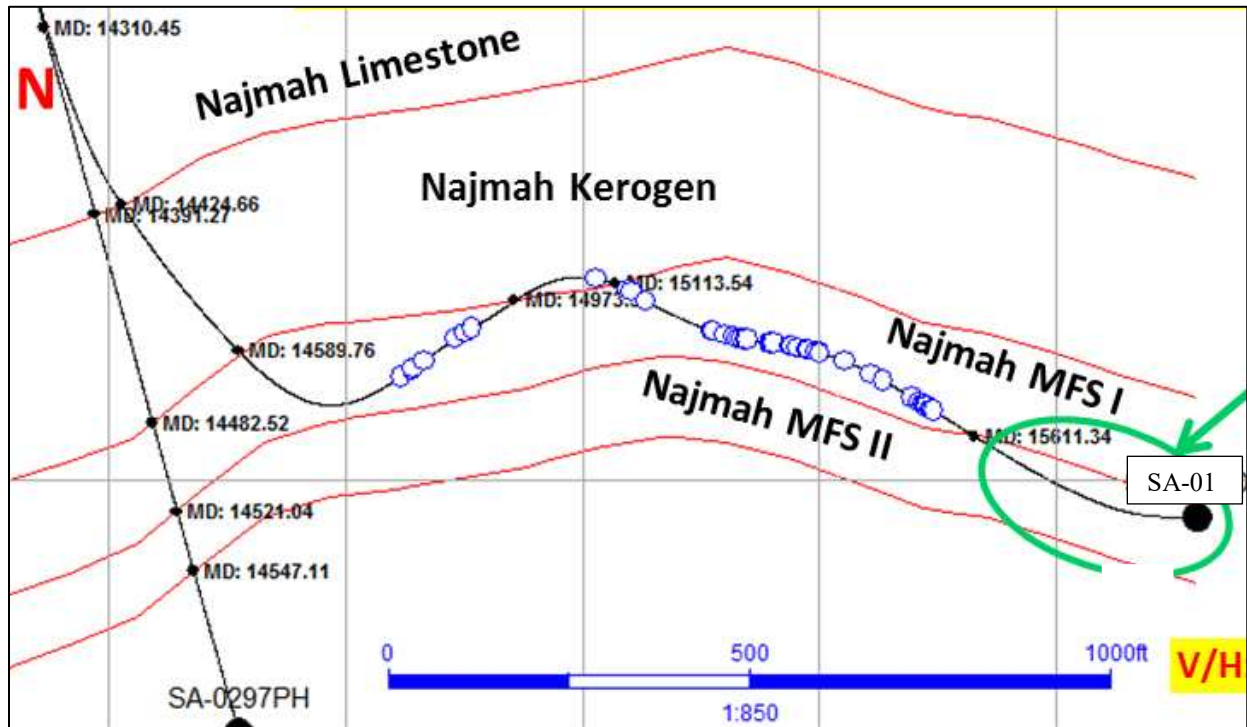


Figure 6.17 Well path along Jurassic formations.

6.1.5 Well Production.

SA-01 started producing in November 2013, the well is producing at a pressure above the dew point (5241 psia). Figure 6.19 shows the well's BHP and WHP on a fixed choke size of 16/64".

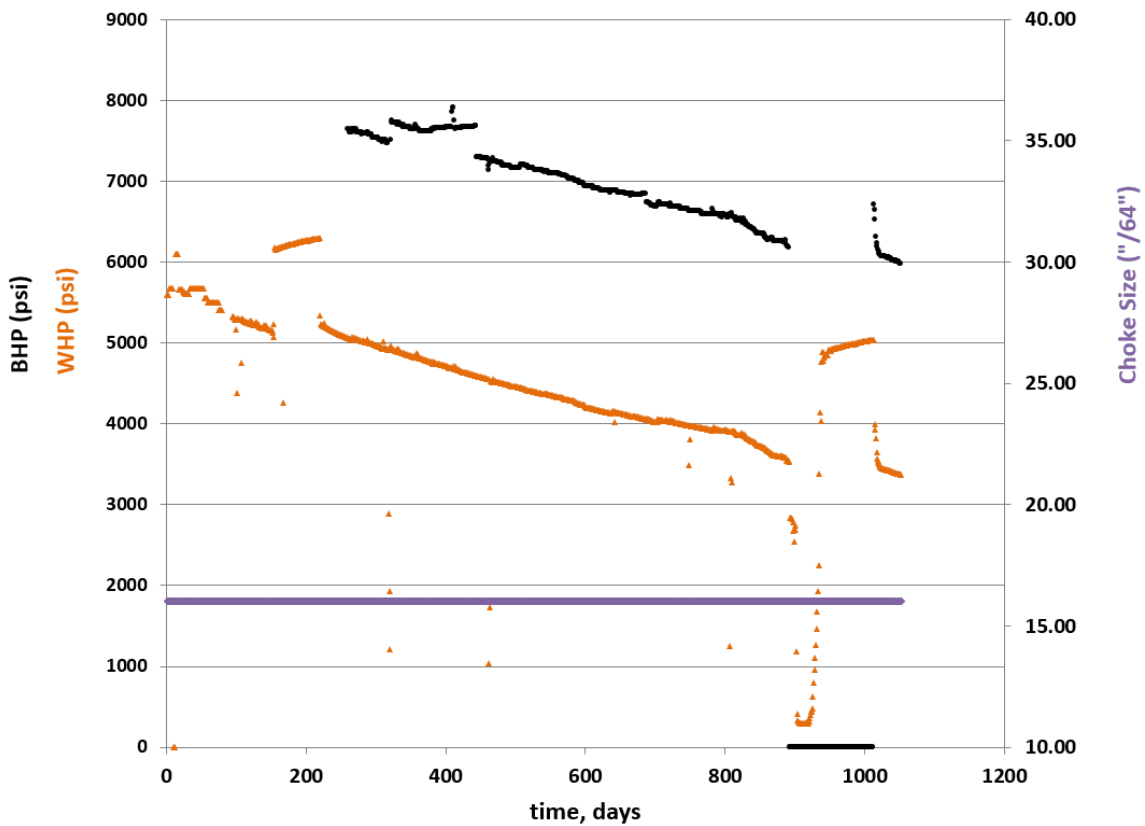


Figure 6.18 BHP and WHP data for SA-01.

The cumulative production up to November 2016 is 4.01 Billion SCF of gas, and 1.1 Million STB of oil. Figure 6.19 shows the daily production of gas, water and oil. It is interesting to point out that the average gas production ranges 4 to 6 MMscf/day. And in the case of water, the production history showed no water production up until September 2016, which was attributed to completion issues as water enters from other formations.

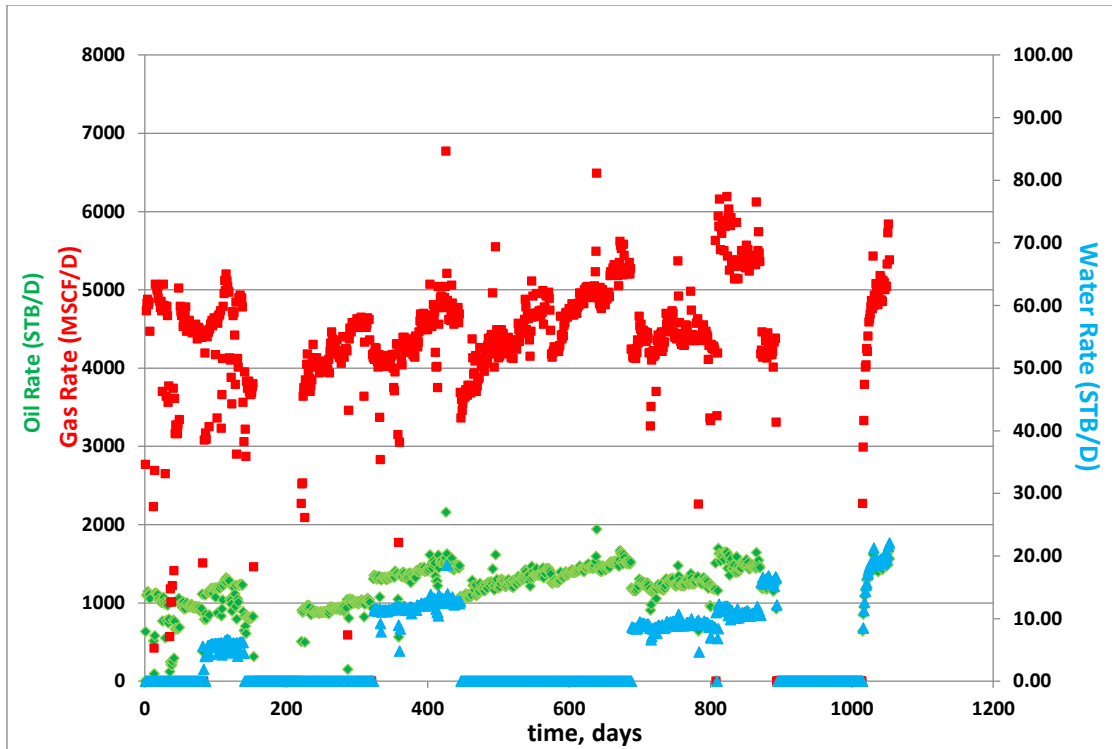


Figure 6.19 SA-01 Production history for oil, water, and gas.

The above data has been incorporated into the model, considering a base constraint of constant gas rate: 2.7 MMscf/day.

6.2 History Matching

To ensure a reliable future forecast, history matching is an essential step in reservoir modeling. It is often an iterative process of modifying uncertain parameters of a reservoir to get a satisfactory match with the actual history data of flow rate and pressure (Netto et al. 2003). Hence, when performing history matching, there are two types of parameters to distinguish:

- Reliable parameters: such as pressure, hydrocarbon PVT analysis, gross thickness, net to gross cutoff values, fluid flow rates, and well locations (Cosentino 2001)
- Uncertain parameters: reservoir permeability, porosity, relative permeability, capillary pressure, reservoir fluid properties, rock properties, water properties and fluid contacts (Mattax and Dalton 1990).

A sensitivity analysis was performed on key fracture parameters, to identify which has a significant impact on the model. The fracture parameters considered for the sensitivity analysis are: effective fracture permeability, fracture porosity, and fracture spacing. Table 6.4 shows the ranges considered for the sensitivity.

Table 6.4 Input parameters for prehistory matching sensitivity analysis

Parameter	Lower range	Middle range	Upper range
$k_{f,eff,(i,j,k)}$ (md)	0.026	0.52	0.78
\emptyset_f	0.01	.02	.03
$L_i L_j$ (ft)	2	5	10
L_k (ft)	2	5	10

The results of the sensitivity analysis indicated that, the model was most effected by fracture porosity and effective fracture permeability, followed by fracture spacing. The optimum combination is indicated in Table 6.5, which showed a good match between history and simulated result across the 3 years of production.

Table 6.5 Modified parameters in history matching process

Property	Modified Values
$k_{f,i}$ (md)	variant based on new $k_{f,eff}$
$k_{f,j}$ (md)	variant based on new $k_{f,eff}$
$k_{f,k}$ (md)	variant based on new $k_{f,eff}$
$k_{f,eff,(i,j,k)}$ (md)	0.52
\emptyset_f	0.01
$L_i L_j$ (ft)	5
L_k (ft)	10

The model was constrained by gas rate while reservoir properties were changed to match average reservoir pressure and condensate production rate. Figure 6.20 shows the match between actual and simulated well bottom hole pressure and Figure 6.21 illustrates the match between actual and simulated gas rate. As indicated above, the uncertain parameters of effective fracture permeability, fracture porosity, and fracture spacing of the model were altered to achieve this match.

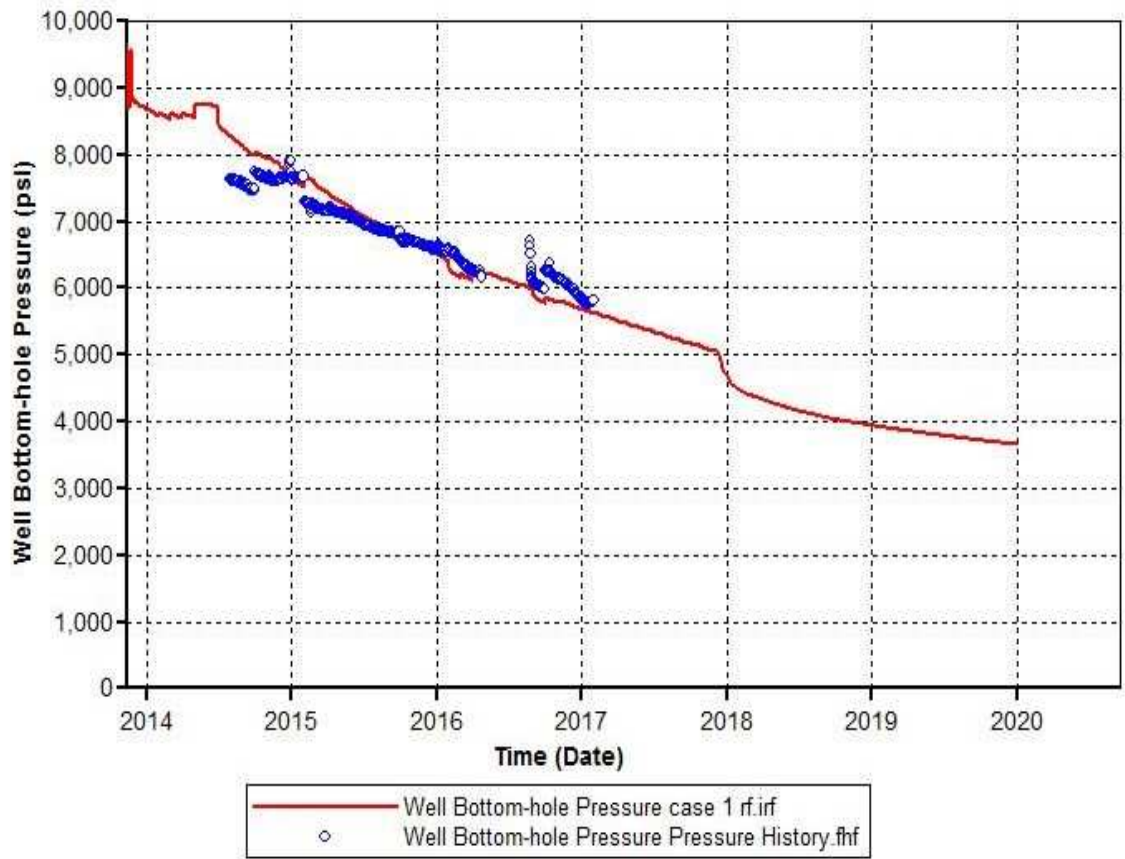


Figure 6.20 SA-01 well bottom hole pressure simulated VS actual.

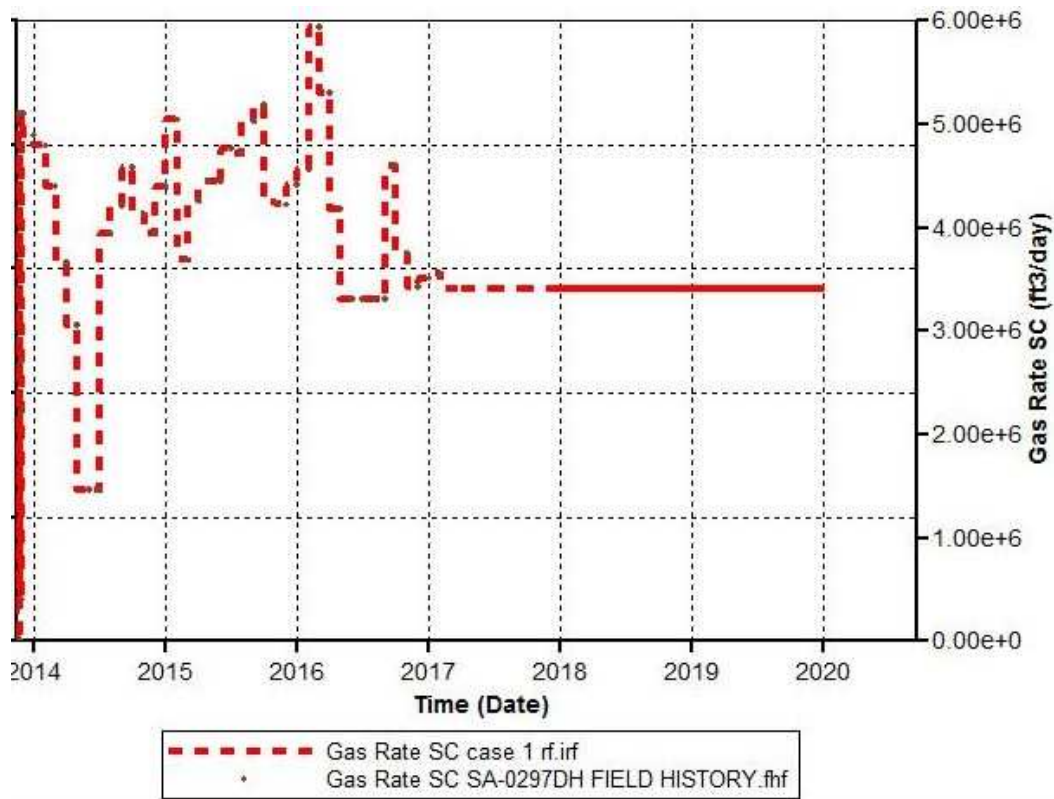


Figure 6.21 SA-01 Gas rate simulated VS actual.

6.3 Hydraulic Fracturing

This section discusses the 3-stage fracturing applied on all 6 cases described earlier (Table 6.6), comparing the cumulative hydrocarbon produced before and after, and evaluating the feasibility of the hydraulic fracturing technique in well SA-01.

Table 6.6 Model cases description for SA-01.

Case No.	Constraint	Water Saturation
1	Constant rate: 2.7 MMscf/day	variant
2	Constant rate: 2.7 MMscf/day	irreducible
3	Constant rate: 4 MMscf/day	variant
4	Constant rate: 4 MMscf/day	irreducible
5	Constant rate: 2.7 MMscf/day	variant
6	Constant rate: 2.7 MMscf/day	irreducible

6.3.1 Case 1: Constant Rate: 2.7MMscf/day, Water Saturation Variant.

Case 1 is the base case scenario, and when applying a three stage fracture system, the behavior profile for bottom hole pressure (BHP) shows an increase of almost 300 psi from time of application as seen on Figure 6.22. However, due to having the gas flow rate as constraint for operation, the model is forced into mimicking the same production with and without hydraulic fracture (HF), as can be observed in flow rate and cumulative rate behaviors in Figures 6.23 to 6.29.

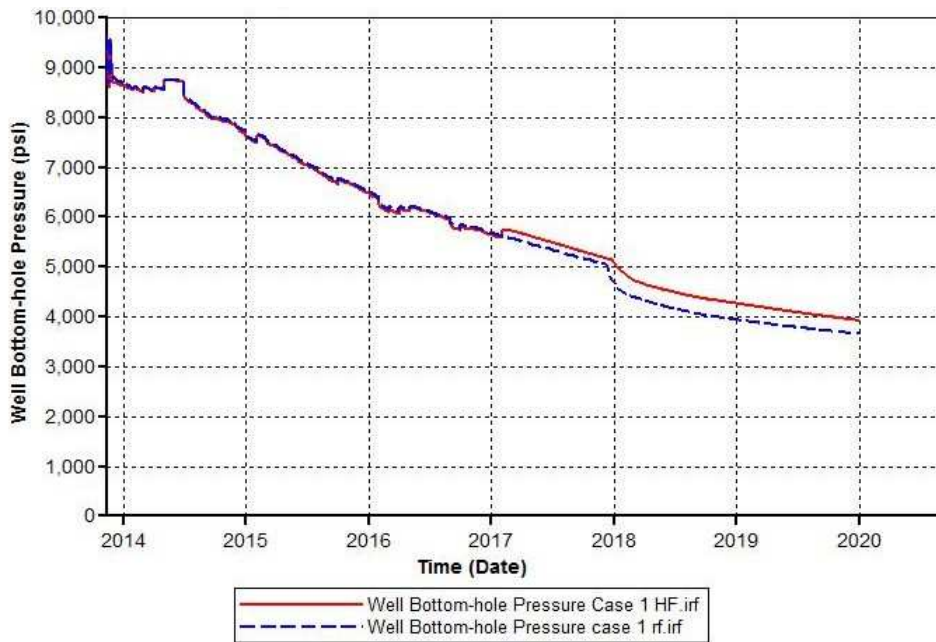


Figure 6.22 Case 1, comparative plot of BHP with and without HF.

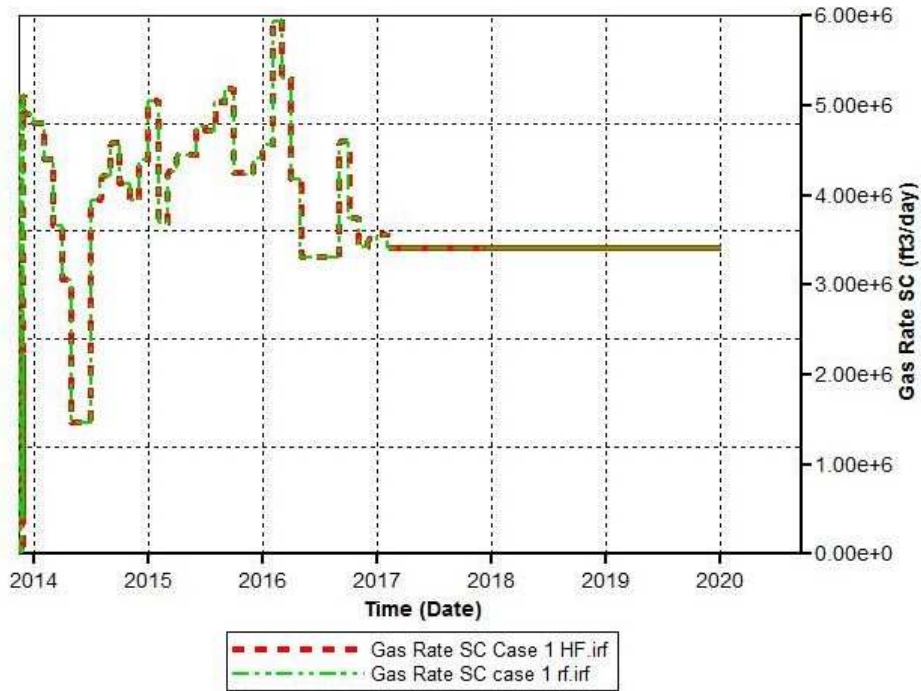


Figure 6.23 Case 1, comparative plot for gas rate with and without HF.

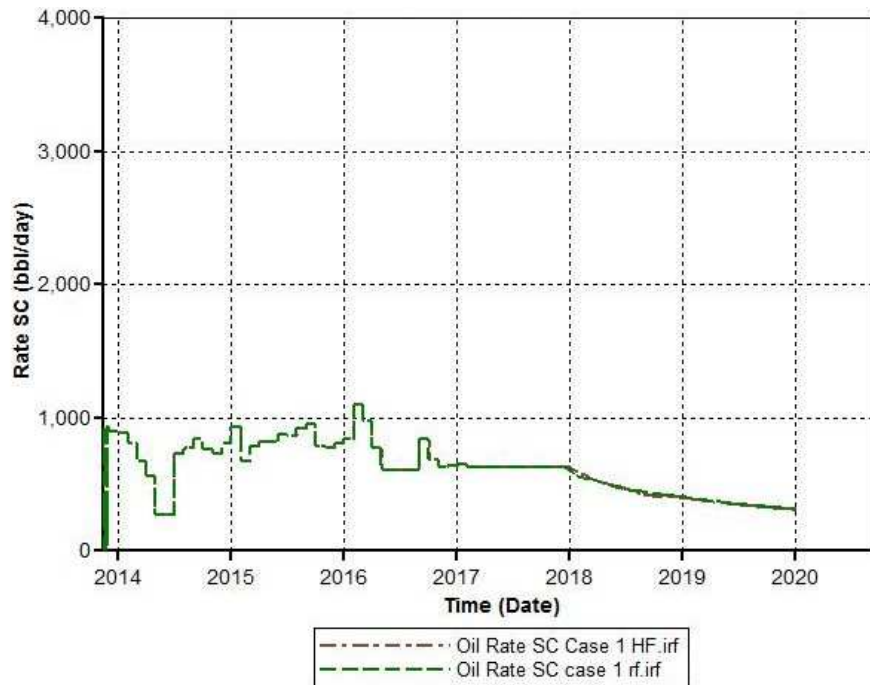


Figure 6.24 Case 1, comparative plot for oil rate with and without HF.

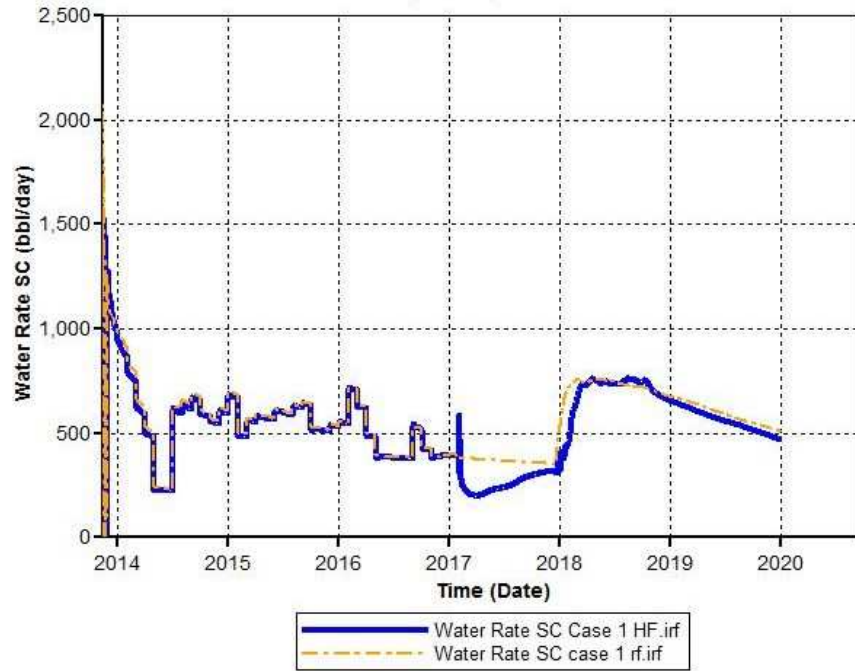


Figure 6.25 Case 1, comparative plot for water rate with and without HF.

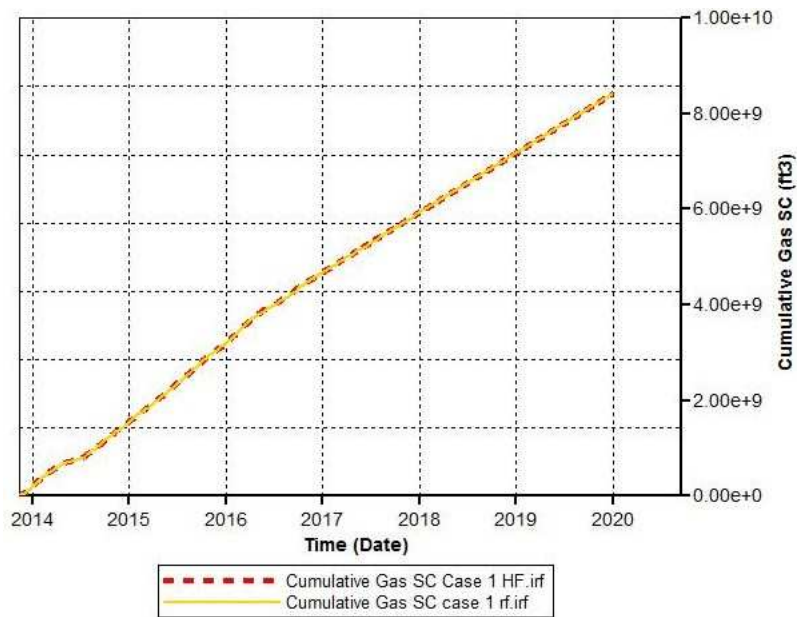


Figure 6.26 Case 1, comparative plot for cumulative gas with and without HF.

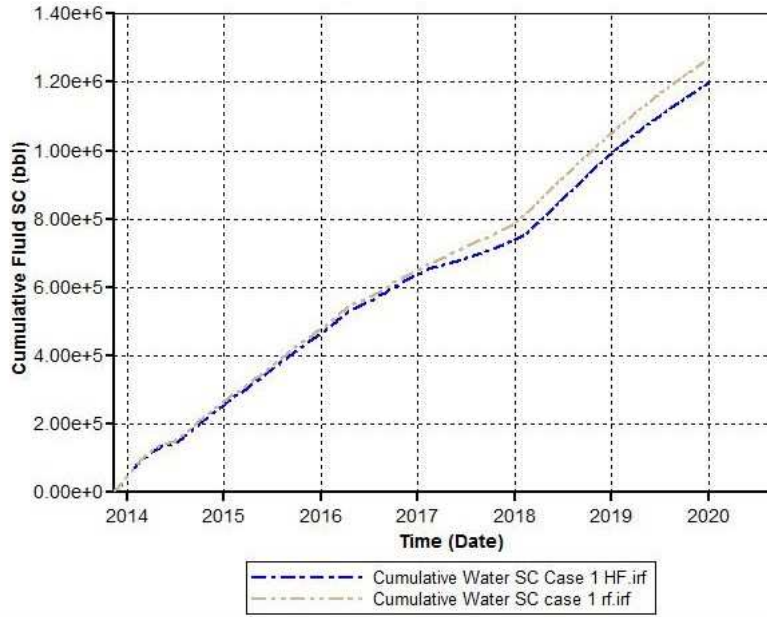


Figure 6.27 Case 1, comparative plot for cumulative water with and without HF.

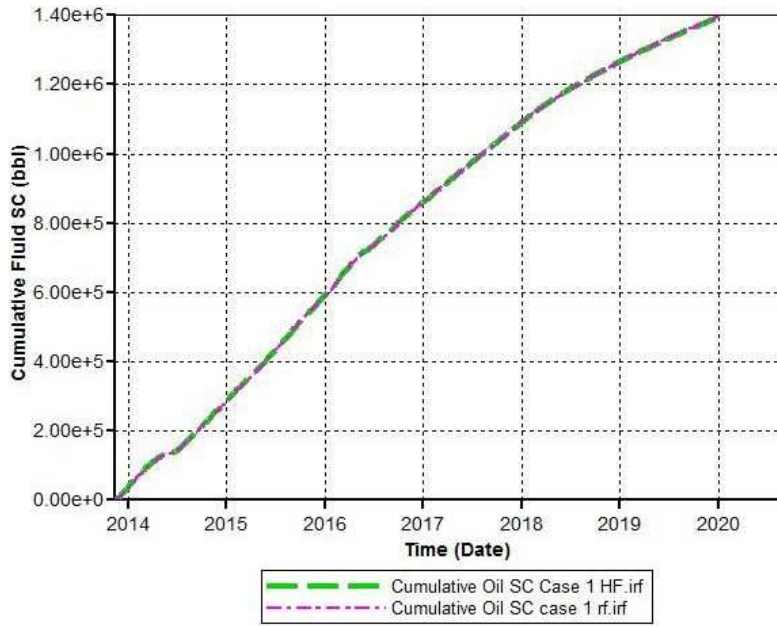


Figure 6.28 Case 1, comparative plot for cumulative oil with and without HF.

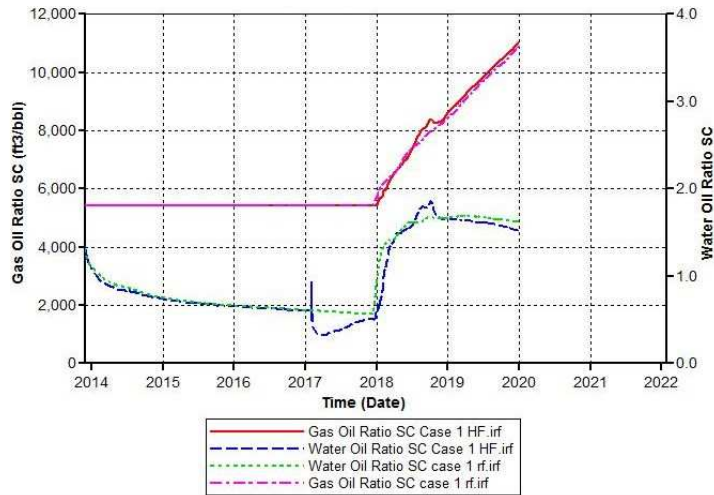


Figure 6.29 Case 1, comparative plot for GOR and WOR with and without HF.

6.3.2 Case 2: Constant Rate: 2.7 MMscf/day, Irreducible.

Case 2 is different than Case 1 in the water saturation treatment, where it is constrained to irreducible status. Again, bottom hole pressure shows an increase of 300 psi, and then gradually matches original profile of BHP by 2019, see Figure 6.30 to Figure 6.34. In terms of response with and without hydraulic fracture, the same behavior is observed as in case 1, due to flow rate operation constraint. The GOR is constant throughout at a value of 5814.6 scf/bbl.

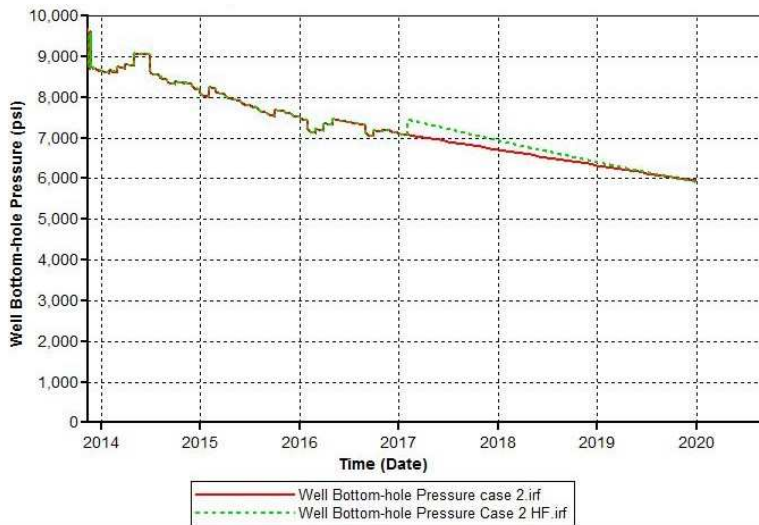


Figure 6.30 Case 2, comparative Plot for well BHP with and without HF.

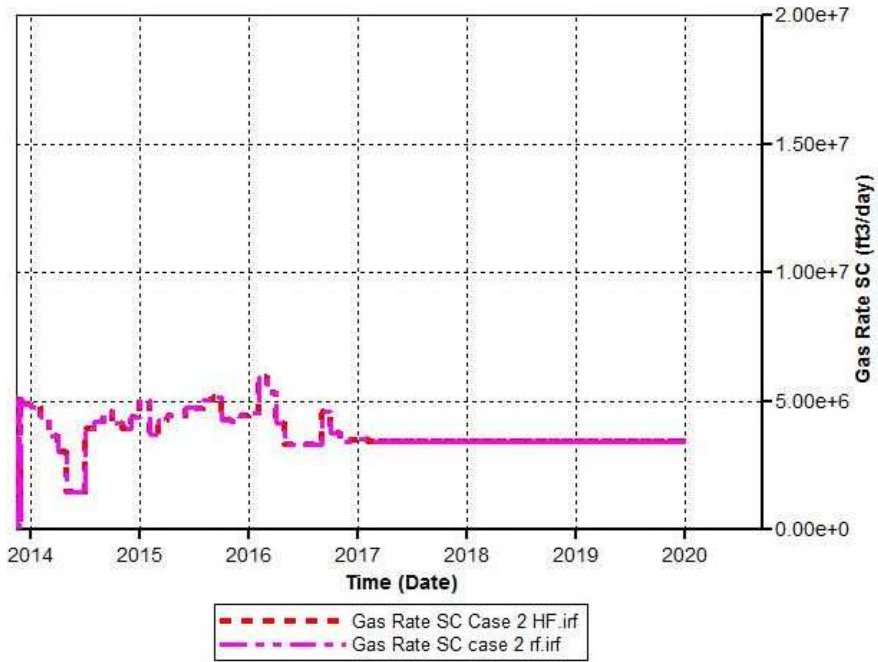


Figure 6.31 Case 2, comparative plot for gas rate with and without HF.

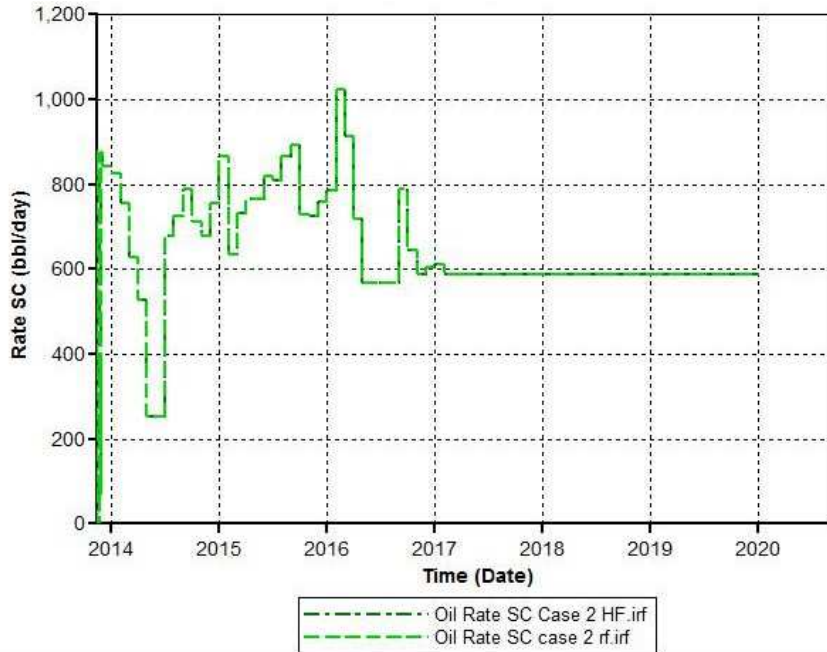


Figure 6.32 Case 2, comparative plot for oil rate with and without HF.

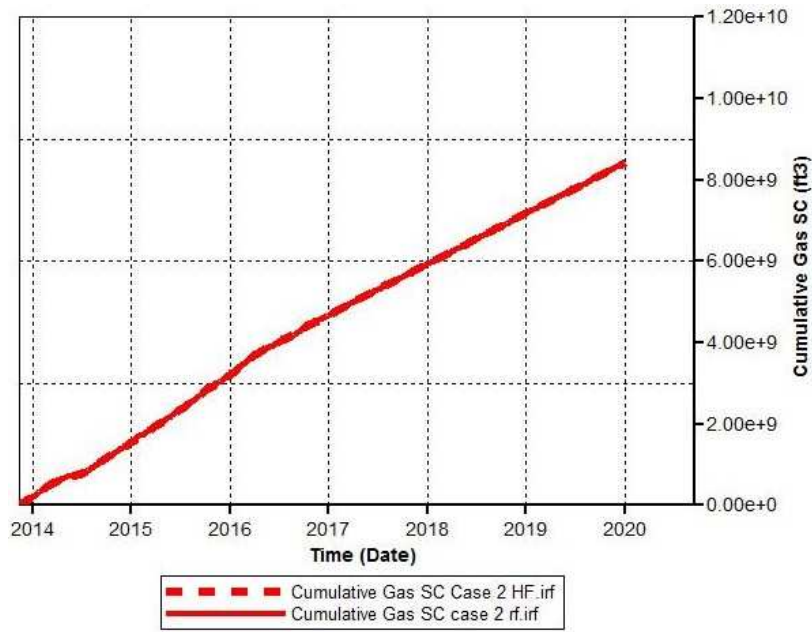


Figure 6.33 Case 2, comparative plot for cumulative gas with and without HF.

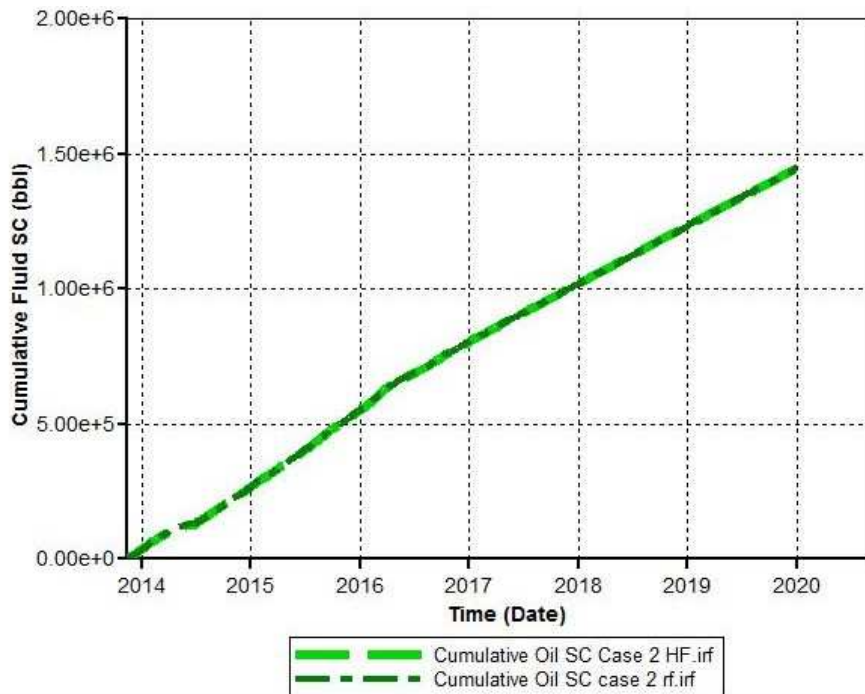


Figure 6.34 Case 2, comparative for cumulative oil with and without HF.

6.3.3 Case 3: Constant Rate: 4 MMscf/day, Water Saturation Variant.

In Case 3, we changed the operation constraint of gas flowing rate from 2.7 MMscf/day to 4 MMscf/day, keeping water saturation as variant. Here we see minimal changes in any of the fluid or pressure behaviors, as can be seen in Figures 6.35 to 6.42, except for a slight decrease in water production as seen in Figure 6.41.

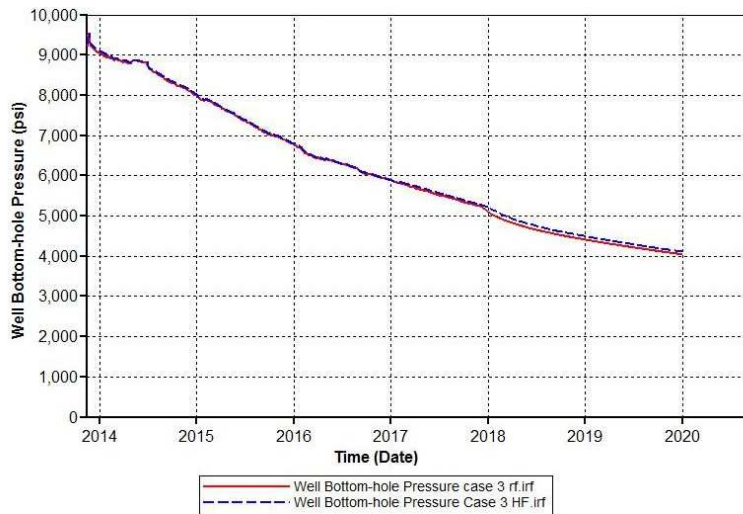


Figure 6.35 Case 3, comparative plot of well BHP with and without HF.

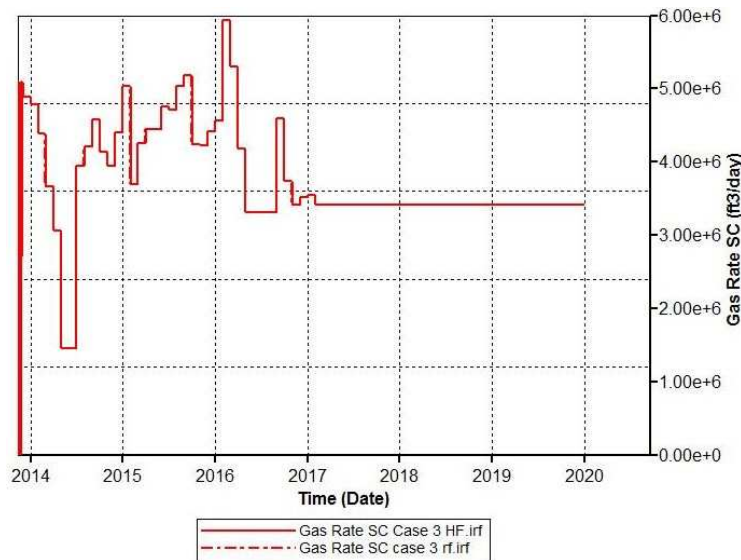


Figure 6.36 Case 3, comparative plot of gas rate with and without HF.

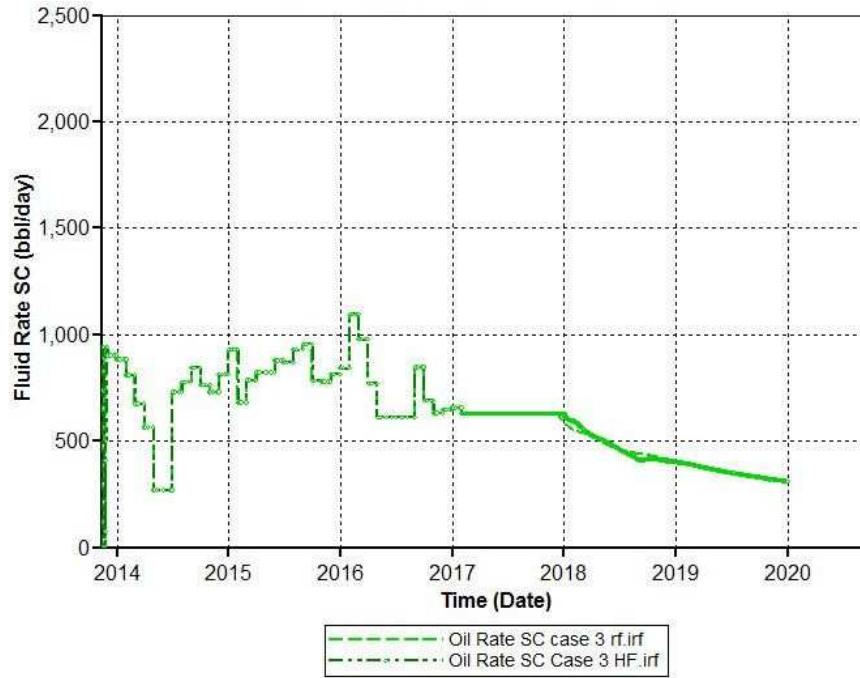


Figure 6.37 Case 3, comparative plot for oil rate with and without HF.

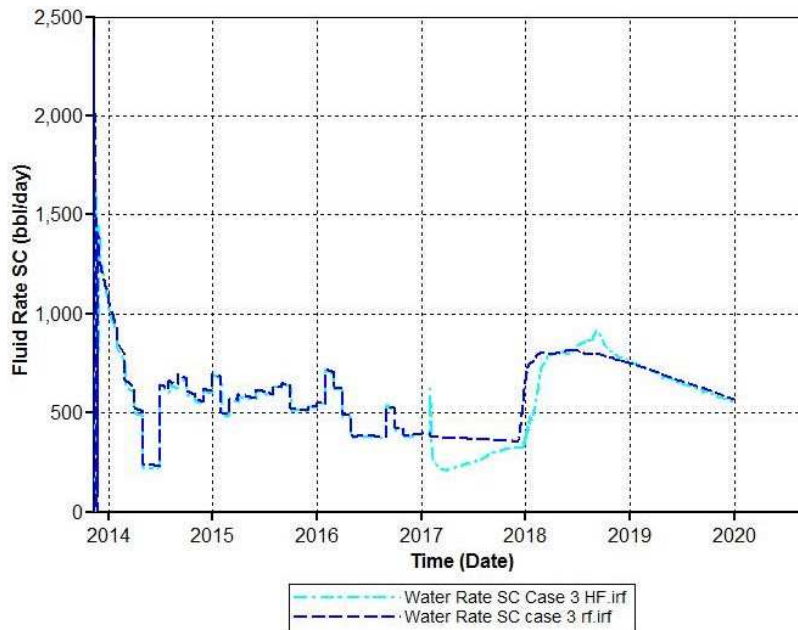


Figure 6.38 Case 3, comparative plot for water rate with and without HF.

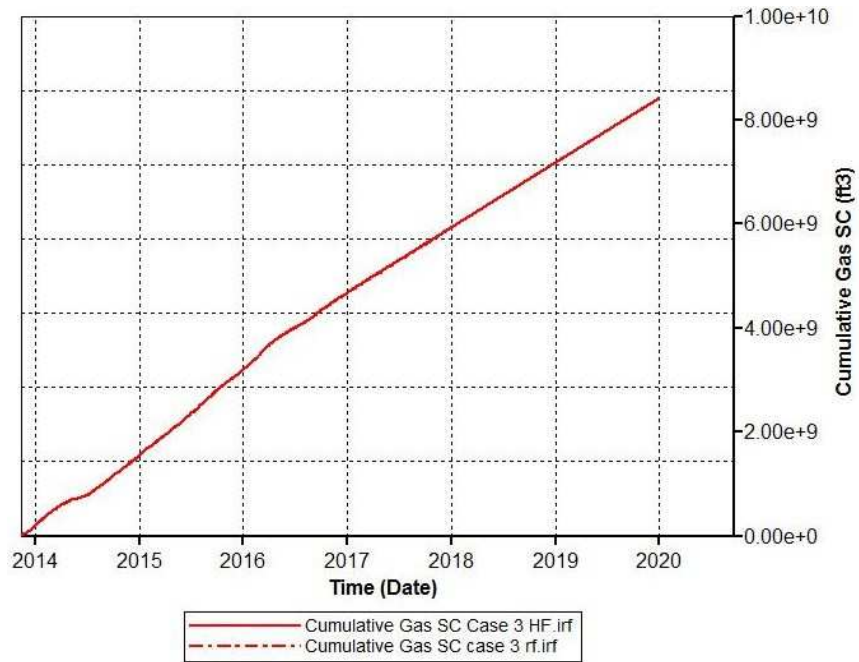


Figure 6.39 Case 3, comparative plot for cumulative gas with and without HF.

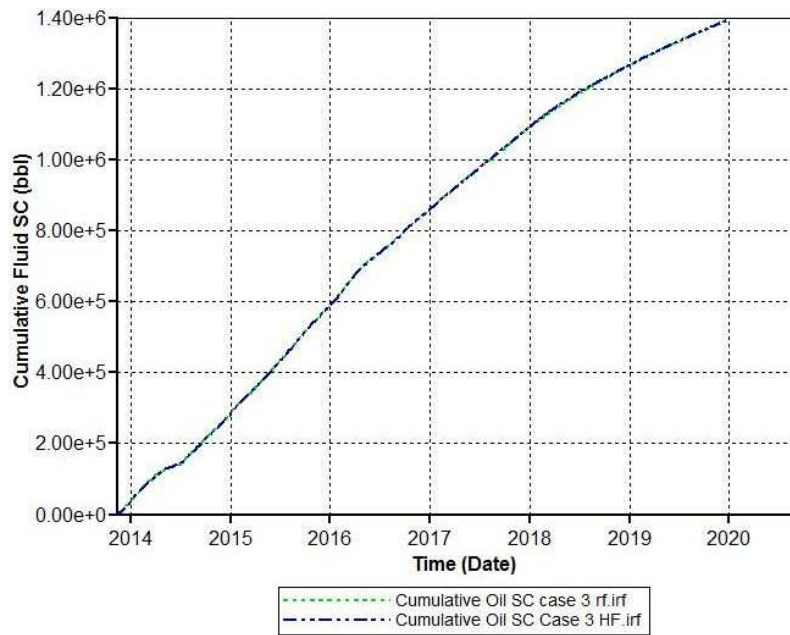


Figure 6.40 Case 3, comparative plot of cumulative oil with and without HF.

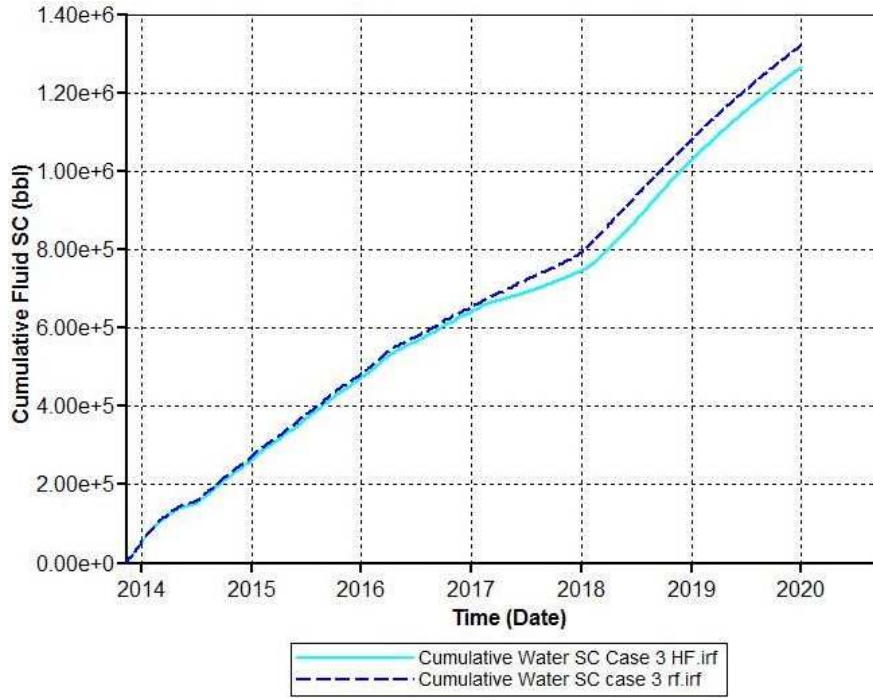


Figure 6.41 Case 3, comparative plot of cumulative water with and without HF.

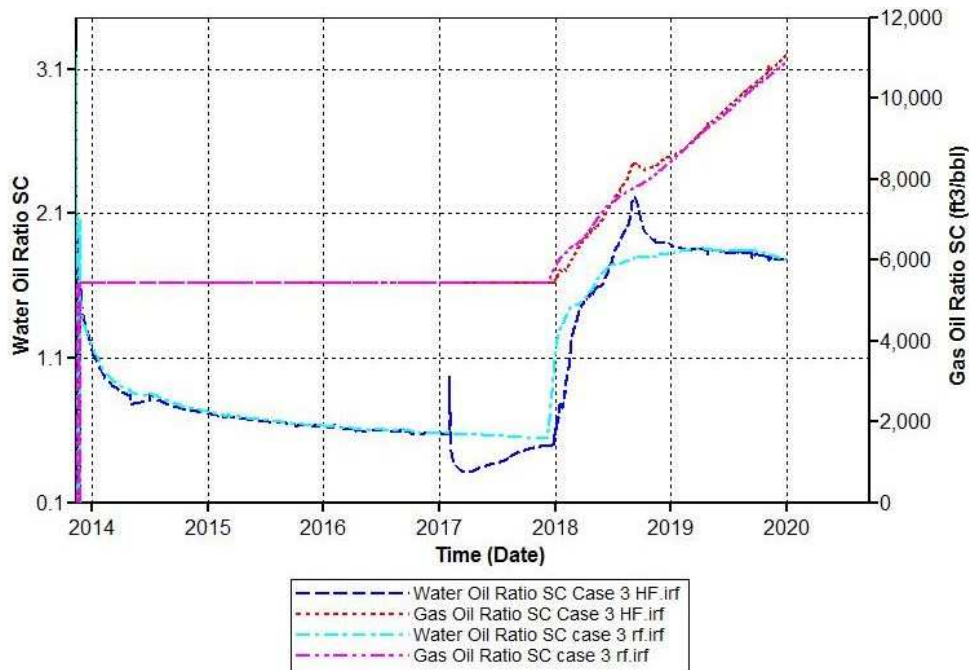


Figure 6.42 Case 3, comparative plot of WOR and GOR with and without HF.

6.3.4 Case 4: Constant Rate: 4 MMscf/day, Water Saturation Variant.

Case 4 is different than Case 3 in the water saturation treatment, where it is constrained to irreducible status. In terms of fluid and pressure behavior, there is no significant change after implementing the three stage hydraulic fracture. See Figures 6.43 to 6.47

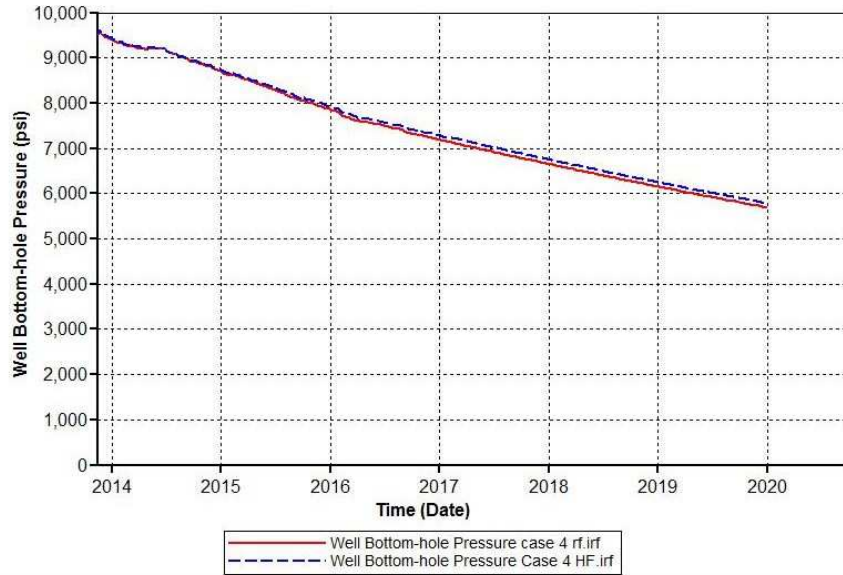


Figure 6.43 Case 4, comparative plot for well BHP with and without HF.

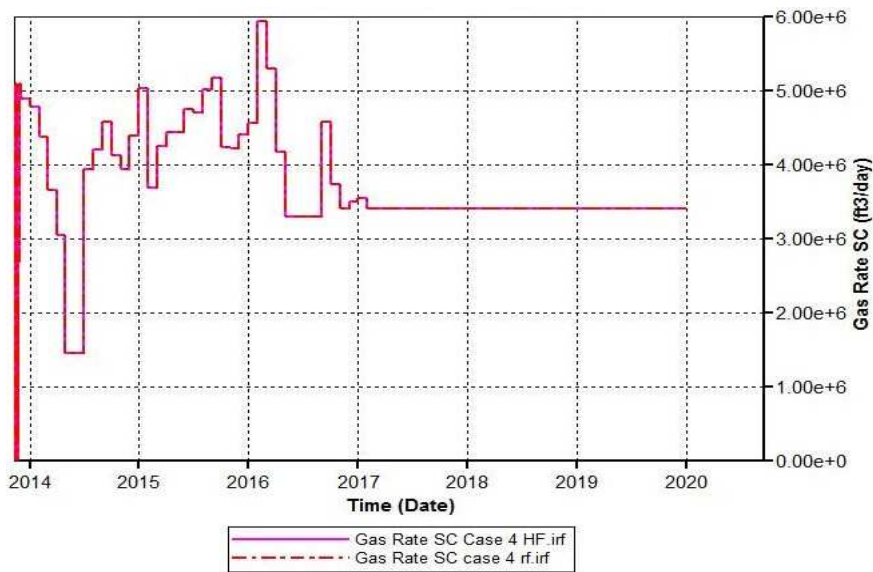


Figure 6.44 Case 4, comparative plot for gas rate with and without HF.

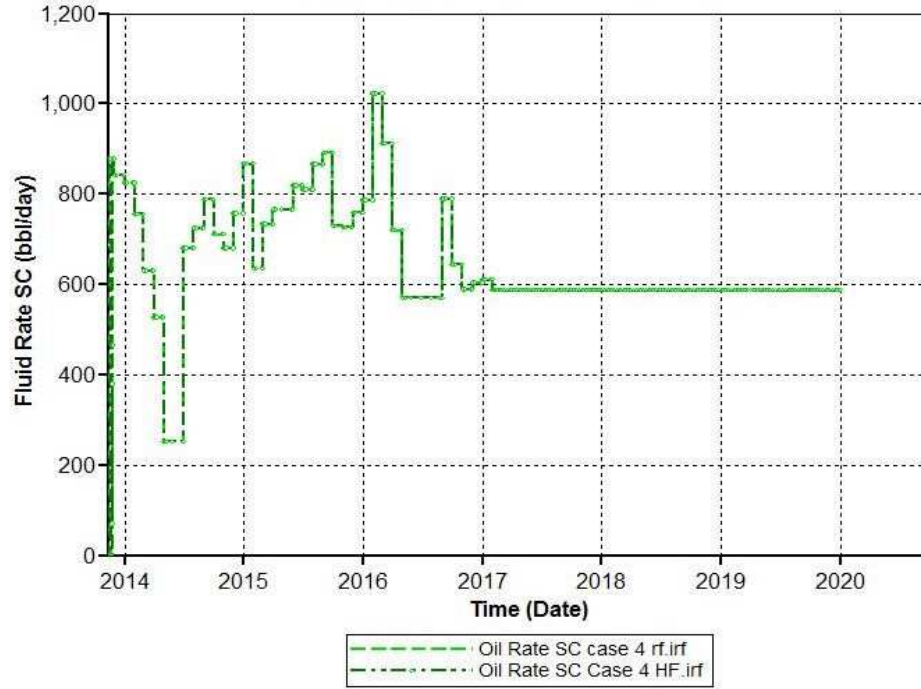


Figure 6.45 Case 4, comparative plot for oil rate with and without HF.

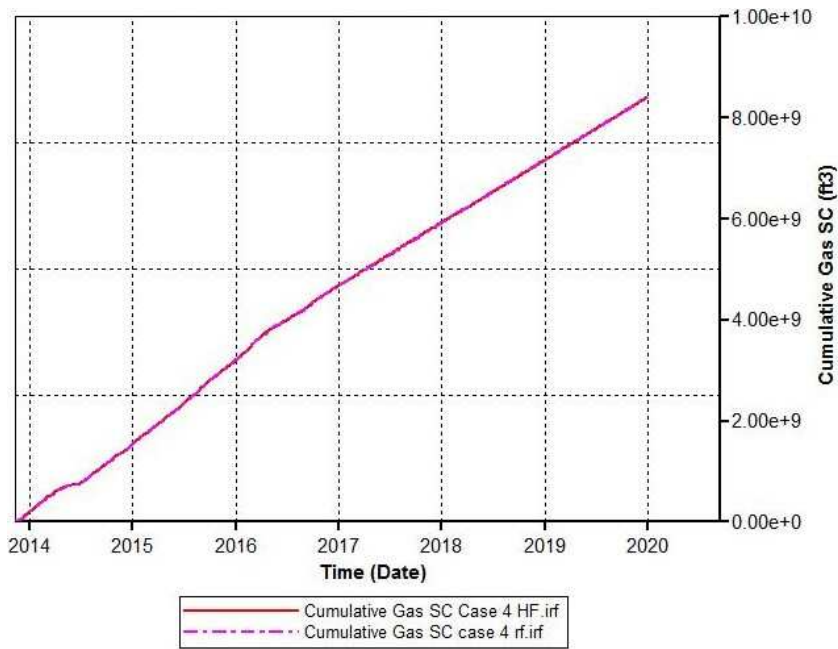


Figure 6.46 Case 4, comparative plot for cumulative gas fluid with and without HF.

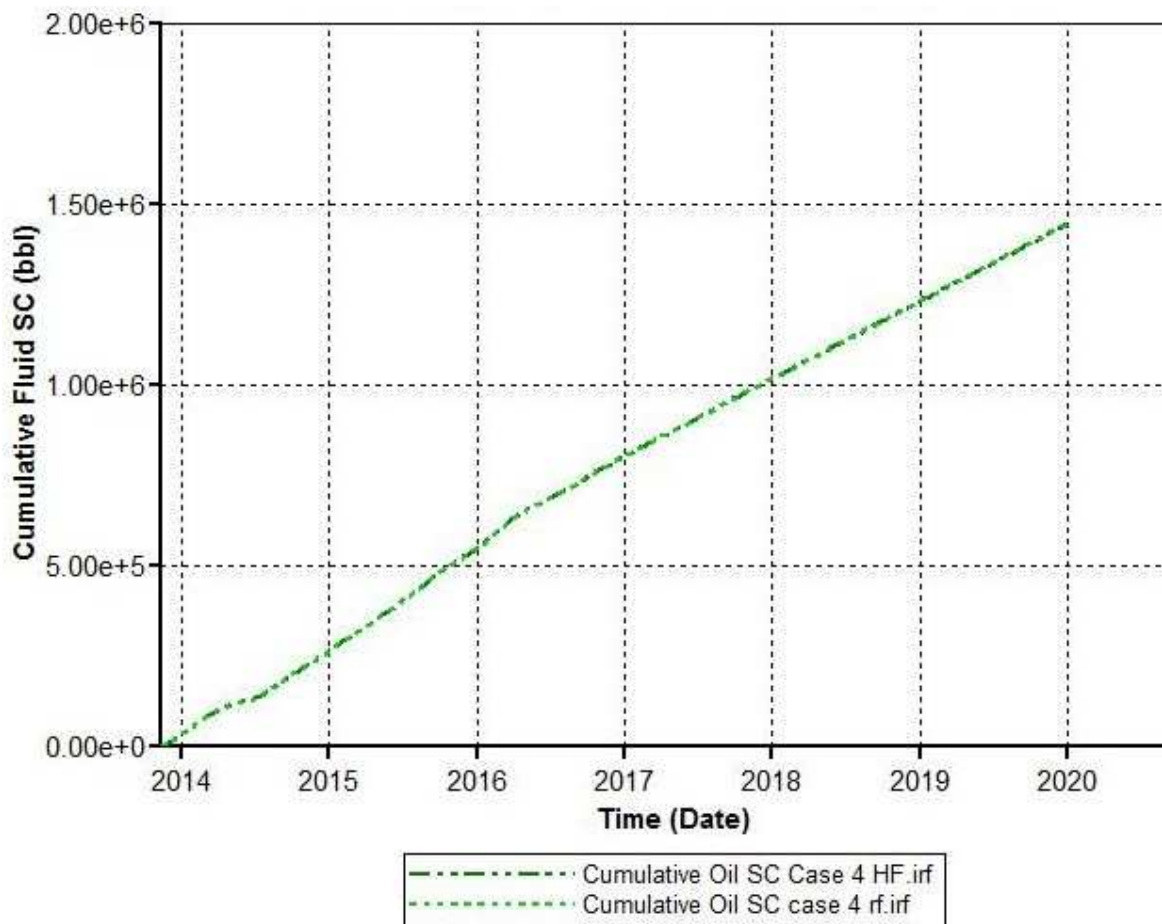


Figure 6.47 Case 4, comparative plot for cumulative oil fluid with and without HF.

6.3.5 Case 5: Constant Rate: 2.7MMscf/day, switched to Constant Pressure.

Case 5 has the original gas flow rate of 2.77 MMscf/day, and an additional constraint at end of history production (2017) switching to constant pressure control of 4000 psi. The initial water saturation is different. the figures below indicate the fluid and pressure behavior (Figures 6.48 to 6.55).

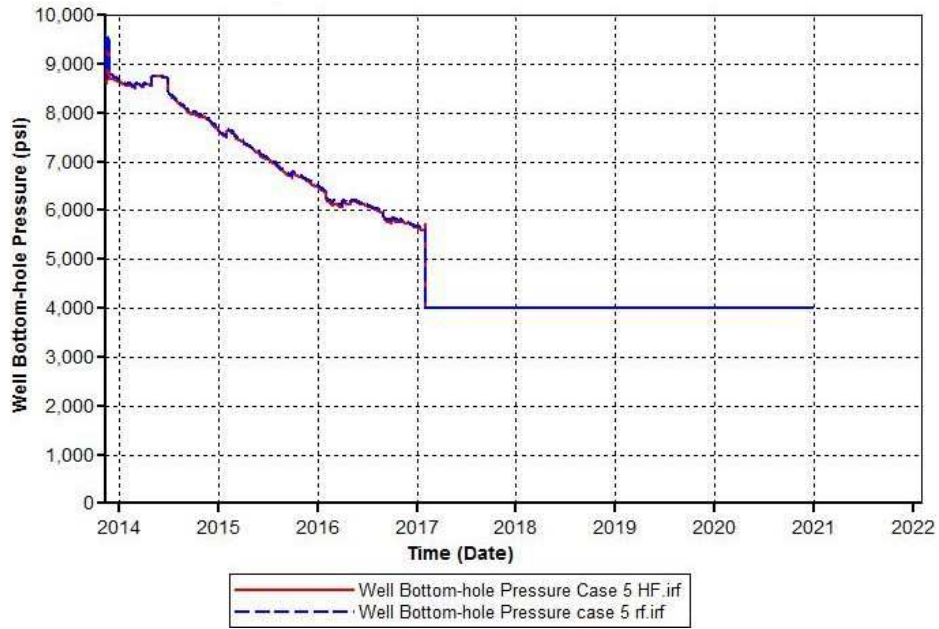


Figure 6.48 Case 5, comparative plot for well BHP with and without HF.

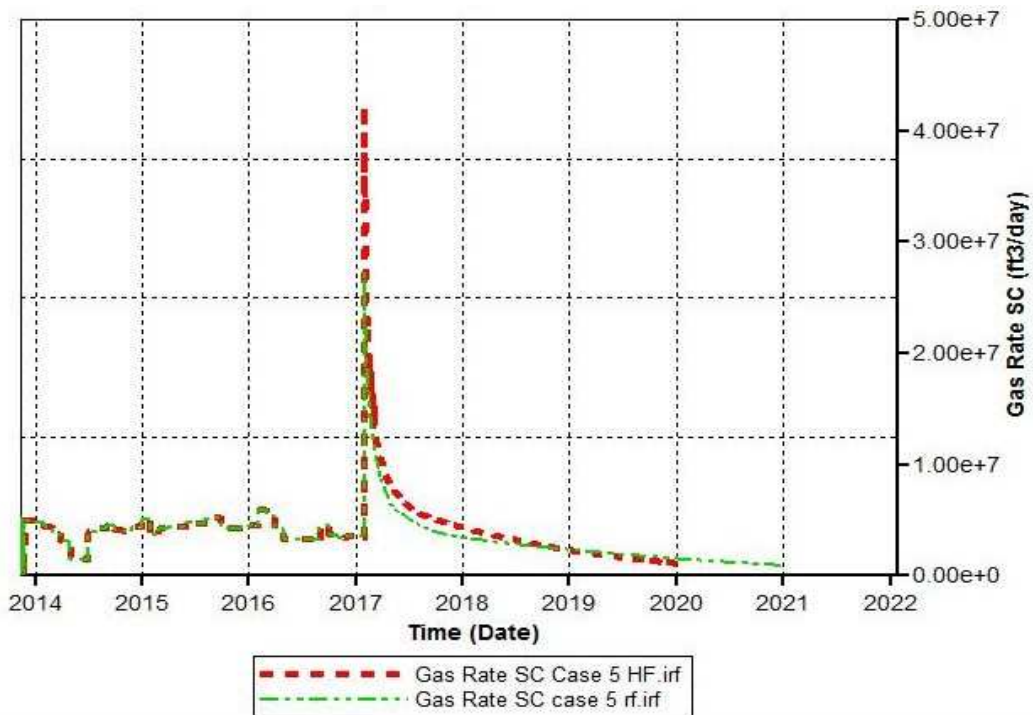


Figure 6.49 Case 5, comparative plot for gas rate with and without HF.

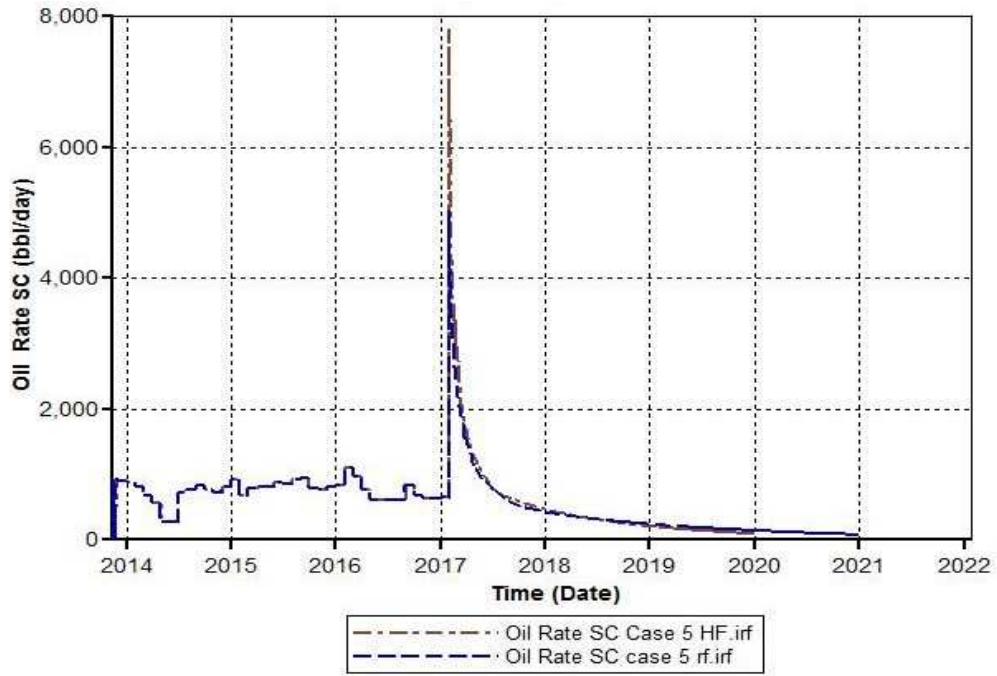


Figure 6.50 Case 5, comparative plot for oil rate with and without HF.

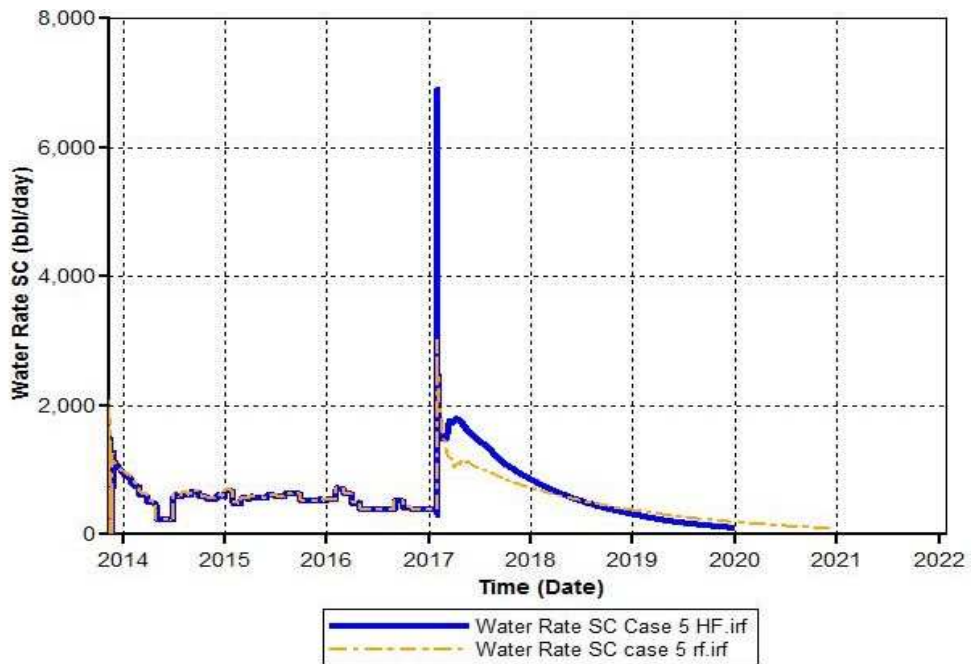


Figure 6.51 Case 5, comparative plot for water rate with and without HF.

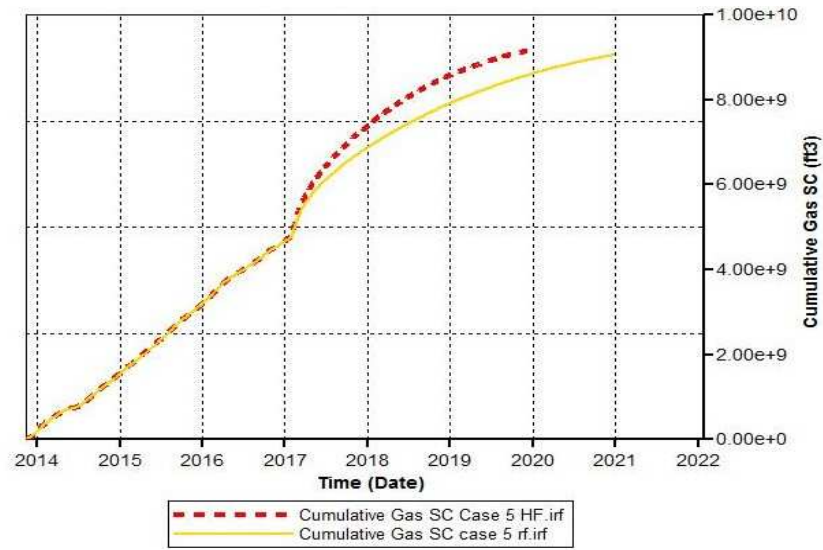


Figure 6.52 Case 5, comparative plot for cumulative gas with and without HF.

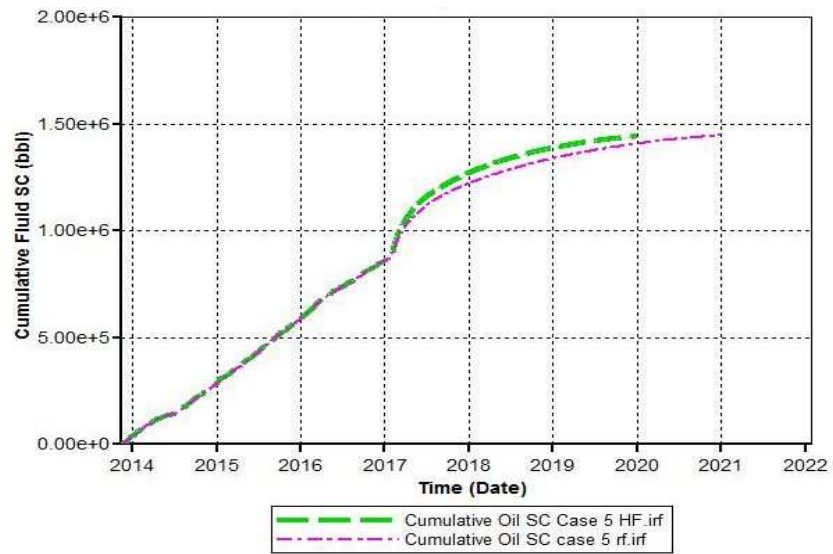


Figure 6.53 Case 5, comparative plot for cumulative oil with and without HF.

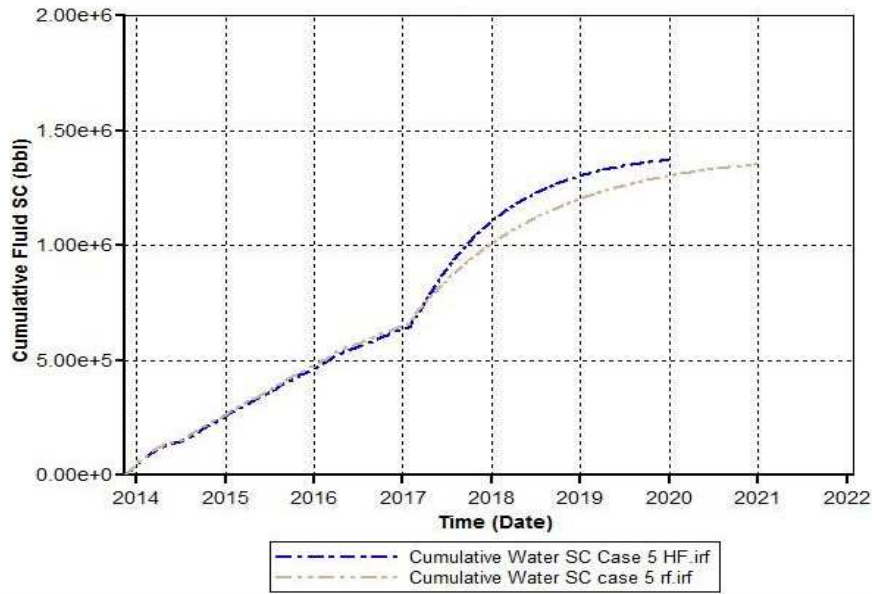


Figure 6.54 Case 5, comparative plot for cumulative water with and without HF.

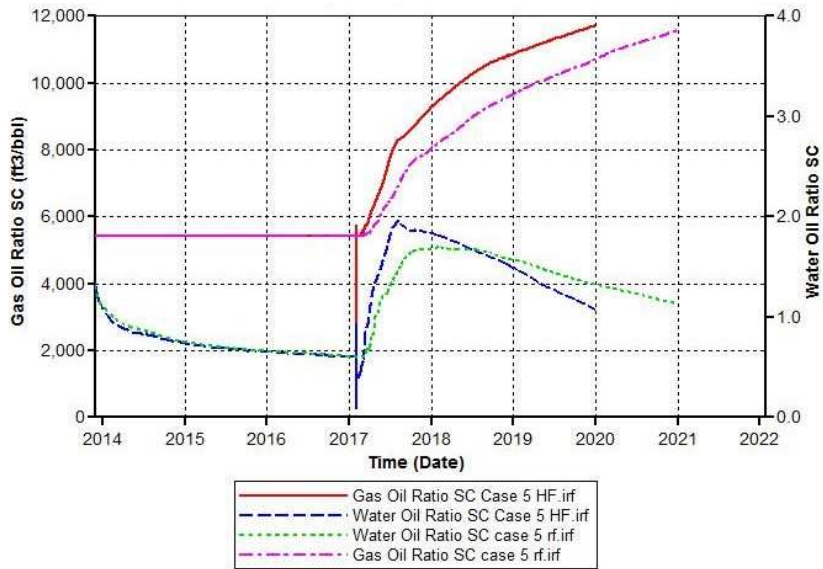


Figure 6.55 Case 5, comparative plot for WOR and GOR with and without HF.

6.3.6 Case 6: Constant Rate: 2.7MMscf/day, switched to Constant Pressure, Immobile Sw

Case 6 is following on the trend of Case 5 with the addition of switching water saturation to irreducible status. Examining fluid and pressure behavior, it is clear that Case 6 delivers the most favorable results in terms of increased cumulative fluid produced as can be seen from Figures 6.56 to 6.60.

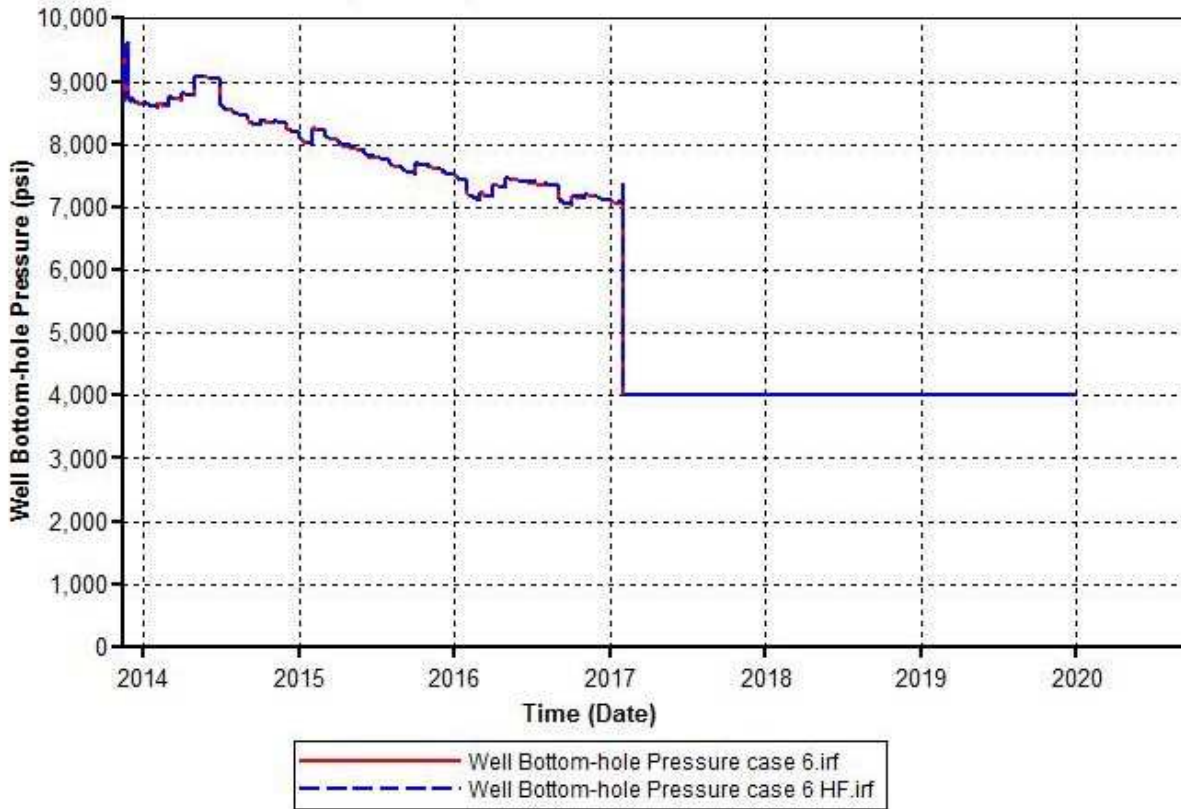


Figure 6.56 Case 6, comparative plot for well BHP with and without HF.

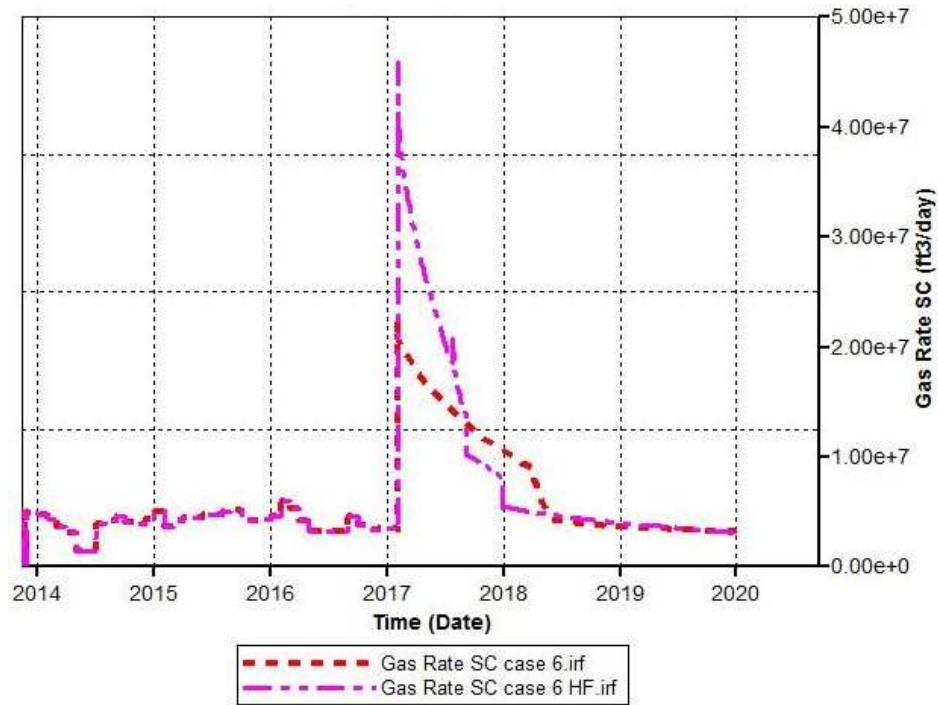


Figure 6.57 Case 6, comparative plot for gas rate with and without HF.

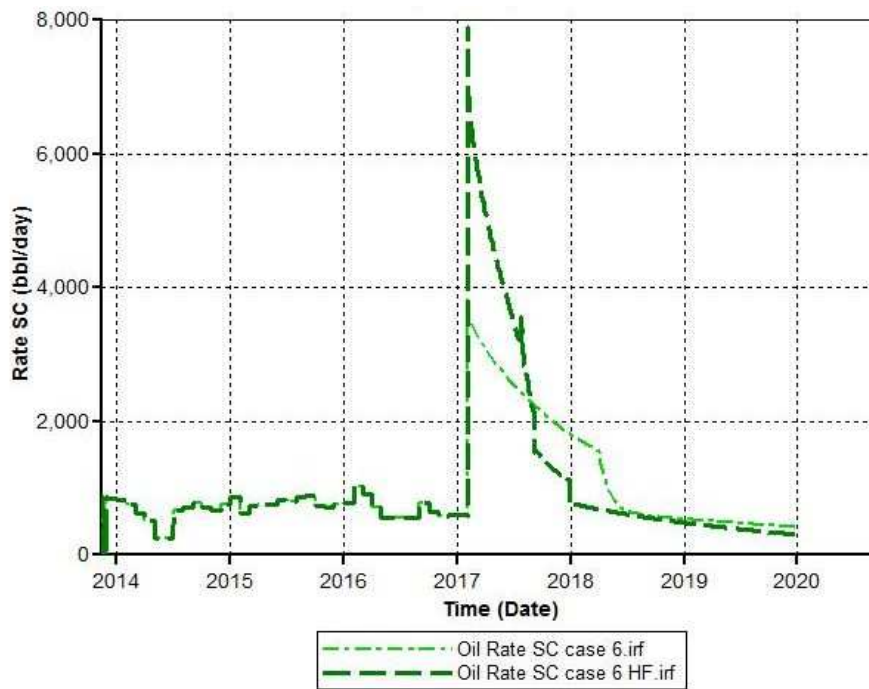


Figure 6.58 Case 6, comparative plot for oil rate with and without HF.

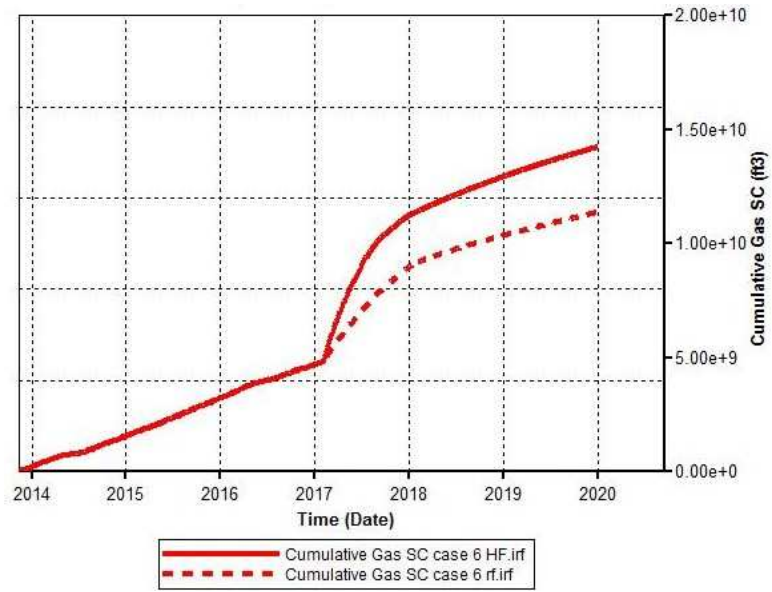


Figure 6.59 Case 6, comparative plot for cumulative gas with and without HF.

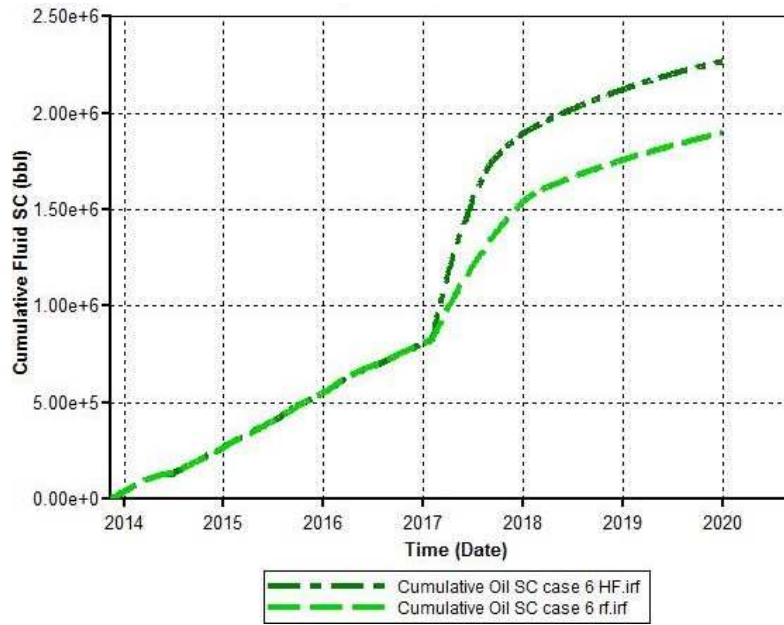


Figure 6.60 Case 6, comparative plot for cumulative oil with and without HF.

CHAPTER 7

CONCLUSIONS AND RECOMMENDATIONS

7.1 Conclusions

The main conclusion of this research is that the horizontal well, which produces from a single Sabriyah strata, and used in this study, performs as effectively as having a three-stage hydraulic fracture embedded in the well. The reason is that the natural fractures provide the improved flow path to the well as with the hydraulic fractures.

Other conclusions of this research study are:

1. The numerical modeling parameters for achieving an acceptable history match are fracture porosity, effective fracture permeability, natural fracture dimensions, and fracture connectivity. History matching included the match of the bottom-hole pressure and flow rate profiles. Water encroachment was not included in the match because of lack of knowledge about the initial water saturation and not understanding the water source entering the reservoir.

2. Sensitivity analysis to grid size revealed that the original grid size in the KOC-provided Petrel static model is too large and, consequently, results in unrealistic pressure and rate profiles.

3. As mentioned earlier, the water encroachment source has not been clearly identified by the reservoir characterization team in Kuwait. This lack of information hinders reliable reservoir performance forecasting; thus, it should become a priority.

4. Pressure analysis of a pressure buildup test conducted on the well, used in this study, and rate transient analysis of the production data from the well proved to be most significant and essential tools for determining the reservoir permeability for reservoir simulation. The calculated effective reservoir permeability was in the range of 0.5 - 0.6 md.

5. Among all production scenarios studied, the case with the constant flowrate of 2.7 MMscf/day at the bottom-hole pressure of about 5000 psia (just below the dew-point pressure), then lowering the bottom-hole pressure to a constant value of 4000 psia, yielded the largest amount of condensate production.

7.2 Recommendations

- Using only one well to assess field performance, as I did in this thesis because of time constraints, is not the best approach. Thus, I recommend a future researcher to conduct reservoir modeling to include a cluster of wells and all producing horizons in a model representing a reservoir sector. The latter will help develop a genuine understanding of reservoir performance and, thereby, arriving at an optimal production scenario for the field.

- A clear understanding of the heterogeneity of the field is essential. Hence, I recommend that the reservoir static model to be revisited.

- To evaluate the effect of production schedule (flow rate magnitude and duration) on the ultimate condensate recovery I recommend constructing a more comprehensive field model and running the model for ten to twenty years.

- Finally, I recommend to evaluate lowering liquid condensation in the reservoir by re-injecting dry gas, separated from the produced gas stream, into the reservoir. This process maintains a higher reservoir pressure, a favorably shift of the phase behavior envelope, and production of injected gas at a later date for use as a major source of energy.

REFERENCES

- Adel, H., Tiab, D. and Zhu, T. 2006. Effect of Gas Recycling on the Enhancement of Condensate Recovery, Case Study: Hassi R'Mel South Field, Algeria. Presented at International Oil Conference and Exhibition, Cancun, Mexico, 31-August to 2 September. SPE-104040-MS. <https://doi.org/10.2118/104040-MS>.
- Al-anzi, E.H., Rao, N.S., Al-Ashwak, S., Kidambi, V.K., Al-ajmi, N.H., Rao, J.D., Al-ateeqi, K.A., Al-Mayyas, R., Olderman, A.S. and Acharya, M.N. 2012. Integrated reservoir delineation and development of deep, tight carbonates: Kuwait case study. SPE Annual Technical Conference and Exhibition, San Antonio, Texas, USA, 8-10 October. SPE-159134-MS. <https://doi.org/10.2118/159134-MS>.
- Al-Eidan, A. J., Rao, N. S., Al-Awadi, M. A., Al-Ajmi, N. H., Pattnaik, C., Al-Ateeqi, K. A. and Dekeyser, T. 2010. Jurassic Tight Carbonate Gas Fields of North Kuwait: Exploration to Early Development. SPE Deep Gas Conference and Exhibition, Manama, Bahrain, 24-26 January. SPE-130914-MS. <https://doi.org/10.2118/130914-MS>.
- Barenblatt, G. I., and Zheltov, Y. P. (1960). Fundamental equations of filtration of homogeneous liquids in fissured rocks. Dokl. Akad. Nauk SSSR, 13, pp 545-548.
- Bello, R. O. and Wattenbarger, R. A. 2008. Rate Transient Analysis in Naturally Fractured Shale Gas Reservoirs. presented at the CIPC/SPE Gas Technology Symposium, Calgary, Alberta, Canada, 16-19 June. SPE 114591-MS. <https://doi.org/10.2118/114591-MS>
- Bratton, T., Canh, D. V., Van Que, N., Duc, N. V., Gillespie, P., Hunt, D. and Nelson, R. 2006. The nature of naturally fractured reservoirs. *Oilfield Review*, **18** (2), 4-23.
- Carman, G.J. 1996. Structural elements of onshore Kuwait: *GeoArabia*, **1** (2): 239–266.
- Chacko, J. 2015. SA-01 PVT Bottomhole Report, Dubai, UAE, June 2015. KOC Private Client Report.
- Cho, Y., Uzun, I., Eker, E., Yin, X., and Kazemi, H. 2016. Water and Oil Relative Permeability of Middle Bakken Formation: Experiments and Numerical Modeling. Presented at the Unconventional Resources Technology Conference, San Antonio, Texas, USA, 1-3 August. URTEC:2456998-MS. <https://doi.org/10.15530/URTEC-2016-2456998>
- CMG [Computer software]. (2012). Manual for GEM, WinProp, Results and Builder. Computer Modelling Group.
- Coats, K. H, 1987, Reservoir Simulation. In *Petroleum Engineering Handbook*, ed. H. B. Bradley, Chap. 48. Richardson, TX: Society of Petroleum Engineers.
- Cosentino, L. 2001. Integrated reservoir studies. 2001 Edition. Paris, France. Institut Français du Pétrole Publications Technip.
- Cronquist, C. 2001. Estimating and Classification of Reserves of Crude Oil, Natural gas, and Condensates, PP 120-144. Society of Petroleum Engineers. Richardson, Texas.

- Fawzi, G., Yawanarjah, S. and Touami, M., 2005. Reservoir Characterization of Fractured Cambrian Reservoirs. SPE Annual Technical Conference and Exhibition, Dallas, Texas, 9-12 October. SPE-96955-MS. DOI: <https://doi.org/10.2118/96955-MS>.
- Gannaway, G.R. and Ibrahim, M., 2016. Multiphase Analytics in a high Water-Cut Environment. SPE Paper 181480, presented at the SPE Annual Technical Conference and Exhibition (ATCE), Dubai, UAE, 26-28 September 2016.
- Gilman, J.R. and Kazemi, H. 1988. Improved Calculations for Viscous and Gravity Displacement in Matrix Blocks in Dual-Porosity Simulators. J.Pet Tech 40 (1): 60-70; Trans., AIME, 285.SPE-16010-PA. DOI: 10.2118/16010-PA.
- Kazemi, H. 1969. Pressure Transient Analysis of Naturally Fractured Reservoirs with Uniform Fracture Distribution. SPE Journal 9 (4): 451—462. SPE-2156-A. <http://dx.doi.org/10.2118/2156-A>.
- Kazemi, H. 2014. Lecture notes on Reservoir Simulation I. PEGN 513A Lecture, Colorado School of Mines, Golden, Colorado.
- Kazemi, H. 2017. Lecture notes on Naturally Fractured Reservoirs. PEGN 613A Lecture, Colorado School of Mines, Golden, Colorado.
- Kazemi, H. and Aime J.M. 1969. Pressure Transient Analysis of Naturally Fractured Reservoirs with Uniform Fracture Distribution. 9 (04). SPE-2156-A. <https://doi.org/10.2118/2156-A>.
- Kazemi, H., Eker, I. and Torcuk, M., 2014. Performance Analysis of Unconventional Shale Reservoirs. In Fundamentals of Gas Shale Reservoirs, ed. R. Rezaee, Chap. 13. Hoboken, New Jersey: John Wiley and Sons.
- Kazemi, H., Merrill Jr, L. S., Porterfield, K. L., and Zeman, P. R. 1976. Numerical simulation of water-oil flow in naturally fractured reservoirs. Society of Petroleum Engineers Journal 16 (Issue 06): 317-326. SPE-5719-PA. <https://doi.org/10.2118/5719-PA>.
- Kerunwal, A. and Uchebuakor, C. 2015. Optimization of Condensate Recovery Using Gas Recycling Technique Department of Petroleum Engineering, Federal University of Technology, University of Port Harcourt, Owerri., Nigeria
- Liu, C., 2008. Continuous Reservoir Simulation Model Upating and Forcasting Using a Markov Chain Monte Carlo Method. M.S. Thesis, Texas A&M University, College Station, Texas (December 2008).
- Mattax, C. C., and Dalton, R. L. 1990. Reservoir Simulation. Richardson, TX: Henry L. Doherty Memorial Fund of AIME, Society of Petroleum Engineers.
- McCain, W. D. 1990. The Properties of Petroleum Fluids. 2nd Edition, PennWell Corp.
- Narhari, S., Al Ashwak, S., Al Doheim, A. and Kidambi, V. 2012. An Integrated Approach for Overburden Drilling Hazard Mapping: Kuwait Case Study, Society of Exploration Geophysicist Annual Meeting, Las Vegas, Nevada, 4-9 November. SEG-2012-0984.

- Nelson, R. 2001. Geologic analysis of naturally fractured reservoirs. Houston, Texas. Gulf Professional Publishing.
- Netto, S., Schiozer, D. J., Ligerio, E. L., and Maschio, C. 2003. History matching using uncertainty analysis. Paper presented at the Canadian International Petroleum Conference. Petroleum Society of Canada. Calgary, Alberta. 10-12 June. PETSOC-2003-145. <https://doi.org/10.2118/2003-145>.
- Nobakht, M. and Clarkson, C. R., 2012. A New Analytical Method for Analyzing Linear Flow in Tight/Shale Gas Reservoirs: Constant-Flowing-Pressure Boundary Condition. SPE Reservoir Evaluation & Engineering **15** (3): 370-384. SPE-143989-PA. <https://doi.org/10.2118/143989-PA>.
- Odeh, A. 1969. Reservoir Simulation ...What is it?. Journal of Petroleum Technology **21**(11):1383-1388. SPE-2790-PA. <https://doi.org/10.2118/2790-PA>.
- Ozkan, E., Brown, M.L., Raghavan, R.S. and Kazemi, H. 2009. Comparison of Fractured Horizontal-Well Performance in Conventional and Unconventional Reservoirs. SPE Western Regional Meeting, San Jose, California, 24—26 March. SPE-121290-MS. <http://dx.doi.org/10.2118/121290-MS>.
- Peng, D. and Robinson, D. 1976. A New Two-Constant Equation of State. Industrial and Engineering Chemistry Fundamentals, **15** (1): 59–64.
- Qanbari, F. and Clarkson, C. 2016. Rate-Transient Analysis of Liquid-Rich Tight/Shale Reservoirs Using the Dynamic Drainage Area Concept: Examples from North American Reservoirs. SPE Low Perm Symposium, Denver, Colorado, 5-6 May, SPE-180230-MS. DOI: <https://doi.org/10.2118/180230-MS>.
- Rao, N. S., Al-Kandari, A. Y. A. M., Kidambi, V. K., Al-Ashwak, S., Al-Qadeeri, B. and Pattnaik, C. (2010, January 1). Understanding Fractures Through Seismic Data: North Kuwait Case Study. SPE Deep Gas Conference and Exhibition, Manamah, Bahrain, Society of Petroleum Engineers. 24-26 January. SPE-130918-MS. <https://doi.org/10.2118/130918-MS>.
- Shi, C. 2009. Flow Behaviour of Gas Condensate Wells. PHD Dissertation, Stanford University. California (March 2009).
- Terry, R. E. Rogers, J. B. 2014. Applied Petroleum Reservoir Engineering. 3rd Edition. San Francisco/ California: Prentice Hall.
- Tivayanonda, V. 2012 Comparison of Single, Double, and Triple Linear Flow Models for Shale Gas/Oil Reservoirs. M. S. Thesis, Texas A&M University, College Station, Texas, U.S.A., (August 2012).
- Tivayanonda, V. 2012. Comparison of Single, Double and Triple Linear Flow Models for Shale Gas/Oil Reservoirs. M.S. Thesis, Texas A&M University, College Station, Texas (August 2012)

- Uzun, I, Eker, E., Cho, Y., Kazemi, H., and Rutledge, J.M. 2017. Assesment of Rate Transient Analysis Techniques for Multiphase Flow in Unconventional Reservoirs: Application to Eagle Ford Formation. Presented at the SPE Western Regional Meeting, Bakersfield, California, USA, 23-27 April. SPE-185737-MS. <https://doi.org/10.2118/185737-MS>
- Uzun, I, Kurtoglu, B. and Kazemi, H. 2016. Multiphase Rate-Transient Analysis in Unconventional Reservoirs: Theory and Application. SPE Reservoir Evaluation & Engineering Journal **19** (04). SPE-171657-PA. <https://doi.org/10.2118/171657-PA>.
- Warren, J. E. and Root, P. J. 1963. The behavior of naturally fractured reservoirs. Society of Petroleum Engineers Journal **3** (03): 245-255. SPE-426-PA. <https://doi.org/10.2118/426-PA>.
- Wattenbarger, R. A., El-Banbi, A. H., Villegas, M. E. and Maggard, J.B. 1998. Production analysis of Linear Flow into Fractured Tight Gas Wells. Presented at the SPE Rocky Mountain Regional/Low-Permeability Reservoirs Symposium, Denver, Colorado, 5-8 April. Paper SPE 39931-MS. <https://doi.org/10.2118/39931-MS>.
- Watts, J. W. 1986. A Compositional formulation of the Pressure and Saturation Equations. SPE Reservoir Engineering **1** (03). SPE 12244-PA. <https://doi.org/10.2118/12244-PA>.
- Winestock, A. G. and Colpitts, G. P. 1965. Advances in Estimating Gas Deliverability, Paper PETSOC 65-03-01 presented at 16th Annual Technical Meeting, Journal of Canadian Petroleum Technology. **4** (03). PETSOC-65-03-01. <https://doi.org/10.2118/65-03-01>.
- Yousif, S. and Nouman, G. 1995. Geological Model of the Jurassic Section in the State of Kuwait, Middle East Oil Show, Manamah, Bahrain, 11-14 March. SPE 29796. <https://doi.org/10.2118/29796-MS>.

APPENDIX
CMG RUN EXAMPLE

This is the log file for case 1 for the GEM run of SA-01:

INUNIT FIELD

WSRF WELL 1

WSRF GRID TIME

OUTSRF GRID SO SG SW PRES

OUTSRF RES ALL

WPRN GRID 0

OUTPRN GRID NONE

OUTPRN RES NONE

** Distance units: ft

RESULTS XOFFSET 0.0000

RESULTS YOFFSET 0.0000

RESULTS ROTATION 0.0000 ** (DEGREES)

RESULTS AXES-DIRECTIONS 1.0 1.0 1.0

**

** Definition of fundamental corner point grid

**

GRID CORNER 24 39 24

CORNERS

2550402.4237 2*2550470.8506 2*2550539.2774 2*2550607.70 Include

'CMGTEMP_002.inc'

DUALPOR

SHAPE GK

*MDPLNRBK 98

** Please don't remove these RESULTS PLNRTEMPLATE keywords.

RESULTS PLNRTEMPLATE NAME 'Planar Template'

RESULTS PLNRTEMPLATE PRIMFRACWIDTH 0.0208

```

RESULTS PLNRTEMPLATE PRIMFRACPERM 10000
RESULTS PLNRTEMPLATE ORIGINALREFINEINTO 19 3 1
RESULTS PLNRTEMPLATE ORIGINALHALFLENGTH 500
RESULTS PLNRTEMPLATE ORIGINAL_LAYERUP 9
RESULTS PLNRTEMPLATE ORIGINAL_LAYERDOWN 4
RESULTS PLNRTEMPLATE END
*PLNRFRAC_TEMPLATE 'Planar Template'
*PLNR_REFINE *INTO 19 3 1
*BWHLEN 500
*IDIR
*INNERWIDTH 2
*LAYERSUP 9
*LAYERSDOWN 4
*PERMI FRACTURE *FZ 104
*PERMJ FRACTURE *FZ 104
*PERMK FRACTURE *FZ 104
*END_TEMPLATE
** 0 = null block, 1 = active block
NULL *MATRIX ALL
6*1 18*0 6*1 18*0 6*1 18*0 15*1 9*0 15*1 9*0 15*1 9*0 2 Include
'CMGTEMP_003.inc'
NULL *FRACTURE ALL
6*1 18*0 6*1 18*0 6*1 18*0 15*1 9*0 15*1 9*0 15*1 9*0 2 Include
'CMGTEMP_004.inc'
POR *FRACTURE CON 0.02
POR *MATRIX ALL
3*0.04732016 3*0.04762381 18*0 3*0.04732016 3*0.04762381 Include
'CMGTEMP_005.inc'
PERMI *FRACTURE ALL
3*20.42566 3*20.25039 18*26 3*20.42566 3*20.25039 18*26 Include
'CMGTEMP_006.inc'

```

```

PERMI *MATRIX ALL
3*0.1114868 3*0.1149923 18*0 3*0.1114868 3*0.1149923 18 Include
'CMGTEMP_007.inc'
PERMJ *FRACTURE ALL
3*20.42566 3*20.25039 18*26 3*20.42566 3*20.25039 18*26 Include
'CMGTEMP_008.inc'
PERMJ *MATRIX ALL
3*0.1114868 3*0.1149923 18*0 3*0.1114868 3*0.1149923 18 Include
'CMGTEMP_009.inc'
PERMK *FRACTURE ALL
20.42566 20.25039 6*26 21.10314 20.57257 20.73019 20.36 Include
'CMGTEMP_010.inc'
PERMK *MATRIX ALL
0.1114868 0.1149923 6*0 0.09793726 0.1085486 0.1053961 Include
'CMGTEMP_011.inc'
TRANSF 'SA_F30' 1.000
18 31 1 IDIR+ 18 32 1 IDIR+ 18 33 1 IDIR+
18 31 2 IDIR+ 18 32 2 IDIR+ 18 33 2 IDIR+
18 31 3 IDIR+ 18 32 3 IDIR+ 18 33 3 IDIR+
18 31 4 IDIR+ 18 32 4 IDIR+ 18 33 4 IDIR+
18 31 5 IDIR+ 18 32 5 IDIR+ 18 33 5 IDIR+
18 31 6 IDIR+ 18 32 6 IDIR+ 18 33 6 IDIR+
12 10 15 IDIR+ 12 11 15 IDIR+ 12 12 15 IDIR+
12 10 16 IDIR+ 12 11 16 IDIR+ 12 12 16 IDIR+
12 10 17 IDIR+ 12 11 17 IDIR+ 12 12 17 IDIR+
12 10 18 IDIR+ 12 11 18 IDIR+ 12 12 18 IDIR+
12 10 19 IDIR+ 12 11 19 IDIR+ 12 12 19 IDIR+
12 10 20 IDIR+ 12 11 20 IDIR+ 12 12 20 IDIR+
12 10 21 IDIR+ 12 11 21 IDIR+ 12 12 21 IDIR+
12 10 22 IDIR+ 12 11 22 IDIR+ 12 12 22 IDIR+
12 10 23 IDIR+ 12 11 23 IDIR+ 12 12 23 IDIR+

```

12 10 24 IDIR+ 12 11 24 IDIR+ 12 12 24 IDIR+
 12 13 1 IDIR+ 12 14 1 IDIR+ 12 15 1 IDIR+
 12 13 2 IDIR+ 12 14 2 IDIR+ 12 15 2 IDIR+
 12 13 3 IDIR+ 12 14 3 IDIR+ 12 15 3 IDIR+
 12 13 4 IDIR+ 12 14 4 IDIR+ 12 15 4 IDIR+
 12 13 5 IDIR+ 12 14 5 IDIR+ 12 15 5 IDIR+
 12 13 6 IDIR+ 12 14 6 IDIR+ 12 15 6 IDIR+
 12 13 7 IDIR+ 12 14 7 IDIR+ 12 15 7 IDIR+
 12 13 8 IDIR+ 12 14 8 IDIR+ 12 15 8 IDIR+
 12 13 9 IDIR+ 12 14 9 IDIR+ 12 15 9 IDIR+
 12 13 10 IDIR+ 12 14 10 IDIR+ 12 15 10 IDIR+
 12 13 11 IDIR+ 12 14 11 IDIR+ 12 15 11 IDIR+
 12 13 12 IDIR+ 12 14 12 IDIR+ 12 15 12 IDIR+
 12 13 13 IDIR+ 12 14 13 IDIR+ 12 15 13 IDIR+
 12 13 14 IDIR+ 12 14 14 IDIR+ 12 15 14 IDIR+
 12 13 15 IDIR+ 12 14 15 IDIR+ 12 15 15 IDIR+
 12 13 16 IDIR+ 12 14 16 IDIR+ 12 15 16 IDIR+
 12 13 17 IDIR+ 12 14 17 IDIR+ 12 15 17 IDIR+
 12 13 18 IDIR+ 12 14 18 IDIR+ 12 15 18 IDIR+
 12 13 19 IDIR+ 12 14 19 IDIR+ 12 15 19 IDIR+
 12 13 20 IDIR+ 12 14 20 IDIR+ 12 15 20 IDIR+
 12 13 21 IDIR+ 12 14 21 IDIR+ 12 15 21 IDIR+
 12 13 22 IDIR+ 12 14 22 IDIR+ 12 15 22 IDIR+
 12 13 23 IDIR+ 12 14 23 IDIR+ 12 15 23 IDIR+
 12 13 24 IDIR+ 12 14 24 IDIR+ 12 15 24 IDIR+
 DIFRAC CON 5
 DJFRAC CON 5
 DKFRAC CON 10
 ** 0 = pinched block, 1 = active block
 PINCHOUTARRAY ALL

```

6*1 18*0 6*1 18*0 6*1 18*0 15*1 9*0 15*1 9*0 15*1 9*0 2 Include
'CMGTEMP_013.inc'
CPOR FRACTURE 7.5e-6
CPOR MATRIX 7.5e-6
**The following is the fluid component
**property data in GEM format.
**The unit system and fluid compositions should
**be specified in the I/O control section.
**The units and compositions specified in WinProp
**are included here as comments for informational purposes.
** PVT UNITS CONSISTENT WITH *INUNIT *FIELD
**COMPOSITION *PRIMARY
**      6.8181000E-01 1.7038000E-01 4.5400000E-02 6.5170000E-02
**      2.3470000E-02 1.3770000E-02
**COMPOSITION *SECOND
**      0.0000000E+00 0.0000000E+00 0.0000000E+00 0.0000000E+00
**      0.0000000E+00 0.0000000E+00
** Model and number of components
MODEL PR
NC 6 6
COMPNAME 'N2 toCH4' 'CO2toIC4' 'NC4toC6' 'C7 toC12' 'C13toC19' 'C20toC36'
TRES 262
VISCOR HZYT
MIXVC 7.4053053E-01
MW
1.6724929E+01 3.6347577E+01 6.9931812E+01 1.2209115E+02 2.1107925E+02
3.5595595E+02
AC
0.0114412 0.126989 0.229965 0.397615 0.657632 0.986799
PCRIT

```

4.6719373E+01 4.7162543E+01 3.4806014E+01 2.6701681E+01 1.7920374E+01
 9.6565182E+00
 VCRIT
 9.8969180E-02 1.6226431E-01 2.9352718E-01 4.7565223E-01 7.9368553E-01
 1.2747608E+00
 TCRIT
 1.9616630E+02 3.3013192E+02 4.6128583E+02 5.9952495E+02 7.2295559E+02
 7.6262055E+02
 PCHOR
 77.0686 120.368 218.139 349.216 570.475 845.375
 SG
 0.315275 0.435728 0.630068 0.767864 0.83806 0.891904
 TB
 -240.472 -53.8234 93.8597 297.213 522.884 776.006
 OMEGA
 0.457236 0.457236 0.457236 0.457236 0.457236 0.457236
 OMEGB
 0.0777961 0.0777961 0.0777961 0.0777961 0.0777961 0.0777961
 VSHIFT
 -0.152409 -0.110652 -0.0391851 0.059581 0.148906 0.203546
 VISVC
 7.9175000E-02 1.4498197E-01 2.3542000E-01 3.8219000E-01 6.3659000E-01
 1.0260000E+00
 BIN
 6.0857333E-03
 2.8960116E-02 8.7310379E-03
 5.9103884E-02 2.8352174E-02 5.8022145E-03
 1.0079892E-01 6.0379501E-02 2.4323362E-02 6.5242944E-03
 1.4664485E-01 9.8951898E-02 5.1985652E-02 2.3897647E-02 5.5912750E-03
 ENTHCOEF

-2.7394751E+00 5.2680330E-01 -2.0420542E-04 3.2775732E-07 -1.1240291E-10
1.3407421E-14
2.5355198E-01 2.1969214E-01 2.7772879E-05 2.4022987E-07 -1.1244398E-10
1.6691060E-14
6.9861099E+00 6.0508494E-02 3.1261745E-04 2.0112555E-08 -3.0075915E-11
4.7252393E-15
0.0000000E+00 -4.3528783E-02 4.2644347E-04 -6.3875523E-08 0.0000000E+00
0.0000000E+00
0.0000000E+00 -3.5302664E-02 4.1554912E-04 -6.1462452E-08 0.0000000E+00
0.0000000E+00
0.0000000E+00 -1.9799547E-02 4.0404851E-04 -5.7694794E-08 0.0000000E+00
0.0000000E+00

ALTER 'SA-01'

3410000.0

*NDARCYCOR FRACTURE BG 'SA-0297DH - Frac_1' *FZ 87.3624

*NDARCYCOR FRACTURE BG 'SA-0297DH - Frac_2' *FZ 87.3624

*NDARCYCOR FRACTURE BG 'SA-0297DH - Frac_3' *FZ 87.3624

DATE 2017 2 2.00000

PRODUCER 'SA-01'

OPERATE MIN BHP 4000.0 CONT

OPERATE MAX STG 10000000.0 CONT

RESULTS TEMP_PROP 'CMGLCustom_Matrix_Por'